Influences of Drive Torque Distribution on Road Vehicle Handling and Efficiency

A Thesis Submitted to The University of Nottingham
for the Degree of Doctor of Philosophy

Joseph W. Griffin, MEng

April 2015

Abstract

With recent developments in active vehicle drivelines and the trend towards the use of electric propulsion in road vehicles, the optimal way to distribute power in a vehicle has become an interesting area of research. Automobiles with Active Torque Distribution (ATD) capabilities demonstrate improved handling and stability, and there is the possibility that energy consumption could be reduced through better distribution of power. Motorcycles that can apply some of the drive torque at the front wheel exist, with the aim of increasing tractive force on low-friction surfaces. Research is required to investigate the effects of torque distribution on the handling and efficiency of motorcycles and automobiles.

In this work, multibody models of both motorcycles and automobiles are created, and are verified with existing mathematical models. The vehicle models include the influences of suspension, aerodynamics and gyroscopic effects, and complex tyre models are used that account for combined lateral and longitudinal slip and the vertical loading situation. Simple driver models are used to control the speed and yaw rate of the vehicles while they undertake a series of on-road manoeuvres.

Left–right torque vectoring is shown to be effective in the alteration of the steady-state handling characteristics of the automobile, and front–rear torque vectoring has a small effect at high speeds. A slight increase is possible in transient responsiveness at moderate speeds, but instabilities can be exacerbated at high speeds. In motorcycles, the torque distribution has only a small effect on handling in steady-state situations.

During straight-running, the optimum efficiency of the both vehicles is shown to occur when the torque is distributed in proportion with the vertical load at the tyres. During cornering, a slight additional bias towards the front wheel(s) is beneficial.

Despite the alteration in handling characteristics made available through ATD, the effects of weight distribution and tyre characteristics still dominate. At normal speeds, almost the same effect on automobile handling can be achieved through left–right torque vectoring in a front- or rear-wheel-drive vehicle, as in a four-wheel-drive vehicle. In these steady-state situations, the energy efficiency of the vehicles varies only by small amounts, with aerodynamic and lateral slip dissipations dominating. The models presented in this thesis, and the results and conclusions obtained from them, offer the designers of future vehicles useful information for the improvement of vehicle handling, efficiency and quality.

Acknowledgements

I'd like to thank Professor Atanas Popov, for the helpful and friendly guidance throughout this research. Your knowledge and ideas were invaluable.

Dr. Guy Charles, thank you for the support, and for the original idea on which this investigation was based.

Thanks must also be given to the Engineering and Physical Sciences Research Council (EPSRC), who funded this research.

Finally, I'd like to thank Ruth, and my parents, John and Claire, for their support.

Contents

Abbreviations

4WD	Four Wheel Drive
ABS	Anti-lock Braking System
ASR	Anti-Slip Regulation
ATD	Active Torque Distribution
CoM	Centre of Mass
CoP	Centre of Pressure
CS	Coordinate System
DoF	Degree-of-Freedom
E-LSD	Electronically-controlled Limited Slip Differential
ECU	Engine Control Unit
ESP	Electronic Stability Program
EV	Electric Vehicle
FWD	Front Wheel Drive
H4V	Hybrid 4-Wheel-Drive Vehicle
HEV	Hybrid Electric Vehicle
ICE	Internal Combustion Engine
ICEV	Internal Combustion Engined Vehicle
LSC	Limited Slip Coupling
LSD	Limited Slip Differential
MSC	Motorcycle Stability Control
NS	Neutral Steer
ODE	Ordinary Differential Equation
OS	Oversteer
PI	Proportional–Integral (control method)
RWD	Rear Wheel Drive
S-AWC	Super–All Wheel Control
SH-AWD	Super Handling–All Wheel Drive

TCS	Traction Control System
US	Understeer

List of Symbols

Latin symbols

A	area
C	a coefficient
F	force
G	gain
$\boldsymbol{H}$	angular momentum
I	inertia
$K_{x,y,\gamma}$	tyre stiffness
K	understeer gradient
M	moment
O	origin
P	power
R	cornering radius
$\mathbf{R}$	rotation matrix
T	torque ratio
a	acceleration
e	error
s	displacement
g	gravitational acceleration
h	height of the centre of mass
l	wheelbase length
m	mass
r	radius
t	track width, or time
v	velocity

Greek symbols

Ω	pitch angle
$\boldsymbol{\Omega}$	angular velocity
α	(tyre) lateral slip angle

$\alpha^\star$	(tyre) lateral slip ratio
β	(vehicle) lateral slip angle
γ	camber angle, or roll angle
δ	steer angle
ϵ	caster angle
θ	heading angle
κ	longitudinal slip ratio
ρ	vertical deflection of the tyre
ρ_{air}	density of air
τ	torque
ψ	yaw angle
ω	angular velocity

Subscripts

0	initial condition
X	global X-axis
Y	global Y-axis
Z	global Z-axis
b	back
f	front
i	inside, or integral
l	left
o	outside
p	proportional
r	right
t	tyre
v	vehicle
w	wheel
x	local x-axis
y	local y-axis
z	local z-axis

Mathematical Notation

$\mathbf{r}$	a matrix (upright bold serif font)
$\boldsymbol{r}$	a vector (italic bold serif font)
r	a scalar (italic mediumface serif font)
:	a colon operator (used in the same way as in a MATLAB script: to specify an array, e.g., $0:1:3 = \begin{bmatrix} 0 & 1 & 2 & 3 \end{bmatrix}$)

List of Figures

List of Tables

List of Publications

A list of the author's publications in chronological order.

[1] J. Griffin, A. Popov and G. Charles. Development of a vehicle model for investigations into torque vectoring drivelines. In *The 11th international symposium on advanced vehicle control*. Seoul, South Korea, 2012.

[2] J. Griffin and A. Popov. Comparisons of active vehicle drivelines and investigations into their efficiency. In *The 23rd international symposium on dynamics of vehicles on road and tracks*. Qingdao, China, 2013.

[3] J. Griffin and A. Popov. Multibody dynamics simulation of an all-wheel-drive motorcycle for handling and energy efficiency investigations. In *The 2nd international symposium on bicycle and motorcycle dynamics*. Narashino, Japan, 2013.

[4] G. Parker, J. Griffin and A. Popov. The effect on power consumption and handling of efficiency-driven active torque distribution in a four wheeled vehicle. In *The 24th international symposium on dynamics of vehicles on roads and tracks*, Due for submission 2015.

[5] J. Griffin and A. Popov. Multibody dynamics simulation of an all-wheel-drive motorcycle for handling and energy efficiency investigations. *Vehicle system dynamics*, Submitted 2014.

Chapter 1

Introduction

Road vehicles accelerate through the application of torque to the wheels. Since the development of the first differential in 1828, engineers have strived for more control over the distribution of torque to manage the individual rotations of the wheels. Limited slip differentials improved traction when one of the wheels is slipping; then electronically controlled braking systems improved the stability of vehicles in dangerous situations; now, through the use of advanced mechanical or electric drivelines, there is the opportunity to actively control drive-torque distribution to influence the handling of the vehicle.

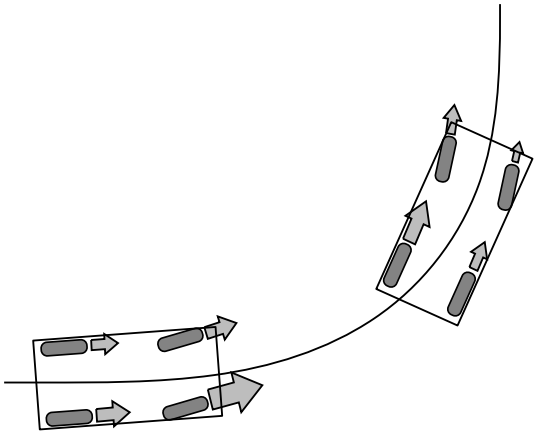

Figure 1.1: Diagrammatic representation of torque vectoring

Torque vectoring, or Active Torque Distribution (ATD), is the process of variably distributing torque between the wheels of a vehicle in order to affect its performance. Performance, here, should be considered as a broad concept encompassing not only the handling and stability of a vehicle but also the fuel efficiency, agility, passenger comfort and driver perception [5]. Figure 1.1 shows one way that torque vectoring could augment an automobile to improve handling during a cornering manoeuvre, with the size of the arrows representing the applied torque.

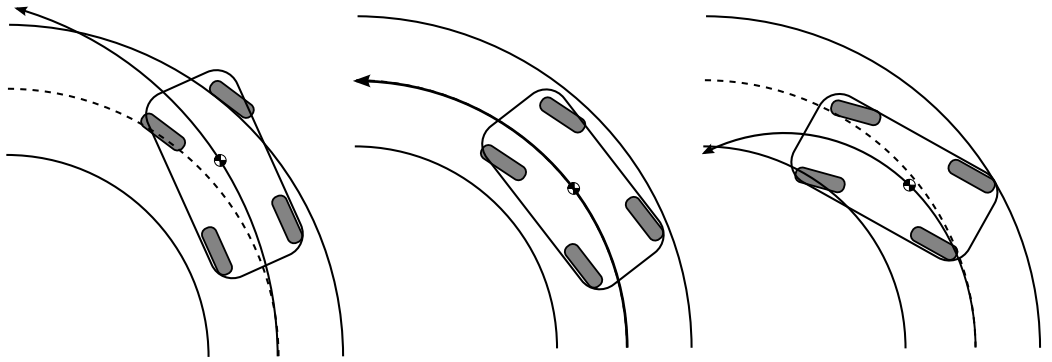

(a) Understeer **(b)** Neutral steer **(c)** Oversteer

Figure 1.2: Handling characteristics

One way to describe the steady-state handling characteristics of vehicles is to classify them as Understeer (US), Neutral Steer (NS) or Oversteer (OS), depending on what happens when they turn, as shown in Figure 1.2. When more lateral slip occurs at the front wheels than the rear, the vehicle is termed US; if the opposite is true, the vehicle is OS. The case when the slips are equal is known as NS. The handling of real vehicles, is, unfortunately, not quite that simple: it is affected by the speed and severity of a manoeuvre, by vehicle properties such as tyre conditions, and by external influences such friction coefficient. Therefore, when the vehicle is in an extreme condition, it can be difficult for drivers to predict how the vehicle will respond to an input.

Over the years, there have been significant efforts to make vehicles more predictable in extreme situations. An Anti-lock Braking System (ABS) helps to prevent locked wheels under braking, while a Traction Control System (TCS) helps to prevent wheels spinning under acceleration. In cornering situations, Electronic Stability Program (ESP) helps keep a vehicle in a controllable condition by limiting the power of the engine, or by applying brakes at one, or more, of the wheels. These systems have proven so effective at reducing the number of crashes and injuries, that the European Commission have made their inclusion in new vehicles compulsory from 2014 [15].

An issue with the above systems is that they can interfere with the driver's intention by reducing speed in extreme situations; therefore, the systems are idle most of the time. Torque vectoring, on the other hand, aims to positively influence the handling and stability of the vehicles without wresting control from the driver, and can thus be active at all times. Control is achieved by redistributing the drive torque, rather than reducing it. In a corner, for example, drive torque might be increased at the outside wheel, and reduced at the inside wheel, to help the vehicle turn into a corner, then, as the vehicle straightens up, more torque might be applied

to the inside wheel to help prevent excessive oversteer. The optimum distribution of torque at any point in a manoeuvre will depend on the current state of the vehicle, its handling characteristics and its environment.

The option to alter the handling characteristics in this way would be beneficial from a safety point-of-view, as the vehicle could be made to handle more predictably. For example, during an extreme or emergency manoeuvre, torque vectoring could be used to help prevent the vehicle spinning. It could also alter the characteristics according to a setting chosen by the driver for a particular situation. Torque vectoring systems can be used in parallel with conventional safety systems, such as ESP: drive torque distribution would be used in normal situations, with the brake-based stability systems becoming active to slow the vehicle in dangerous situations.

A potential advantage of ATD is that it helps to control the vehicle in a manoeuvre without the application of wheel brakes, which waste energy both through heat, and through subsequent acceleration to recover the lost speed. Furthermore, it actually offers the potential to save energy, compared to a standard vehicle. When a wheel slips over the ground, energy is dissipated as heat; choosing the distribution of torque to minimise the slip will minimise the amount of energy lost. Clearly, it is important to minimise the energy consumed for environmental and monetary reasons. Part of this research is to determine how much energy could be saved through the use of ATD, and in what situations.

Torque vectoring could also help improve traction when one, or more, of the wheels experiences low friction, or low vertical load. Open differentials—the most common type—distribute torque approximately evenly between the wheels. If one wheel starts to spin, for example, because of loose ground or reduced vertical load in a corner, the other drive wheel(s) are limited by the torque applied at the spinning wheel. Limited slip differentials have tried to address this [3], and torque vectoring offers the next logical development.

Various types of torque vectoring drivelines have been implemented in a small, but increasing, number of automobiles; it has not yet been seen in motorcycles. TCS and ABS are currently utilised on some larger-engined road bikes, and the systems are becoming more popular. There are also a few specialist motorcycles, primarily for off-road use, that can apply a portion of the drive torque at the front wheel using mechanical or hydraulic actuation. With electric motors reducing in size and cost, front- or two-wheel-drive motorcycles might become more common. It is therefore appropriate to investigate the potential impact of varying the distribution of torque on the handling and efficiency of motorcycles, for safety and environmental reasons.

Traditionally, the quality of a product would be determined through subjective experience, which, particularly for vehicle manufacturers, would be a long and expensive processes involving the development and refinement of prototypes. The

qualities that customers look for in vehicles will include how the vehicle feels to drive, and how it handles. By quantifying these characteristics in an objective and scientific manner, the need to collect subjective data can be reduced. With modern computers, detailed models of motorcycles and automobiles can be created to represent their real-world counterparts, meaning their characteristics can be compared before a vehicle is even built.

In this investigation, accurate multibody models of both a motorcycle and an automobile are created, and verified with documented mathematical models. Parameters studies are undertaken to investigate the effects of torque distribution. The influence on handling characteristics and efficiency will be quantified and reported, and, thus, the impact on quality analysed objectively. This information is important to the designers of future vehicles for the improvement of their handling and efficiency. Ultimately, however, it will be up to the consumers to decide whether ATD technology improves their driving or riding experience.

Chapter 2

Literature Review

2.1 Introduction

This chapter presents some history of torque distribution in automobiles and the current state-of-the-art technology in the field of torque vectoring. Motorcycles that can apply drive torque to both wheels are rare, and are considered. Electric propulsion provides an exciting opportunity to instantly and accurately control the amount of torque the wheels receive, especially if separate motors are used for each wheel; therefore, the use of electric motors in vehicles is also commented upon.

The method of investigation into torque vectoring will be through the use of computer modelling; the accuracy of which will determine how successfully the characteristics can be captured. Section 2.3 considers potential modelling methods for both the automobile and the motorcycle, and determines the methodology for the remained of the thesis.

This literature review provides the basis upon which the investigation is built.

2.2 History and Current Technology

This section summarises the advances made in controlling the distribution of torque in vehicles, and the history of stability control. Automobiles and motorcycles are considered separately, and the use of electric motors for vehicle propulsion is discussed.

2.2.1 Automobiles

Over the years, features have been introduced in automobiles to make them safer. Besides improving what happens when they crash, preventing crashes altogether has been major area of investigation. This has been achieved by the implementation of driver aids including stability control.

Introduction to Stability Control

Drivers generally control the longitudinal motion of their vehicle using the brake and accelerator pedals, and the lateral motion using the steering wheel; however, these controls cannot alter the vehicle's motion directly, only through the generation of forces at the tyre-road interaction. In normal driving, the forces generated at the tyres vary approximately linearly with slip, as the driver would expect, but as slip continues to increase, the tyre forces become saturated. Considering lateral motion, once the tyres have become saturated (at a sideslip angle of around 15° for a typical passenger-car tyre [77]) no extra turning force is generated for an increase in steering wheel angle, which might be unexpected behaviour as far as the driver is concerned. This can be seen in Figure 2.1b. Figure 2.1a shows a similar saturation effect in longitudinal motion once the wheels have reached about 20 % slip, when the wheels are considered to be locked (during braking) or spinning (during acceleration).

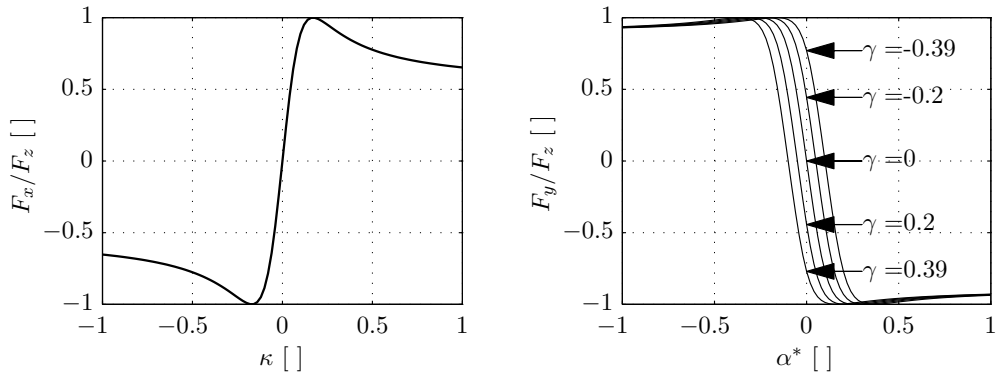

(a) Longitudinal **(b)** Lateral

Figure 2.1: Tyre characteristics

As the longitudinal slip of a tyre increases, its ability to generate lateral force is reduced, until the point where the tyre is locked and it can produce no lateral force whatsoever. It is this fact that makes Anti-lock Braking System (ABS) appealing, so that lateral control can still be maintained under heavy braking. The approximately circular shape of Figure 2.2 shows the maximum magnitude of the tyre forces in the longitudinal and lateral directions, F_x and F_y, respectively. The force available from the tyres approaches an ellipse known as the *friction circle*. This means that maximum lateral force is available with zero longitudinal slip and vice versa, and the maximum is reduced in conditions of combined lateral and longitudinal slip. A well-designed stability controller will allow the driver to approach this maximum magnitude but not exceed it. Unfortunately, this often requires an estimation of the available friction, which is not a directly measurable characteristic.

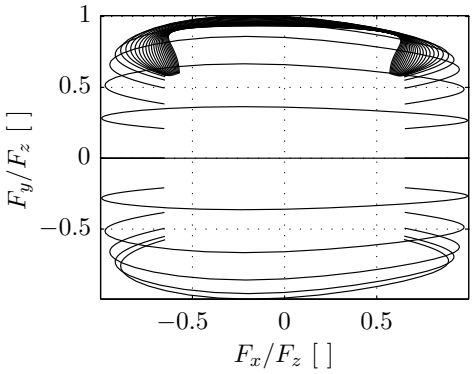

Figure 2.2: Tyre force circle, $\alpha^\star = -1 : 0.04 : 0.20$

As the majority drivers spend most of their time driving with their tyres operating in the linear region, any unexpected non-linearity might cause a loss of control, which could lead to an accident. When the lateral force at a wheel has become saturated, the centrepetal force pushing the wheel outward is no longer balanced by the friction force. This means that the affected wheels will start to drift out of the turn. If this happens more at the front wheels than the rear, understeer is occurring and the vehicle is taking a straighter path than that intended by the driver. If saturation occurs at the rear first, oversteer will occur and the vehicle will start to spin. The case where slip occurs evenly at the front and rear wheels, regardless of speed, is known as neutral steer [75]. These phenomena are depicted in Figure 1.2. Vehicle manufacturers have introduced various systems to try to help reduce excessive oversteer or understeer and, therefore, improve stability and safety. SOme of these systems will be introduced chronologically to demonstrate how chassis control theory has advanced over the years.

Traditional Brake-Based Electronic Stability Programs

In 1936, Bosch filed a patent application for an "Apparatus for Preventing Lock-Braking of the Wheels of a Motor Vehicle" but it was not until October of 1978 that their Antiblockiersystem (or ABS) went into production on the Mercedes-Benz S-class. An ABS system requires the addition of three main components to a traditional hydraulic braking system: a rotational speed sensor on each of the wheels, an electronic control unit and a hydraulic modulator that is capable of independently varying the braking pressure at each of the wheels' brakes. When the brakes are applied, the sensors monitor the deceleration of the wheels and the electronic control unit compares the signals to the expected deceleration values stored in its memory. If it detects that a wheel is at risk of locking, a signal is sent to the hydraulic modulator to reduce the braking pressure, hence allowing the wheel's slip to be

reduced and tyre force generation to remain in the linear region. The control unit will continue to monitor the wheel's speed and increase the braking pressure, if required, until the possibility of a locked wheel is detected again; thus, a new cycle begins. This happens up to 40 times a second - faster than even expert drivers can manage [55]. By preventing the saturation of tyre force in the longitudinal direction, ABS prevents the loss of steerability of a vehicle due to locked wheels, which is useful in an obstacle-avoidance manoeuvre.

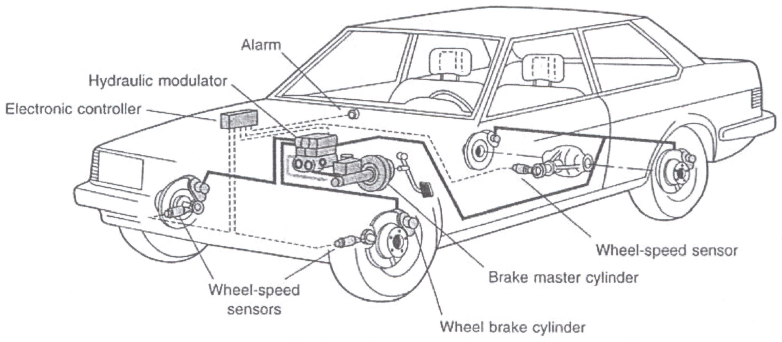

Figure 2.3: ABS by Bosch, 1984, [22]

Bosch continued to work in this area and, in 1987, introduced the first Traction Control System (TCS) called Anti-Slip Regulation (ASR) in Mercedes-Benz and BMW vehicles. Other manufacturers soon followed suit with similar systems. A TCS uses many of the same components as the ABS described above but aims to control the vehicle when excessive slip is detected under acceleration. A TCS attempts to control longitudinal slip in two ways: by reducing the power from the engine and/or by braking one or more of the wheels that are at risk of spinning. It is necessary that the braking system is able to provide a braking force without any pressure from the driver and that the engine output power can be controlled by the Engine Control Unit (ECU). The Saab TCS, which was introduced on the 9000 model in 1992, intervened in several ways at different speeds to improve stability: at low speeds, the wheel brakes would be applied first, followed by a reduction in engine power if the desired vehicle motion was not achieved; at higher speeds, the engine power would be reduced first, followed by the intervention of the braking system.

The first Electronic Stability Program (ESP) system was available on the Mercedes-Benz S-class in 1995 [48] and has since been made available, in some form, by most vehicle manufacturers. Indeed, the European Commission have made their inclusion in new vehicles compulsory from 2014 [15]. The ESP system controls the TCS and ABS to ensure that the wheels neither spin nor lock during a manoeuvre, which improves the vehicle's stability; however the difference between an ESP system and the two basic subsystems of which it comprises, is in its influence on lateral

vehicle dynamics. The ESP system monitors the driver's intent using steering wheel angle, and throttle and brake sensors, and compares this to the vehicle's actual handling behaviour, computed from lateral acceleration and yaw velocity sensors amongst others [50]. The system will intervene if the expected yaw rate and measured yaw rate differ. This intervention might be that a braking force is applied at one or more of the wheels, to correct the vehicle's yaw, or that torque from the engine is reduced by a command from the ECU.

Piyabongkarn *et al.* [48] state that ESP reduces single-vehicle crashes by 67% in the USA. While this is a significant improvement in vehicle safety, the use of the braking system as an actuator means that the vehicle's longitudinal speed is often compromised.

There are many advanced stability control systems that aim to improve vehicle yaw response such as Porsche Torque Vectoring, which features as an option on the Porshe 911 Turbo, and Mercedes-Benz Torque Vectoring, which features in the S-Class. Both of these systems actively apply brakes to one of the rear wheels to generate an additional yaw force. The limitations are that the brakes must be used, sacrificing longitudinal speed, and only 50% of the rear wheels' torque can be varied.

Having reviewed many of the available yaw rate and sideslip control methods, Manning and Crolla [37] conclude that, "Brake-based systems offer the best solution for pure safety and stability, [...] but do interfere in the driver's longitudinal speed demand."

Active On-Demand Centre Couplings

The Volvo XC90 uses a Haldex Limited Slip Coupling (LSC) to connect the front and rear drive shafts when its stability controller deems it necessary. The Haldex LSC is one example of many on-demand couplings that are available, which all work in a similar way: the system attempts to alter the handling characteristics by transferring torque from the front to the rear. By increasing the torque at the rear, the longitudinal slip there is increased. As shown in Figure 2.2, this will reduce the rear wheels' ability to generate lateral force, and, therefore, oversteer is induced. The controller will monitor the vehicle's yaw rate to see if it is lower than the desired yaw rate and actuate the coupling to modify the vehicle's dynamics and, hence, try to correct the path. Another perceived benefit of the active centre coupling is that during high-speed, straight-line driving, torque at the rear wheels can be reduced relative to the front, which might improve the stability of the vehicle.

Electronically Controlled Limited Slip Differentials

A differential is required in a vehicle to allow the left and right wheels to turn at different speeds. This is necessary in a turn, as the outer wheels follow a circle of larger radius than the inner wheels and, therefore, must turn faster. They were first used on Panhard-Levassor vehicles produced in 1891 and have since come into use in the drives of almost all vehicles [3]. The simplest type of differential is known as an 'open' differential, which always transfers the same amount of torque to each of the wheels. Problems arise with this type of differential if one of the drive wheels is on a low-friction surface such as ice, or if vertical load is reduced in a corner. In this situation, it will take only a small amount of torque to make the wheel spin and only the same amount of torque can be applied to the other drive wheel(s) making acceleration slow or impossible. A Limited Slip Differential (LSD) attempts to get around the problem by using spring-loaded clutches in the differential that fight relative motion between the half-shafts.

An Electronically-controlled Limited Slip Differential (E-LSD) shares many of the same components as an LSD, with the addition of an electronic controller for a clutch that is mounted between one half-shaft and the ring gear of the differential. When hydraulically actuated by the controller the clutch provides an additional path for torque transfer. In effect, this clutch attempts to lock the two half-shafts together, reducing their relative motion. In a corner, it can attempt to make the wheel speeds the same, which tries to force the vehicle to take a straighter path. In other words, it can increase its tendency to understeer, which can be used, by the controller, to correct oversteer. Like the active centre coupling, however, there is a limitation to the E-LSD in that torque can only be transferred from the outside wheel, which is turning faster, to the inside wheel, which is turning slower. This makes it impossible for the system to correct understeer. Hancock *et al.* [21] state that, "The controlled LSD does not appear to be such an effective tool for yaw moment control [compared to an overdriven active differential]".

Having simulated a vehicle with an active centre differential and an E-LSD, Piyabongkarn *et al.* [49] find that the vehicle, "Can always effectively provide understeering yaw moments but can provide oversteering torque moments only during on-throttle manoeuvres."

Torsen Differentials

A passive device that attempts to apply more torque to the wheel(s) with more traction is the Torsen Differential. This device exploits the fact that worm gears cannot be back-driven and so, when slip between the shafts starts to occur, worm gears in the differential start to lock up and more torque can be passed to the slower

spinning shaft [61]. They can be used in the drive axle(s) or as a centre differential and can be designed to transmit up to five times more torque to the slower spinning shaft.

Having been introduced in the Quattro in 1987, many Audis use a Torsen differential as the centre differential. The Front Wheel Drive (FWD) Ford Focus RS has used one in its front axle since 2002, and the Four Wheel Drive (4WD) Subaru Impreza WRX STi has used one in its rear axle since 2007. A limitation of this device is that torque cannot be transferred to a faster shaft. Also, if one wheel was to come off the ground completely, for example, in an off-road situation, no torque can be applied to the wheel that still has traction.

Honda's SH-AWD

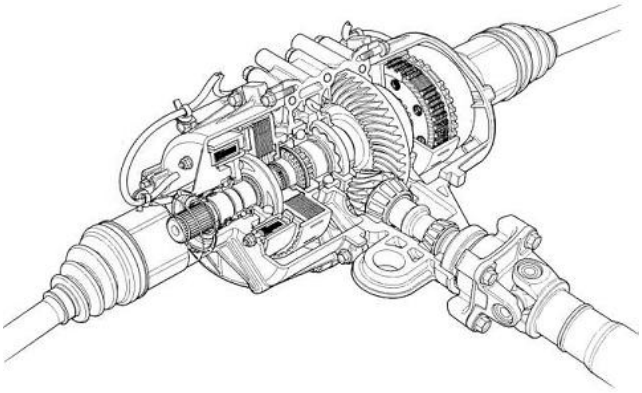

Figure 2.4: Honda's Super Handling–All Wheel Drive (SH-AWD) [24]

A torque vectoring system or Active Torque Distribution (ATD) system can directly control the distribution of torque to the front or rear axles and the inside or outside wheels, and as such, is suitable for inducing both understeer and oversteer to correct a vehicle's path. Transferring torque laterally across the axle generates a larger longitudinal force on that sideof the vehicle and hence generates a yaw moment. Rajamani [50] states that, "The ultimate all-wheel drive system is one in which torque transfer to each of the four wheels can be independently controlled." Honda introduced SH-AWD on its Legend model in 2004 [54]. This system has the ability to split torque 70:30 to 30:70 between the front and rear axles and 100:0 to 0:100 between left and right wheels at the rear. It uses electromagnetic clutches in the rear differential that are actively controlled by the stability control system. These apply torque to the required half-shafts from shafts that are geared-up from the main input shaft, hence overcoming the problem of transferring torque from a slower shaft to a faster one. The use of overdriven shafts to transfer torque has led to this type

of differential being called an 'overdriven differential'. The major limitation of the SH-AWD device is that it cannot transmit torque between the half-shafts when the torque from the input shaft is zero, i.e., it can only vector torque during on-throttle manoeuvres; However, this is often not a problem because the brake-based stability control system can aid with yaw control without interfering with the driver's intent under deceleration.

Mitsubishi's S-AYC

In April 1996, Mitsubishi Motors Corporation equipped its Lancer Evolution IV with Super–All Wheel Control (S-AWC) [57]. The system could vector toque between the left and right rear wheels to control the yaw moment acting on the vehicle regardless of whether the vehicle is accelerating or decelerating [56]. It is different from SH-AWD in that the overdriven shafts it uses, via actuated clutches, to transfer torque are driven from the half-shafts themselves, rather than the input shaft; it is this that makes the system able to transfer torque even during off-throttle manoeuvres.

In 2008, Mitsubishi launched the Lancer Evolution X, which upgraded the above system with a hydraulically actuated multi-plate clutch in its centre differential to control the torque delivered to the front and rear axles, hence achieving torque vectoring between all four wheels. The system is electronically controlled by Mitsubishi's S-AWC, which controls all of the vehicle's stability programmes [72].

MIRA's Hybrid 4-Wheel-Drive Vehicle

The above systems show the evolution of the concept of ATD and improvements in vehicle stability have been proven [48]. The systems are, however, complex and expensive, limiting their implementation to only the luxury-sport market. With the recent introduction of electric motors in vehicles, there is potential for the benefits of torque vectoring to be realized more simply and cheaply. Shino and Nagai [67] investigate the feasibility of wheel torque control of a small-scale electric vehicle with promising results.

In 2008, engineers at MIRA Ltd. developed the Hybrid 4-Wheel-Drive Vehicle (H4V). This is a FWD Skoda Fabia that has been modified with twin rear electric motors for the purpose of ATD [47]. The motors can both be energised in the forwards direction to make the vehicle effectively 4WD in low friction situations or high acceleration demand. Alternatively, the motors can be energised oppositely to create a yaw moment without affecting the longitudinal speed of the vehicle. During this operation, the negative torque required at one motor is used to regenerate power for the other motor, which is providing a positive torque, meaning that very little extra power is consumed. Finally, both motors can be used to regenerate power,

either from coasting down a hill, for example, or to use excess power from the engine and keep it at its most efficient. With this vehicle they demonstrated the potential improvements in handling dynamics made possible by the use of electric motors for torque vectoring.

A simulation of another hybrid vehicle with torque vectoring capabilities currently in development is given by Milehins *et al.* [42] where improvements in the vehicle handling behaviour over the equivalent uncontrolled vehicle are shown.

Automobile Stability Control Summary

Torque vectoring has started to prove itself as a method of improving stability in automobiles with mechanical drivelines. The logical next step is to investigate how it could be implemented in other electric and hybrid electric vehicles, where the individual wheel torques can be accurately and easily controlled. In his PhD thesis, Rieveley [52] concludes that, "The simulated results of the variable torque distribution yaw moment control within the hypothetical BMW 330i hybrid vehicle are promising." The hybrid vehicle being studied here was a FWD BMW 330i modified with 3 electric motors, one at each of the rear wheels and one connected in series with the engine. In numerical simulations using the same model, Rieveley and Minaker [53] show that the use of torque vectoring increases the side-slip angle of the vehicle during cornering events. This might have an effect on driver comfort and tyre longevity and could also increase the chances of loss of control.

Having compared different types of ATD, Osborn and Shim [45] state that, "Control of front–rear torque distribution alone delivers almost the same performance enhancement as fully independent control, for a considerably lower investment in hardware." The potential exists, therefore, to investigate the effect of different hardware layouts in the context of electric vehicles.

The ATD system can be used successfully with other stability control systems that might be present in a vehicle because their ranges of operation do not often encroach on each other. Under normal situations, ATD can aid the driver without hindering longitudinal progress, so the controller can use the ATD system earlier than traditional systems without fear of aggravating the driver. As the car is pushed further to its limit of adhesion, the traditional brake-based stability control system will become active at the point when avoiding a crash is more important than maintaining longitudinal velocity.

2.2.2 Motorcycles

In conditions of low traction and when high performance is required, there has been a trend towards the use of All-Wheel-Drive (AWD) in vehicles with four or more wheels.

Not only that, designers have been striving for control over exactly how much torque each of the wheels receives and in which situations. This is demonstrated through the use of locking and limited slip differentials and, more recently, electronically controlled differentials in the form of ATD, as described above. There are two major, but surmountable, barriers to the use of torque vectoring in motorcycles: providing power to the front wheel, and control over the system.

Motorcycle Front Wheel Drive

There are a few notable cases where AWD motorcycles have been developed and tested in the industry; for example, by Öhlins and Christini. Öhlins have developed both off-road and on-road motorbikes that use a hydraulic pump and motor to transfer up to 15 % of the torque to the front wheel, depending on the "conditions and throttle position" [28]. Christini have managed to transfer torque to the front wheel of off-road bikes by mechanical means [10]. Here, the front wheel is driven, through a freewheel, at around 80 % of the speed of the rear; thus, for torque to be applied, the rear wheel must be spinning faster than the front. Christini claim better hill climbing performance and that, "With the front wheel under power, it is nearly impossible to wash out the front end." Their system is complex: a chain is driven from the engine sprocket to a gearbox, clutch and shaft assembly that transfers torque to gears within the head tube. These mesh with gears on the lower triple clamp which, through chains, turn drive shafts that run parallel to each of the forks to a freewheel on the hub of the front wheel. Both manufacturers' systems require excess slip at the rear wheel before a drive torque is applied at the front wheel, and the amount of torque transferred is fixed by the design of the system.

There exists pedal-powered bicycles that have an assistance motor located in the hub of the front wheel. With advances in electric motor technology, it is feasible that electric motors could be used to directly power the front wheel of a motorcycle, and as such, the amount of torque applied there could be instantly and accurately controlled. However, this may present additional difficulties with the increase in unsprung mass and gyroscopic effects that would need to be investigated.

Motorcycle Stability Control

The stability systems mentioned for automobiles have not seen the same levels of acceptance in motorcycles, although they are becoming more common. ABS and TCS were first implemented in the BMW K1 in 1988, and have been used in a variety of large-engined motorcycles. Bosch has recently developed Motorcycle Stability Control (MSC), which incorporates a lean and pitch angle sensors, to help control the systems as the motorcycle corners. Bosch claim "motorcycle stability control

can help in two thirds of the motorcycle accidents occurring in bends due to rider error" [4].

Results have been presented concerning ATD in 4-wheeled vehicles showing that transferring power between the front and rear axles could have a small effect on the understeer gradient of the vehicle and could, for example, be used to help prevent a car with an oversteer tendency from spinning during high speed cornering [45]. There is therefore the possibility that such torque vectoring systems will have similar effects in two-wheeled vehicles. The difference between front and rear tyre shape and force generating characteristics play a more important role in motorcycle simulation, in comparison to a vehicle with four identical tyres.

Changing the distribution of power between the wheels of a motorcycle could give the designer more control over its handling characteristics. Anecdotal evidence suggests that powering the front wheel makes the motorcycle feel more stable in a turn and gives more traction when accelerating on soft surfaces. This research aims to investigate the optimal way to distribute torque, and to determine the extent to which the designer can influence the handling, efficiency, and ride quality in a variety of conditions and situations.

2.2.3 Electric and Hybrid Electric Vehicles

Introduction

Recently, with more stringent regulations on emissions and fuel efficiency, and concerns about energy resources, alternatively-fuelled vehicles have attracted more attention from consumers, manufacturers and governments. Research and development of Electric Vehicles (EVs) and Hybrid Electric Vehicles (HEVs) has focussed on direct replacements for current Internal Combustion Engined Vehicles (ICEVs), as passenger vehicles constitute an integral part of our lives yet are a major source of urban pollution and other environmental problems. Many governments are providing incentives to stimulate transition to low- and zero-emission vehicles. In the UK, new ICEVs and HEVs with an emission level of less than $100\,\mathrm{g\,km^{-1}}$ of CO_2, and all new EVs, do not have to pay road tax.

When passenger cars were first starting to appear in the mid-nineteenth century, EVs were in direct competition with steam-powered and ICE-powered vehicles and outsold them in many cases. The first car to achieve over 60 mph, La Jamais Contente in 1899, was powered by two direct drive electric motors attached to the rear wheels [9]. In 1900, Ferdinand Porsche, who was working for Lohner coachworks at the time and later founded the vehicle manufacturer Porsche, built a 4WD EV with electric motors mounted in the hubs of each of the wheels [3], shown in Figure 2.5. In this vehicle, the batteries alone weighed 1800 kg, which proved too heavy and

were an obstacle to the vehicle's success. Consequently, Porsche reduced the size of the battery bank and added an Internal Combustion Engine (ICE) coupled to a generator, thus creating the first HEV in 1903.

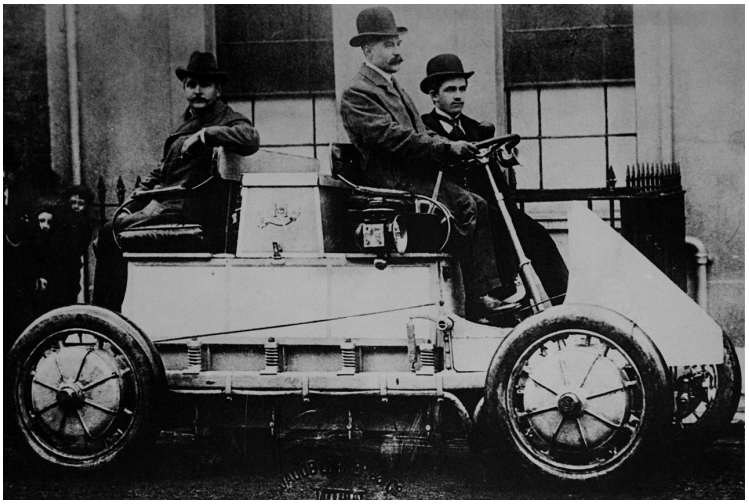

Figure 2.5: Lohner-Porsche Mixte Hybrid, 1900

By the 1920s, the invention of the starter motor, reduced purchasing costs (driven by Ford's mass production of the Model T) and the inconvenience of recharging led to the demise of early electric vehicles. Interest began to be revived during the oil crises of the 1960s, and development of the enabling technologies since then has allowed automotive manufacturers to bring EV and HEV to the market with increasing levels of success.

General Motors introduced the first modern EV, the Saturn EV1, to a limited market in 1995; however, their expensive battery packs and long recharge times prevented widespread acceptance. To address these problems, Toyota introduced the first modern HEV, the Toyota Prius, in 1999, which used a 1.5 l ICE to keep the batteries charged [70]. Since then various engineering improvements have led to increasing acceptance of alternatively powered vehicles. The current state-of-the-art will be summarised in the following sections.

Electric Vehicles

Hussain [25] defines an EV as a vehicle in which the power source is portable and electromechanical or electrochemical in nature, and where traction effort is supplied only by an electric motor. EVs generally use batteries to store the energy they gain when charged, usually from the electricity grid where the power source ranges from fossil fuels to renewable sources.

They are generally characterised by having no tailpipe emissions and a high efficiency [8] but are hindered by their high initial cost (mainly due to the batteries)

and long charging times. Issues with battery longevity mean that the high initial cost is unlikely to be offset [7]. The range of these vehicles is often short when compared to ICEVs and, although the range is increasing, the long charging times required after discharge means that they are only practical for local journeys.

The Californian firm, Tesla, produce the Roadster and Roadster Sport. These high-performance electric sports cars are capable of 125 mph and the Roadster Sport can reach 60 mph in 3.7 s (the same as a Pagani Zonda CS12 S). The 53 kW h lithium-ion battery pack gives it a 245 mile range and can be fully recharged in 3.5 h by using a 70 A connector although this can take 32 h using a standard US 15 A 120 V power outlet [68]. At USD 109 000, this car is unlikely to receive widespread acceptance but currently sets the standard for high-performance electric vehicles.

Hybrid Electric Vehicles

A HEV is one in which there are two or more main sources of power. In general, the power sources are an ICE and an electric motor but many other possibilities exist. The two main classifications are series and parallel, although some vehicles exhibit properties of both [19].

In a series hybrid, the battery-powered electric motor provides the only source of traction while the other power source, usually an ICE, is used only to generate electricity to charge the batteries. This means that, when necessary, the ICE can run at its most efficient speed, helping to keep emissions low. The batteries, in this case, are acting to buffer the electrical energy flow from the generator to the motor. The simple drivetrain and lack of a mechanical link between the generator and motor allow for flexibility of design but a drawback of this architecture is that both a generator and an electric motor are required. In other systems, the same component can fulfil both tasks. Also, the ICE, generator and motor must all be designed for maximum power for sustained high-speed driving [25].

A parallel hybrid is one in which either, or both, of the power sources can deliver power to the wheels at any time. In general, the ICE and electric motor are coupled mechanically before the transmission. This mechanical link allows the generator and motor functions to be carried out by the same electrical component in different situations. Maximum power output is determined from the sum of the ICE and electric motor, although the maximum power is not sustainable indefinitely as the batteries discharge. Parallel hybrids require more complex control than series hybrids, as power flows have to be regulated from two sources.

A variant of this architecture is known as a *through-the-road parallel* hybrid. In general, an ICE powers the front wheels while one, or more, electric motor is used to power the rear wheels. When required, the rear motor can be used as a generator to charge the batteries with power being supplied to the motor-generator through

the road. Compared to a similarly-sized ICEV, fuel efficiency can be improved by 20–30 % [25], while high-load performance can also be increased when the two propulsion units are used in parallel. When two independently controllable motors are used at the rear, this configuration can provide some degree of torque vectoring [42]. Kaiser *et al.* [31] report an improvement in transient response of such a vehicle, after studying the effects with a mathematical automobile model.

There are two main methods of supplying the power to the wheels: having one or multiple electric motors. A vehicle with a single powerplant has one motor, the power from which is split mechanically between the wheels. If it is a HEV, the electric motor will usually share the rest of the powertrain with the ICE. By connecting the electric motor to the powertrain using a planetary gearset, the HEV can operate in either series or parallel mode using the motor to generate electricity when excess power is available [8]. In the context of torque vectoring, when powered by a single powerplant the vehicle still requires the complex gearboxes of the type used in SH-AWD and S-AWC with the associated costs and other limitations.

The other alternative is to have separate motors for each of the powered wheels. These can either be hub-mounted or mounted inboard with a simple transmission. Hub mounted motors mean that no cabin space is used up but will increase the unsprung mass with detrimental effects on vehicle ride and handling. Both options allow for direct control of the torque delivered at each wheel using the feedback that is easily available from the motors. This means that the concept of torque vectoring is easier to realise than in singe powerplant vehicles.

One problem that is apparent for the distributed drive type is that when torque vectoring is requested by the controller, the maximum power of the vehicle cannot be used. For example, if a vehicle with four distributed motors needs to vector torque 30:70 front–rear and 30:70 left–right, it can only use around half the power output compared to when all four individual motors are producing their maximum power.

Electric Propulsion Summary

Currently, most EV and HEV are designed to be efficient and use as little fuel as possible and, as such, are less focussed on dynamic and exciting driving. However, vehicles such as the Tesla Roadster and some high-performance Lexus hybrids show that there is a market for energy-efficient sports and luxury vehicles. Electric propulsion is also becoming more popular in motorcycles and scooters.

Possibilities exist, particularly with vehicles with more than one tractive power source, for dynamics to be improved significantly over conventional vehicles. This study will investigate the methods of torque vectoring as a means of improving the dynamics within the context of both conventional and electric vehicles to discover the benefits and limitations.

2.3 Vehicle and Tyre Modelling

By creating accurate models of dynamic systems, one can precisely predict responses of systems to a range of inputs, thus negating the necessity for empirical testing, which has associated cost savings. Dynamic models of mechanical systems aim to predict the changes in state of the system over time.

2.3.1 Vehicle Modelling

Modelling is especially applicable to the analysis of automotive vehicles where computer simulations can replace many of the prototypes a manufacturer might have to construct to evaluate new technology. Vehicle suspension characteristics can be analysed to predict the *ride* response to a range of theoretical road-surface inputs, and vehicle handling and stability can be analysed. Given vehicle parameters such as mass, inertia and tyre properties, the response of the vehicle to driver input such as steer angle or throttle position can be calculated. Over the years, vehicle modelling has developed and become more useful as vehicle technologies have improved and computers become more powerful.

Mathematical Models

In the early twentieth century, research was concentrated on the pneumatic tyres and how they respond to side forces but results were hampered by a lack of experimental facilities [36]. In the 1930s, a sufficient understanding of the tyre was achieved to allow the steady-state turning behaviour of vehicles to be studied. With influence from the aerospace industry in the 1960s, investigations into the stability and control of vehicles began, with multi-degree of freedom systems being used to predict directional responses of a vehicle. These models are now being used in on-board controllers that directly influence vehicle dynamics through the control of stability systems, which is known as model-based control.

The well-known *bicycle model* [18] is one of the simplest models for studying the handling of four-wheeled vehicles, but is not suitable for limit-handling scenarios, where tyre forces become non-linear. The bicycle model assumes that the forces generated at the left and right wheels of each axle are approximately equal, and that their combined effect can be assumed to act at the centre of the axle; thus the simplified model resembles a bicycle. The model is generally used to calculate the yaw-rotational motion and the lateral acceleration, and uses the approximation that lateral tyre forces vary linearly with lateral tyre slip. For further information about the bicycle model and its analysis, see [2]; the model will be introduced here in Section 3.3.2. While the model, with relatively few parameters, can provide good

insight into the handling and stability of vehicles, it is unsuitable for torque vectoring studies since the tyre forces at each side are assumed to be equal.

With the addition of a longitudinal Degree-of-Freedom (DoF) for the vehicle body, and a rotational DoF for each of the wheels, the bicycle model can be extended for the purposes of torque vectoring research. Dynamic weight distribution can be accounted for so that, in a corner, the outside wheels experience more vertical load than the inside wheels: an important characteristic for torque vectoring investigations. Osborn and Shim [45] present this type of seven-DoF model for the investigation of torque vectoring drivelines in automobiles. This model is described fully in Section 3.3.3, and later verified and used for investigations into the effects of torque distribution. The model is still relatively simple and can provide good insight; however, when lateral accelerations are high, suspension and roll motions, which are ignored, will become important. At this point, the equations of motion required to describe the system accurately become too cumbersome to derive by hand; thus, software can be used to derive the equations automatically, as will be described later.

For bicycles, the earliest model was developed by Whipple [74], which considered rigid bodies and wheels that roll without slip on a level road. In general, the difference between bicycle and motorcycle dynamics is the assumption that slip does occur at the wheels of a motorcycle, leading to a model developed by Sharp [63]. The model has a mass to represent the steering system, which rotates about the steer axis of the rear frame. The rear frame includes the mass of the rider. The front and rear wheels wheels each have a tyre model that includes the effect of tyre slip and lag—a characteristic that had previously been ignored. The model was used for stability analysis with good success, and has since been used as a basis for much of the motorcycle dynamics research [64]. Other useful models are presented by Koenen [32] and Meijaard and Popov [40] and there is ongoing research by Kageyama and Kuriyagawa [30].

Multibody Models

Vehicle models are generally derived using multi-body dynamics, which is a logical continuation of the classical mechanics introduced by Newton and has been transformed by the advent and development of the computer. The system is modelled as a set of connected rigid bodies that may undergo translational and rotational motions relative to each other. The number of components and subsystems in a typical real vehicle makes comprehensive modelling impossible so simplified models need to be developed. There are many different reasons why one might want to simulate vehicles; these reasons will determine the type of model one produces.

Three dimensional modelling is now possible thanks to improvements in computers and software, where a model is built that closely represents the real system. The

shear number of equations of motion required to describe the system makes it almost essential that a computer program is used to derive them. Models created in this way are often very detailed and require significant computing power.

A number of different programs are available: SimMechanics [69] is useful for the three-dimensional modelling of rigid bodies in user defined geometries; CarSim [39] is a program that derives the equations of motion symbolically and can then simulate the dynamic behaviour of the vehicles using the model to produce animations and plots of variables. Both programs allow the user to investigate transient and steady state behaviour of systems under various inputs. MSC Adams [44] has apparently been used to model a scooter with good success [6]. Vehicle modelling specific programs, such as CarSim and Adams, often have an easy-to-use front end, but control is taken away from the user about the method of solution, which might be proprietary, and the software is often not be backed by documented code verification.

A variety of software now allows the computation of numerical solutions to the complex mathematical problems presented by the simulation of dynamic systems. Torque vectoring has the potential to affect many areas of vehicle performance. Longitudinal modelling is sufficient to investigate the effect that torque vectoring has on traction, but three-dimensional modelling is essential to investigate whether torque vectoring can improve vehicle handling.

For an automobile, a simple multibody model could include bodies that represent the main chassis and the four rotating wheels. The motions of these bodies, relative to each other and to the global coordinate system, can be defined by the user. In this way, steering actuation, drive torque and suspension motions can be modelled. This approach is used in Section 3.3.4 to describe a vehicle model suitable for torque vectoring investigations.

Vehicle Modelling for Torque Vectoring Investigations

As mentioned previously, torque vectoring was first introduced by Honda and Mitsubishi in the 1990s. Around this time, research was published by both companies to determine the efficacy of torque vectoring in improving handling and stability [54, 73]; however, a mathematical model of such a vehicle was not available.

The two-DoF of freedom model can be augmented with the moments generated by a difference in torque at the driving wheels; however, this does not account for lateral weight-transfer, and is only suitable for analysis of steady-state situations.

Abe [2] presents equations of motion, developed from the bicycle model, for vehicles with passive and active yaw-moment control. This is achieved by calculating the moment-inducing effects of, for example, locked or viscous-type differentials and then re-deriving the handling characteristics. This has the advantage that the handling caracteristics of vehicles with and without the driveline augmentations can

be compared directly; however, the model assumes linear tyre characteristics and, thus, might not be accurate near and beyond the limit of adhesion.

He *et al.* [23] present a model of a vehicle that can move with all six-degrees of freedom and uses it to analyse the combined effects of torque vectoring, active steering and traditional brake-based stability systems. The influence on handing is demonstrated for the uncontrolled systems and an integrated controller is developed. The vehicle model, and the subsystems containing the differential and braking systems, are relatively simple, but good insight is shown into the advantages and disadvantages of the systems.

As mentioned, Osborn and Shim [45] presented a seven-DoF automobile model in MATLAB and Simulink [69], which was used to evaluate the performance of front–rear and left–right torque vectoring in acceleration manoeuvres. It includes lateral, longitudinal and yaw motions of the vehicle body, plus the rotations of the rotations of the wheels; it accounts for dynamic weight transfer but ignores suspension and roll motions. It showed good potential improvements in a vehicle ability to follow a target radius when accelerating on a low-friction surface. However, it uses a relatively simple tyre model that is not accurate at high levels of combined lateral and longitudinal slip.

A ten-DoF model of a Rear Wheel Drive (RWD) automobile with a torque vectoring differential was presented in the PhD thesis of Hancock [20] and results published [21] to show the effect of an overdriven differential compared to open and limited-slip differentials. The model is based in Simulink and accounts for longitudinal, lateral and heave motions, and yaw, roll and pitch rotations of the vehicle body, plus the individual rotations of the wheels. The *Magic Formula* tyre model is used to model the tyre forces, as will be described later. Whilst the model provides good insight, it does not lend itself to easy modification to extend its application to, for example, electric drive at each of the wheels.

The EU-funded research group, E-VECTOORC (Electric-Vehicle Control of Individual Wheel Torque for On- and Off-Road Conditions) [17], is currently researching the effects of torque distribution on handling and strategies for the implementation of torque vectoring with other vehicle stability control systems. The various possible driveling layouts for electric vehicles are compared and the effect on the handling characteristics considered [13].

The work presented in this thesis aims to build on the research presented elsewhere, and expand on it, especially concerning the effect of torque vectoring on efficiency. Also, the effect on handling and efficiency of active torque distribution in motorcycles has not been considered, and is an interesting area of research.

2.3.2 Tyre Modelling

Accurate tyre models are essential for vehicle dynamics simulations. This section will summarise the available methods of calculating the forces and moments generated by a tyre, given its current situation.

Physical Models

At low slip ratios, the response of the tyre can be calculated easily, as the tyre material deforms elastically in the contact patch. The model can be extended to allow for sliding in the contact patch, using the *brush model* [46]. For basic simulations, with small slip magnitudes and without camber, this simple model might suffice; however, at large slip magnitudes, this model no longer accurately predicts the relationship between slip and force. To attempt to derive equations that model all the processes in the contact patch, such as heat dissipation, would be impractical; therefore semi empirical methods are often used.

Semi-Empirical Models

Prof. Pacejka, along with others at TU-Delft, developed the *Magic Formula* tyre model [46] to address the large deviations observed in experimental results from analytical models such as the *brush model*. The semi-empirical model is a set of equations that relate tyre load, lateral and longitudinal slips, camber angle and vehicle speed to the generated forces and moments.

Many versions exist, from the four-parameter model for approximating only lateral or longitudinal forces, to complex models, accounting for combined slip and camber angle, that calculate all six principle forces and moments. For more details, see Section 3.6.2.

The *Magic Formula* was extended to improve its applicability to motorcycle tyres, and the large camber angles they experience. Meijaard and Popov [40] present a simpler, but, perhaps, more usable model with fewer parameters.

Finite Element Models

Finally, finite element analysis of the contact patch can provide an accurate representation of the processes involved; however, they are computationally too expensive to be of use in multibody dynamics simulations.

2.3.3 Vehicle Modelling Summary

This section has briefly introduced vehicle modelling for investigations into active torque distribution. Good insight can be gained into the handling of automobiles

and motorcycles using relatively simple mathematical models, and the influence of torque vectoring can, to some extent, be analysed with small changes to these models. However, for more accurate results to be obtained, especially as the vehicles approach the limit of adhesion, more complex models are required so that suspension and individual wheel rotations can be modelled.

Calculation of the response of tyre force to slip also requires consideration: at low slip magnitudes a linear tyre model will usually suffice, but as manoeuvres become more aggressive, a more complex tyre model including saturation and the effects of combined lateral and longitudinal slip is required.

Vehicle and tyre modelling will be discussed in more detail in Chapter 3, where the various levels of complexity required for different investigations is considered.

2.4 Research Methodology

This research conforms to the scientific method: tests are conducted that produce repeatable and measurable results, from which conclusions are drawn to answer the question, "What are the influences of drive torque distribution on road vehicle handling and efficiency?"

Having studied the available literature and analysed state-of-the-art technology, it appears that there is potential for the energy consumption of automobiles to be reduced by varying the drive torque distribution. Therefore, testing will be carried out using mathematical automobile models to calculate the energy efficiency in various situations. Analysis of the results will show if a reduction in energy consumption is possible and will quantify the reduction in that case.

Following on from research into the effects of torque distribution on the handling of four-wheeled vehicles, the possibility exists for both the handling and efficiency properties of motorcycles to be influenced by the torque distribution. Again, models will be created to allow the simulation of situations in which the properties can be analysed. Changes in handling and efficiency will be quantified and, thus, conclusions about the effects will be made.

The effect on the subjective quality of the vehicles is considered only through the effect on specific and measurable characteristics of the behaviour of the vehicles.

Documented mathematical models will be compared with the complex multibody models, allowing both the verification of results in normal situations, and any differences that arise between the models in extreme situations to be analysed.

The aims and objectives of the research are specified below, and the presentation of the thesis summarised.

2.4.1 Aims and Objectives

The aim of this thesis is to determine how the drive torque distribution can be varied in order to affect the handling and efficiency of automobiles and motorcycles. In order to achieve this, the following objectives are specified:

- Research technology available for varying the distribution of torque between the wheels of two- and four-wheeled vehicles.
- Research automobile and motorcycle modelling techniques that are suitable for investigations into the effects of torque distribution.
- Create and verify models of sufficient complexity to capture the characteristics of vehicles with active torque distribution in situations approaching the limit of stability.
- Investigate the effect of ATD on the handling of automobiles and motorcycles.
- Investigate the effect of ATD on the efficiency of automobiles and motorcycles.
- Critically evaluate whether torque vectoring would be beneficial to vehicles of today and tomorrow.

2.4.2 Thesis Outline

The research is organised into chapters. Brief descriptions of their content are given below, in order to give an overview of the structure of the thesis.

Chapter 1: Introduction

A general introduction to the topic is presented, and the motivation behind the research is summarised.

Chapter 2: Literature Review

For interest and background information, a brief history of torque distribution in vehicles is given, with an assessment of the current state-of-the-art technology in the field of ATD. Available modelling techniques for both motorcycles and automobiles are critically reviewed, and the research methodology summarised. Based on this, the aims and objectives of the research are specified.

Chapter 3: Vehicle Modelling

The modelling of automobiles, motorcycles, wheels and tyres is considered in this chapter. The ways in which the simulation models can be controlled is also described.

Simple mathematical models that are suitable for initial investigations are presented, along with more complex multibody models for ATD investigations.

Chapter 4: Model Verification

The above models are verified by using simple models to verify more complex models within the regions that they are expected to be similar. Also, forces and moments are balanced against the effects they produce, and energy conservation throughout the model is checked.

Chapter 5: Vehicle Handling

Using the vehicle models developed in Chapter 3, the influence of ATD on handling is considered, including straight line and steady-state cornering situations for two- and four-wheeled vehicles. The transient response of automobiles is also considered.

Chapter 6: Energy Efficiency

Using the aforementioned vehicle models, the influence that ATD can have on efficiency is investigated in straight-line and steady-state cornering situations.

Chapter 7: Conclusions and Future Work

The major findings of the research are presented, with some suggestions for future work.

Chapter 3

Vehicle Modelling

Active Torque Distribution (ATD) is the process of controlling the amount of torque that the individual wheels of a vehicle recieve in specific situations. Research has shown that it can be used to influence the handling of automobiles [45]; models described in this section will be used to verify and quantify that effect.

The effect of torque distribution on the handling of motorcycles has not been considred, and is an interesting area of research. A model of a motorcycle that can independently vary the drive torque at its wheels will be created. It is also interesting to consider the effect on energy consumption of these systems in both the automobile and the motorcycle; therefore, the models of the vehicles will be of sufficient complexity to capture this characteristic.

Since validation of the vehicle models with real ATD motorcycles and vehicles is out of scope for this research, the models will be verified using previously accepted models of the vehicles from the literature.

The automobile model is developed from the well-known *bicycle model*, and by using a seven-Degree-of-Freedom (DoF) mathematical model presented by Osborn and Shim [45]. At low speeds with a large turning radius, the mathematical and multibody models should be equivalent, giving confidence that the complex multibody model of the automobile is accurate.

The motorcycle model will use the geometeric definition of a motorcycle turning with camber and a four-DoF model presented by Seffen *et al.* [59] after Sharp and Limebeer [66]. A steady-state model of the motorcycle, derived from the *bicycle model* for automobiles, will also be presented. Finally, a multibody motorcycle model is outlined, based on the models of Sharp and Limebeer [66] and Meijaard and Popov [40].

Linear and non-linear tyre models will be considered from Pacejka [46] and Meijaard and Popov [40], for use in the vehicle and motorcycle respectively. Simple driver

models, capable of controlling the vehicle models to acheive a specified manoeuvre will be described.

3.1 Introduction

To allow the investigation of how torque distribution affects a vehicle, a mathematical model of the vehicle is required. The level of complexity of the model is determined by the characteristics that need to be captured.

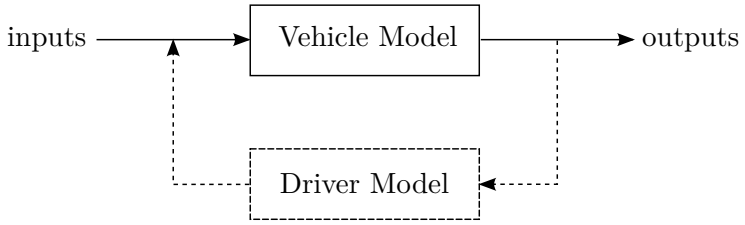

Figure 3.1: The vehicle can be thought of as an open- or closed-loop system

The vehicle can be thought of as an open-loop system, where the driver inputs influence the motion of the vehicle, as shown by the solid lines in Figure 3.1. The required outputs of the vehicle model will vary according to what is important to the investigation: for simple handling investigations of four-wheeled vehicles, this will be the yaw rate and the lateral acceleration, but to allow comparisons of more complex models, more outputs will be needed, such as the position and orientation relative to a point in space, the angular velocities of the individual wheels and the overall power consumption.

To allow accurate comparisons of different vehicles, it may be necessary to have the different vehicles undertaking the same manoeuvre at the same speed, irrespective of what driver inputs are needed to reach that state, in which case a driver model is needed. The driver model represents the human driver of the vehicle and responds to speed, position or yaw-angle errors and adjusts the inputs to the vehicle accordingly. The addition of a driver model makes the system into a closed loop, as shown by the dashed lines in Figure 3.1. Driver models will be dealt with in Section 3.7, and until that point the vehicles are considered open-loop systems.

3.2 Coordinate Systems

The number of different Coordinate Systems (CSs) involved in multibody vehicle simulation can present a challenge to a dynamicist. The CSs referred to hereafter broadly follow those outlined in [27] and are described below:

1. The *global* CS, referred to with a subscript XYZ, is fixed in space with its origin at an arbitrary point. The Z-axis points vertically upwards and the X–Y plane is horizontal and coincident with the ground.

2. The *vehicle intermediate* CS, with subscript notation xyz, moves with the vehicle and has its origin below the centre of mass when the vehicle has no roll or pitch. The z-axis remains vertical at all times but the x- and y-axes are rotated with a yaw angle equal to that of the vehicle's chassis or mainframe.

3. The *vehicle* CS, with subscript notation $xyzv$, has its origin at the same point as the *vehicle intermediate* CS but the zv-axis rolls with the vehicle mainframe about the xv-axis and pitches about the yv-axis. The xv–zv plane is thus the vehicle's plane of symmetry.

4. The *tyre* CS, with subscript notation $xyzt$, exists for each tyre and has its origin at the wheel centre. The zt-axis remains vertical but the xt- and yt-axes are rotated with a yaw angle equal to that of the tyre.

5. The *wheel* CS, with subscript notation $xyzw$, also exists for each tyre and has its origin at the same point as the *tyre* CS, but the zw-axis cambers with the wheel about the xt-axis, which remains horizontal. The xw–zw plane is thus the wheel's plane of symmetry.

Where subscripts are given as a group, the quantity represents a vector in that coordinate system (e.g., $\boldsymbol{v}_{xyzt}$ is velocity vector in the *tyre* CS). Where subscripts are given individually, the quantity refers to the specific component of the vector (e.g., v_{xt} is the velocity in the longitudinal direction of the *tyre* CS). Figure 3.2 shows the CSs for a motorcycle turning with camber; the same CSs and subscripts are applicable to four-wheeled vehicles.

The following convention will be followed in mathematical expressions: a scalar is represented in italic medium-face serif font, e.g., R, r, ω; a vector is represented in italic bold serif font, e.g., $\boldsymbol{R}$, $\boldsymbol{r}$, $\boldsymbol{\omega}$; and a matrix is represented in upright bold serif font, e.g., $\mathbf{R}$, $\mathbf{r}$.

3.3 Automobile Models

In this section, four-wheeled vehicle models of increasing complexity will be introduced. Firstly, the *bicycle model*, which is a simple model that allows good insight into the handling of four-wheeled vehicles, with some restrictions. Secondly, a 7-DoF model will be described that is similar in many respects but that allows individual wheel torques to be specified. Finally, a multibody model allowing a fuller description of the vehicle will be outlined. Presenting the models sequentially allows the evolution

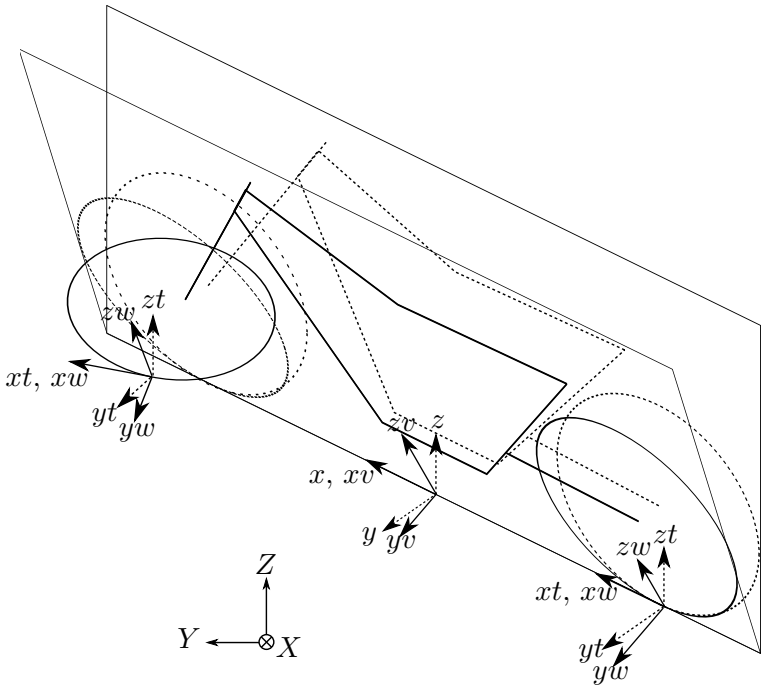

Figure 3.2: Vehicle coordinate systems

of a model capable of capturing the effect of torque vectoring to be described. At each stage, the simpler model allows the more complex model to be verified, and is then used to further the investigation.

3.3.1 Geometric Description

When a vehicle turns at very low speed, its wheels can be assumed to roll perfectly, without slip, along the surface of the road. If the vehicle is making a turn of radius R about a point at the centre of the turn, O, then the perpendiculars from each of the wheels must pass through O. Assuming only the front wheels are steered, which is the case in most four-wheeled vehicles and shown in Figure 3.3, the angle of the wheels relative to the vehicle x-axis in this no-slip condition is known as the Ackermann angle.

By assuming that angles are small, and using a value for the steer angle, δ, equal to the average of the inside and outside steer angles, δ_i and δ_o respectively, using trigonometry it can be seen that

$$\delta = \frac{l}{R}, \tag{3.1}$$

where l is the wheelbase. In an ideal, no-slip situation, the vehicle can be assumed to be a particle located at the centre of mass; thus, the longitudinal velocity, v_x, is

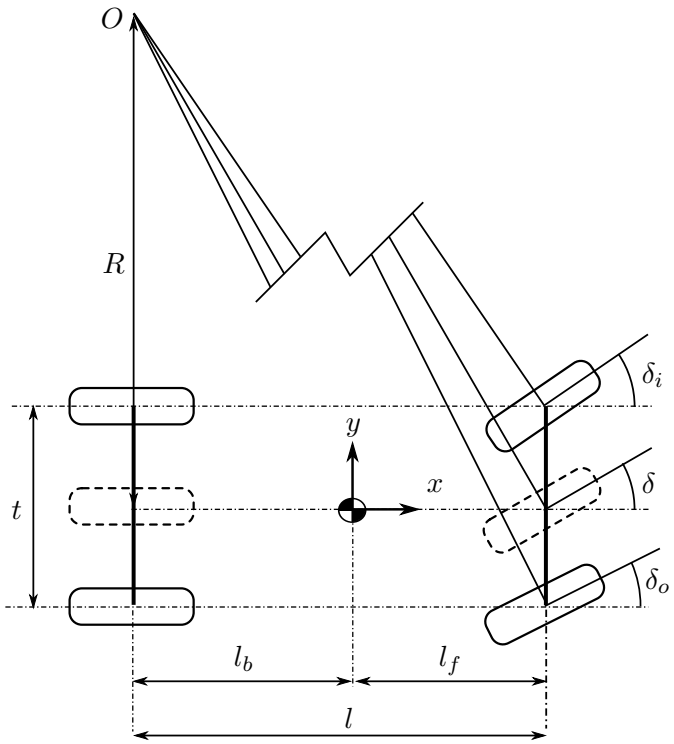

Figure 3.3: Geometry of a turning automobile

related to the speed of yaw rotation, or yaw rate, $\dot{\psi}$, by the equation

$$\dot{\psi} = \frac{v_x}{R}, \tag{3.2}$$

and to the lateral acceleration, a_y, by the equation

$$a_y = \dot{\psi} v_x = \dot{\psi}^2 R = \frac{v_x^2}{R}. \tag{3.3}$$

These equations for a vehicle cornering without slip are useful when comparing with vehicles moving at higher speeds.

3.3.2 The *Bicycle Model*

During cornering at all but the slowest speeds, real wheels will experience lateral slip due to the lateral acceleration of the vehicle, at which point the above equations are no longer valid. To investigate high-speed cornering, a more complex description of the vehicle motion is necessary, and the well-known *bicycle model* is one such option. Note: the *bicycle model* is the name given to a simplified model of a four-wheeled vehicle, and is not to be confused with models of motorcycles elsewhere in the thesis.

When the slip angles are small, the left and right slip angles can be considered to be equal, and if there is also negligible roll, then it is suitable to consider the left

and right wheels to be concentrated at the intersecting point of the xv-axis and the front and rear axles [2], as shown by the dashed lines of Figure 3.3.

If the left and right tyres of each axle have the same characteristics, then the lateral forces generated there will be equal. The horizontal forces perpendicular to the vehicle's direction of travel, F_y, are

$$2F_{y\,f} = F_{y\,fl} + F_{y\,fr} \tag{3.4}$$

$$2F_{y\,b} = F_{y\,bl} + F_{y\,br}, \tag{3.5}$$

for the front and back axles, respectively, where the subscripts fl, fr, bl and br refer to the front-left, front-right, back-left and back-right tyres.

The equation governing the lateral motion of a vehicle at a contant longitudinal speed, v_x, can now be written, from Newton's second law, as

$$m\left(\dot{v}_y + \dot{\psi}v_x\right) = 2F_{y\,f} + 2F_{y\,b}, \tag{3.6}$$

where m is the mass of the vehicle, $\dot{v}_y$ is the time-rate-of-change of lateral velocity and $\dot{\psi}$ is the time-rate-of-change of yaw angle, or yaw rate.

The lateral tyre forces also result in a yaw moment about the centre of gravity, with the motion described by the equation

$$I\ddot{\psi} = 2l_f F_{y\,f} - 2l_b F_{y\,b}, \tag{3.7}$$

where I is the inertia of the vehicle about the vertical z-axis, and l_f and l_b refer to the distance from the centre of gravity to the front and back axles respectively.

In this case where small angles are being considered, the force generating characteristics of the tyres can be assumed to vary linearly with slip angle, in the opposite direction to the lateral slip,

$$F_{yt} = K_y\alpha, \tag{3.8}$$

where K_y refers to the cornering stiffness of the tyre, and α is the slip angle, which is defined as the difference between the tyre travelling direction and the tyre heading direction. The subscript t refers to the *tyre* CS, which, for the front wheels, is rotated through the steer angle, δ, relative to the *vehicle* CS.

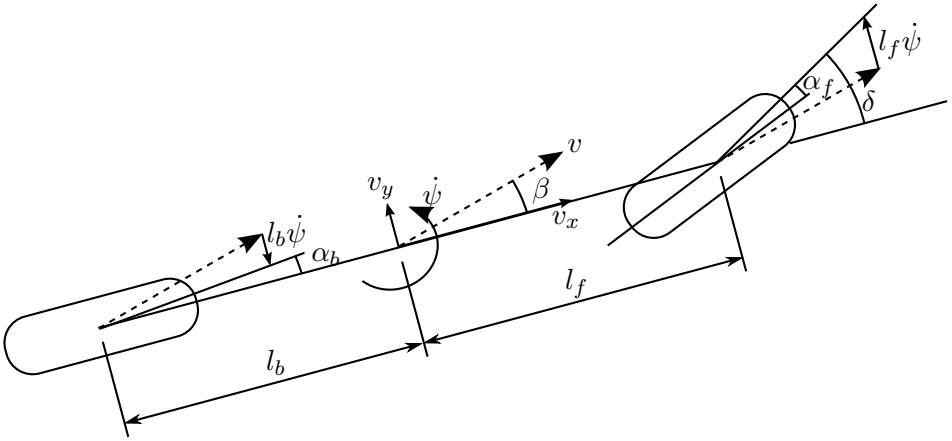

Figure 3.4: Slip angles

The slip angles at the front and rear can be calculated using the vehicle motion

$$\alpha_f = \beta + \frac{l_f\dot{\psi}}{v} - \delta \tag{3.9}$$

$$\alpha_b = \beta - \frac{l_b\dot{\psi}}{v}, \tag{3.10}$$

where β is the vehicle side slip angle, equal to v_y/v_x, and v is the resultant vehicle velocity, which, when angles are small, is approximately equal to v_x. This situation is shown in Figure 3.4.

Equations (3.9) and (3.10) are used with Equation (3.8) to find the tyre forces, which are then substituted in Equations (3.6) and (3.7) to get the equations of motion in terms of the motion itself

$$m\left(\dot{v}_y + \dot{\psi}v_x\right) = -2K_{yf}\left(\frac{v_y + l_f\dot{\psi}}{v_x} - \delta\right) - 2K_{yb}\left(\frac{v_y - l_b\dot{\psi}}{v_x}\right) \tag{3.11}$$

$$I\ddot{\psi} = -2l_fK_{yf}\left(\frac{v_y + l_f\dot{\psi}}{v_x} - \delta\right) + 2l_bK_{yb}\left(\frac{v_y - l_b\dot{\psi}}{v_x}\right). \tag{3.12}$$

These equations of motion can be solved as a set of first order, simultaneous Ordinary Differential Equations (ODEs) using MATLAB, with the function given in Appendix B.1.

The *bicycle model* is a very useful tool and allows a surprisingly detailed and insightful investigation into the handling of four-wheeled vehicles to be undertaken; however, some assumptions are made that limit the use of the model, as follows:

- Small steer and slip angles are assumed.

- The tyres have a linear characteristic, and the forces generated on each side of the axles are equal.

- The longitudinal speed is constant, and there is no longitudinal slip. Tyre aligning moments are also neglected.

To allow the study of the impact of torque vectoring on handling, it is necessary to take into account the effect of the items mentioned above, in particular, the more complex characteristics of a road tyre, and the influence of longitudinal slip. For this reason, a more complex mathematical model of the vehicle is developed.

3.3.3 Seven-Degrees-of-Freedom Model

An automobile model capable of capturing the characteristics of a vehicle with torque vectoring must have wheels that can rotate, and thus generate force, independently of each other; i.e., with their own rotational DoF. This will also affect the vehicle's longitudinal motion, and as such, the model must have a longitudinal DoF, as well as the lateral and yaw-rotational DoFs of the *bicycle model*. This results in seven DoFs.

The model assumes that roll and pitch motions are small, and thus suspension is not modelled, but the influence of lateral and longitudinal weight transfer due to acceleration is included as this affects the tyre forces. Torque can be applied at any wheel, and it is assumed that exactly the requested wheel torque is applied instantaneously.

Again, using Newton's second law as for the *bicycle model*, but including the longitudinal DoF and also without assuming small steer angles, the equations of motion for longitudinal, lateral and yaw motion become

$$\begin{aligned} &m\left(\dot{v}_x - \dot{\psi} v_y\right) = \\ &\left(F_{x\,fl} + F_{x\,fr}\right)\cos\delta - \left(F_{y\,fl} + F_{y\,fr}\right)\sin\delta + F_{x\,bl} + F_{x\,br} + F_{\text{aero}} \end{aligned} \tag{3.13}$$

$$\begin{aligned} &m\left(\dot{v}_y + \dot{\psi} v_x\right) = \\ &\left(F_{x\,fl} + F_{x\,fr}\right)\sin\delta + \left(F_{y\,fl} + F_{y\,fr}\right)\cos\delta \quad + F_{y\,bl} + F_{y\,br} \end{aligned} \tag{3.14}$$

$$\begin{aligned} &I\ddot{\psi} = \\ &\left[\left(F_{x\,fr} - F_{x\,fl}\right)\cos\delta + \left(F_{y\,fr} - F_{y\,fl}\right)\sin\delta\right]\frac{t_f}{2} + \left[F_{x\,br} - F_{x\,bl}\right]\frac{t_b}{2} \\ &+ \left[\left(F_{y\,fl} + F_{y\,fr}\right)\cos\delta + \left(F_{x\,fl} + F_{x\,fr}\right)\sin\delta\right] l_f + \left[F_{y\,bl} + F_{y\,br}\right] l_b, \end{aligned} \tag{3.15}$$

where t_f and t_b are the distances between the front and back wheels respectively, known as the track width. Other quantities are shown in Figure 3.5. These equations are similar to those presented by Osborn and Shim [45] with the addition of an

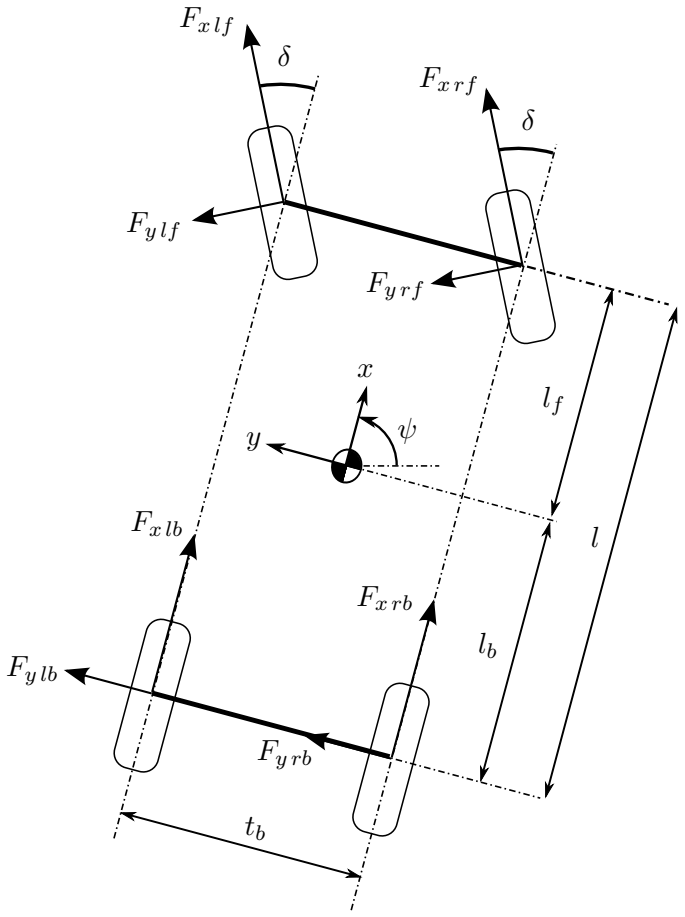

Figure 3.5: Schematic of the seven degrees of freedom model

aerodynamic drag force and the option to have a different track widths at the front and rear.

The equations of motion governing the rotation of the individual wheels are all of the same form; for example, the equation for the front-left tyre is

$$I\dot{\omega}_{fl} = \tau_{fl} - F_{x\,fl} r_{fl} \tag{3.16}$$

where τ is the applied torque to the wheel, and r is the wheel radius, as shown in Figure 3.6. Tyre rolling resistance moment, M_y, is assumed to be zero in the current model, but is accounted for by more complex models described later.

The tyre forces in the model are no longer assumed to vary linearly with slip, and are affected by vertical load and the combined slip situation. The tyre models are described in Section 3.6. The calculation of the variables used by the tyre models will now be outlined.

The vertical force, F_z, experienced at each wheel results from the accelerations of the vehicle mass in its three principle directions. The forces are determined by

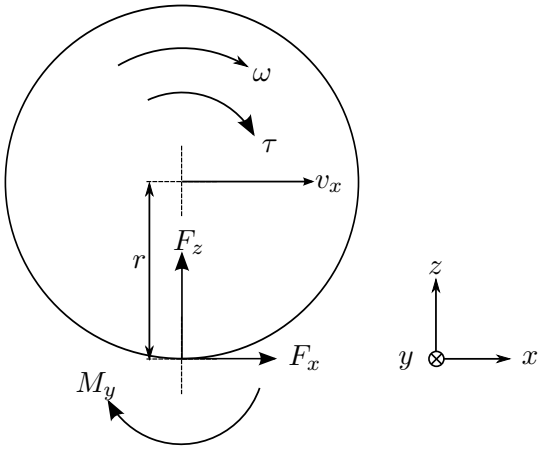

Figure 3.6: Schematic of the wheel

the equations

$$F_{z\,fl} = \frac{mgl_b}{2l} - \frac{mha_x}{2l} - \frac{ml_r a_y}{2t_f} \tag{3.17}$$

$$F_{z\,fr} = \frac{mgl_b}{2l} - \frac{mha_x}{2l} + \frac{ml_r a_y}{2t_f} \tag{3.18}$$

$$F_{z\,bl} = \frac{mgl_f}{2l} + \frac{mha_x}{2l} - \frac{ml_f a_y}{2t_b} \tag{3.19}$$

$$F_{z\,bl} = \frac{mgl_f}{2l} + \frac{mha_x}{2l} + \frac{ml_f a_y}{2t_b}, \tag{3.20}$$

where g is the acceleration due to gravity and h is the height of the centre of mass. In simulation, the longitudinal and lateral accelerations are taken from the left-hand side of Equations (3.13) and (3.14) at the previous time step.

The speed of the wheel centre in each of the *tyre* coordinate systems is required, along with the rotational speed of the wheel, to allow the calculation of the tyre slips, and hence the tyre forces. Firstly, the longitudinal tyre velocity, v_{xt}, is calculated using the equations

$$v_{xt\,fl} = \left(v_x - \frac{\dot{\psi} t_f}{2}\right)\cos\delta + \left(v_y + \dot{\psi} l_f\right)\sin\delta \tag{3.21}$$

$$v_{xt\,fr} = \left(v_x + \frac{\dot{\psi} t_f}{2}\right)\cos\delta + \left(v_y + \dot{\psi} l_f\right)\sin\delta \tag{3.22}$$

$$v_{xt\,bl} = v_x - \frac{\dot{\psi} t_b}{2} \tag{3.23}$$

$$v_{xt\,br} = v_x + \frac{\dot{\psi} t_b}{2}. \tag{3.24}$$

Similarly, the lateral tyre velocity, v_{yt}, is calculated with

$$v_{yt\,fl} = \left(v_y + \dot{\psi} l_f\right) \cos\delta - \left(v_x - \frac{\dot{\psi} t_f}{2}\right) \sin\delta \tag{3.25}$$

$$v_{yt\,fr} = \left(v_y + \dot{\psi} l_f\right) \cos\delta - \left(v_x + \frac{\dot{\psi} t_f}{2}\right) \sin\delta \tag{3.26}$$

$$v_{yt\,bl} = v_y - \dot{\psi} l_r \tag{3.27}$$

$$v_{yt\,br} = v_y - \dot{\psi} l_r. \tag{3.28}$$

The longitudinal speed of rolling, v_r, for each wheel is found by multiplying its angular velocity, ω, by its radius, r; for example,

$$v_{r\,fl} = \omega_{fl} r_{fl}. \tag{3.29}$$

Equations (3.21) to (3.29) are used to find the tyre longitudinal slip ratio, κ, and the lateral slip angle, α, and thence with the vertical load and tyre model to find the tyre lateral and longitudinal forces at each wheel, as described in Section 3.6.

To include the effect of aerodynamic drag, a force is assumed to act on the vehicle in the opposite direction to the vehicle's heading. The pitching moment generated by the aerodynamic force is assumed to be small; thus, the force is assumed to act at the origin. The magnitude of the force is calculated with

$$F_{\text{aero}} = -1/2 \rho_{\text{air}} A C_{\text{drag}} v_x^2 \tag{3.30}$$

where ρ_{air} is the density of air, A is the frontal area and C_{drag} is the coefficient of drag.

These equations can now be solved as a set of ODEs using MATLAB, with inputs of steer angle and the four individual drive torques. The function for doing so is presented in Appendix B.2.

The 7-DoF model provides a suitable platform for investigations into the effect of ATD in automobiles, especially when a non-linear tyre model is used; however, still there are some important assumptions and limitations:

- It is assumed that the wheels are rigidly attached to the vehicle, and there is no camber, or toe-in or toe-out. Roll and pitch motions are assumed to be negligible. As such, the model is only suitable for simulating steady-state, or quasi-steady-state, situations.
- Any changes to the vehicle description, such as rear-wheel steer or additional axles, would require the equations of motion to be re-derived and re-coded by hand.

- While the tyre model no longer assumes a linear relationship between slip and force, the variation of horizontal load with vertical load, and the effect of combined slip, are still rudimentary. Tyre moments are not included.

To address the above issues, and for other reasons described below, a multibody model was developed.

3.3.4 Multibody Model

SimMechanics, a graphical multibody modelling suite from The Mathworks [69], was chosen for the development of a multibody model, as it allows modelling, control and evaluation of the system in one environment. Equations of motion are generated automatically from the block diagram, based on the specified bodies, joints and constraints. The resulting ODEs are solved using MATLAB solvers, which can be modified to the requirements of the user. MATLAB is used for parameterizing and post-processing.

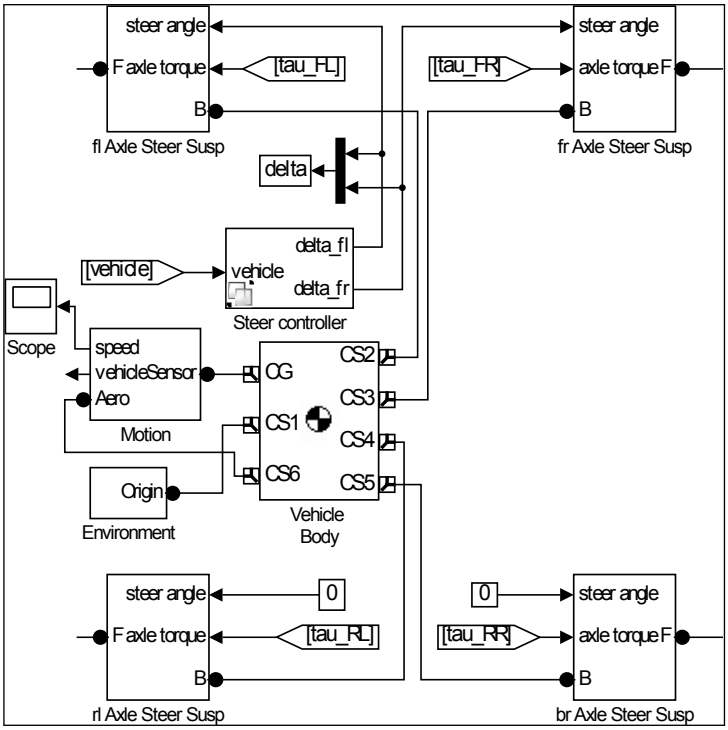

Figure 3.7: Part of the vehicle model block diagram

In SimMechanics, the multibody model is described in block diagram form with bodies, joints, sensors and actuators connected in a similar way to Simulink models [69]. Figure 3.7 shows part of the top-level view of the vehicle model, which will be described in this section.

Model Environment

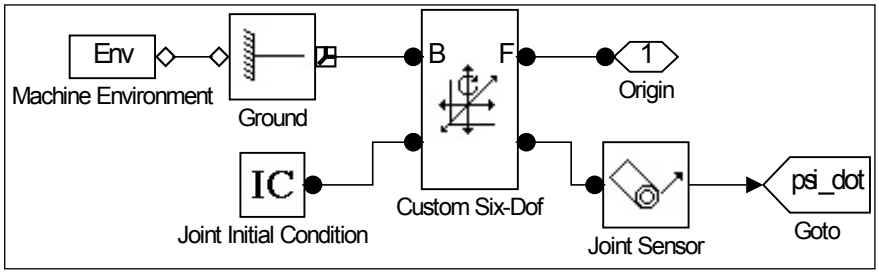

Figure 3.8: Defining the model environment and initial conditions

In the subsystem shown in Figure 3.8, gravity and other simulation parameters are set in the *Machine Environment* block, and a point in space defined by the *ground* block, which is the origin of the *world* or global CS. A CS attached to the vehicle is connected to the *ground* block through a joint that allows six degrees of freedom. Initial conditions, such as longitudinal speed, are also set here, and a *sensor* is used to record the yaw rate for use elsewhere in the model.

Vehicle Body

The lumped mass of the vehicle body is defined by the *body* block in Figure 3.7: its mass and inertia matrix are specified, along with the necessary CSs. A CS, which moves and rotates with the body, is required at each point where a joint or sensor is to be attached, and at the points where forces or moments are to be applied. The origin of the first CS is defined directly below the centre of mass of the vehicle, which is coincident with the origin at the start of the simulation, and from which the relative positions of the other CSs are specified. These include the vehicle's centre of mass, the aerodynamic centre of pressure, and the locations of the connections to the four wheels. Values are set from a MATLAB script of model parameters.

Aerodynamic lift and drag forces are applied to the CS at the centre of mass according to the equations

$$F_{\text{aero},xv} = -0.5\rho_{\text{air}} C_{\text{drag}} v_{xv}^2 \tag{3.31}$$

$$F_{\text{aero},zv} = 0.5\rho_{\text{air}} C_{\text{lift}} v_{xv}^2. \tag{3.32}$$

Steering and Suspension

Connected to the CS at each of the wheels is an identical copy of a *variant subsystem*: the two user-selectable variants give control over whether a suspension model is included in the joint description. In both cases, the *base* of the joint is connected to the vehicle body and the *follower* is connected to a wheel body.

When no suspension model is required, e.g., for verification with simplified models, the joint allows only an angle of rotation to be specified relative to the local z-axis, and rotation about the local y-axis. This allows the steer angle of the individual wheel to be specified, and defines the roll degree-of-freedom of the wheel; a torque can be applied about this axis of rotation, if required.

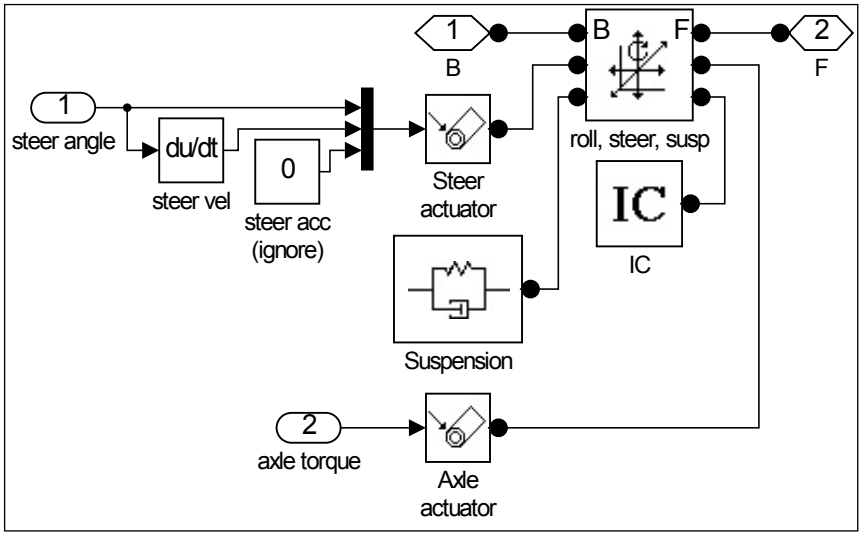

Figure 3.9: Variant wheel joint subsystem including a suspension model

When a suspension model is required, e.g., where roll motion might be important and for transient manoeuvres, then another degree of freedom is introduced that allows the wheel hub to move in the direction of the local zw-axis, with specified spring and damping coefficients. This variant is shown in Figure 3.9. The linear suspension model is intended as a tool to investigate the importance of suspension in the response, rather than to capture the complex motion and characteristics of a real vehicle suspension system.

The steer angle of the left and right wheels is calculated from an equivalent vehicle steer angle, δ, using equations that satisfy Ackermann geometry, as shown in Figure 3.10. The left and right steer angles, δ_l and δ_r respectively, are

$$\delta_l = \arctan\left(\frac{l}{{}^{l}/_{\tan\delta} - {}^{t_f}/_{2}}\right) \tag{3.33}$$

$$\delta_r = \arctan\left(\frac{l}{{}^{l}/_{\tan\delta} - {}^{t_f}/_{2}}\right), \tag{3.34}$$

and the equivalent vehicle steer angle can be calculated from the wheel steer angles

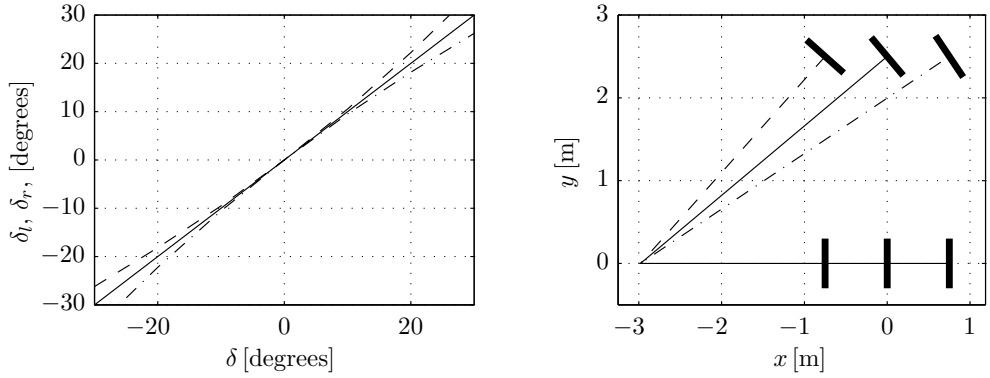

(a) Ackermann steering angles **(b)** Ackermann steering geometry

Figure 3.10: Ackermann steering. – – –Left wheel; ——Imaginary centre wheel; – · –·Right wheel.

using

$$\delta = \operatorname{arccot}\left(\frac{\cot\delta_l + \cot\delta_r}{2}\right). \tag{3.35}$$

Wheels

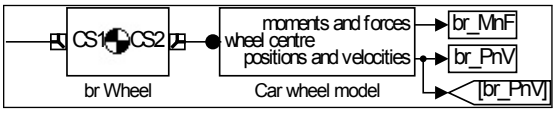

Figure 3.11: Part of the vehicle model showing the wheel

Wheel bodies are connected to each of the axle joints, and their mass and inertia properties specified. Two CSs are required, both of which are coincident with, and moving with, the centre of mass of the wheel. The first for connecting to the hub, and the second for the application of the tyre forces and moments. Because SimMechanics CSs move and rotate with the body to which they are attached, no CS can be specified at the contact patch, thus the tyre forces must be applied at the centre of mass, and the effect of the offset taken into account mathematically, as will be discussed in Section 3.5.

The *car wheel model* subsystem in Figure 3.11 contains the wheel kinematics calculations, and tyre force and moment calculations. It also outputs the data for use elsewhere in the model and saves it as variables for the processing of results.

Multibody Model Summary

The five masses of the multibody model are now defined, and the allowable motions specified, given 14 degrees of freedom. The calculation and application of tyre forces

will be discussed in Sections 3.5 and 3.6. By prescribing or controlling the individual steer angles and drive torques, the response of the vehicle can be calculated for a given simulation length. Control over the steer angles and drive torques will be discussed in Section 3.7.

3.3.5 Automobile Modelling Summary

This section has described how models of increasing complexity were used to allow the development of a four-wheeled-vehicle model capable of simulating the effects of torque vectoring. The models described were:

- the geometric description of a vehicle turning at low speed;
- the *bicycle model* for simple handling investigations;
- a seven-degree-of-freedom model for non-linear handling investigations and preliminary torque vectoring studies;
- a multibody model suitable for use with a complex tyre model for further study of torque vectoring.

With each increase in complexity, it is possible to gain further insight into the handling of vehicles through the inclusion of, for example, load transfer effects, combined tyre slip and suspension models. At each stage, the simpler models provide the basis for verification of the more complex models, as will be described in Chapter 4.

3.4 Motorcycle Models

Compared to other multi-wheel vehicles, single track vehicles represent quite a different challenge to the dynamicist because their motion is more complex. Cambering and self-steering characteristics, for instance, can often be ignored when modelling automobiles; however, they are fundamental to the motion of a motorcycle. Trail and gyroscopic effects also influence the handling and stability [33]. The modelling of motorcycles includes sideslip at the tyre contact points; sideslip is usually ignored in the modelling of bicycles, where non-holonomic rolling constraints are usually preferred. Following a process similar to the modelling of the automobile above, this section will describe motorcycle models of increasing complexity, to allow investigation into the effects of varying torque distribution.

3.4.1 Geometric Description

Consider a motorcycle as point mass, m, negotiating a corner of constant radius, R, at a steady speed, v_x. By assuming that the steer angle of the motorcycle is small,

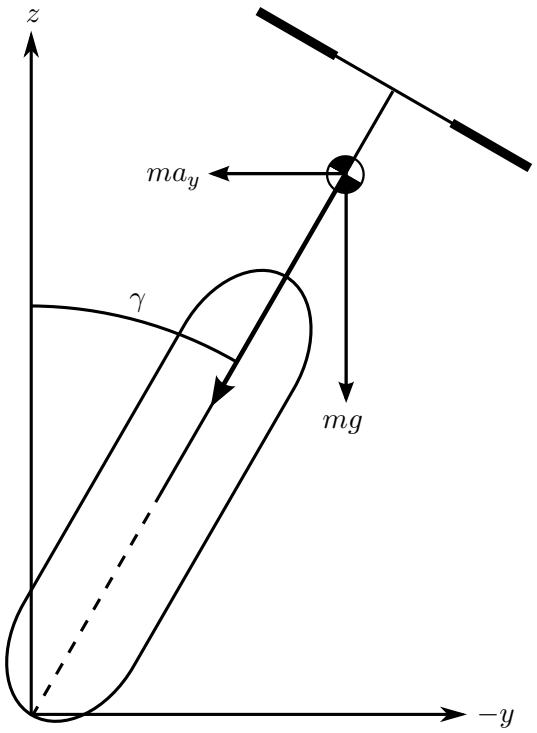

Figure 3.12: Camber angle of a simplified motorcycle viewed from the rear.

so that the camber angle of the front wheel, γ_f, is the same as the frame and rear wheel, γ_b, and that the tyres are disc-like, the camber angle can be calculated by resolving the gravitational and centripetal forces, as shown in Figure 3.12. Using the substitutions from Equation (3.3), the following equation is obtained,

$$\gamma \approx \tan\gamma = \frac{\cancel{m}a_y}{\cancel{m}g} = \frac{v_x^2}{gR} = \frac{\dot{\psi}v_x}{g}. \tag{3.36}$$

This equation can be used, for example, for verification of the motorcycle models in steady state, but is of limited use in the analysis of the dynamics of motorcycles because of the assumptions made.

3.4.2 Steady-State Model

The simplified equations of motion for the automobile known as the *bicycle model*, given in Equations (3.6) and (3.7), are valid for a motorcycle; however, only in steady state conditions. Only one tyre force is applied at each axle, thus, the equations can be written

$$m\dot{\psi}v_x = F_{yf} + F_{yb} \tag{3.37}$$

$$I\ddot{\psi} = l_f F_{yf} - l_b F_{yb} = 0. \tag{3.38}$$

The camber of the tyres generates lateral force in addition to the side slip velocity, which must be accounted for by the tyre model. Assuming that tyre force is linearly proportional to both sideslip angle and camber angle, the tyre forces are

$$F_{yf} = K_{\alpha f}\alpha_f + K_{\gamma f}\gamma_f \tag{3.39}$$

$$F_{yb} = K_{\alpha b}\alpha_b + K_{\gamma b}\gamma_b, \tag{3.40}$$

where K_α and K_γ are the lateral stiffness and camber stiffness of the tyres, respectively.

Using the substitutions from the *bicycle model* in Equations (3.9) and (3.10) with Equation (3.36), the steady-state equations are

$$\begin{aligned} m\dot{\psi}v_x = &\left(K_{\alpha f} + K_{\alpha b}\right)\beta + \\ &\left(\frac{l_f K_{\alpha f} - l_b K_{\alpha b}}{v_x} + \frac{\left(K_{\gamma f} + K_{\gamma b}\right)v_x}{g}\right)\dot{\psi} - K_{\alpha f}\delta \end{aligned} \tag{3.41}$$

$$\begin{aligned} 0 = &\left(l_f K_{\alpha f} - l_b K_{\alpha b}\right)\beta + \\ &\left(\frac{l_f^2 K_{\alpha f} + l_b^2 K_{\alpha b}}{v_x} + \frac{\left(l_f K_{\gamma f} - l_b K_{\gamma b}\right)v_x}{g}\right)\dot{\psi} - l_f K_{\alpha f}\delta, \end{aligned} \tag{3.42}$$

This model is useful for investigating how the steady-state handling characteristics of a motorcycle vary with tyre and mass distribution properties. This analysis of motorcycle handling is not common, although similar equations are presented by Kageyama and Kuriyagawa [30]. It is limited by the following assumptions:

- The model is only valid in steady state.
- Steer angle, δ, is used as an input, but motorcycles are usually controlled with a combination of steer torque and lean torque [33]. The actual steer angle is generally not used by the rider to control a motorcycle, except perhaps at very low speeds, nor is it important for feedback.
- The motorcycle consists of only one lumped mass, rather than multiple connected bodies, each with mass and inertia properties. The motion of these bodies, relative to each other, are considered to be important in the handling of a motorcycle.

Because of these limitations, a more complex motorcycle model is required for torque vectoring investigations.

3.4.3 Dynamic Motorcycle Model

A model of a motorcycle suitable for dynamics investigations was created by Sharp [63], from which many subsequent motorcycle models have been based. Seffen *et al.* [59] presented equations of motion of the form

$$\mathbf{M}\begin{bmatrix}\ddot{y}\\ \ddot{\psi}\\ \ddot{\delta}\\ \ddot{\gamma}\end{bmatrix} + \mathbf{N}\begin{bmatrix}\dot{y}\\ \dot{\psi}\\ \dot{\delta}\\ \dot{\gamma}\end{bmatrix} + \mathbf{P}\begin{bmatrix}\delta\\ \gamma\end{bmatrix} + \mathbf{G}\left[\tau_s\right] = 0, \tag{3.43}$$

where y is the lateral displacement, ψ is the yaw angle, δ is the steer angle and γ is the lean angle. The first and second time derivatives are represented by a $\dot{}$ and a $\ddot{}$, respectively. The model has four degrees of freedom. The steer torque, τ_s, is applied about the axis of rotation of the handlebars. $\mathbf{M}$, $\mathbf{N}$, $\mathbf{P}$ and $\mathbf{G}$ are matrices of motorcycle parameters and the reader is referred to [59] for their definition. This derivation of the equations of motion ignores rider lean torques. The equations of motion were coded in MATLAB [69] and are given in Appendix B.5.

The model is very useful for motorcycle handling investigations; however, it is limited by the following assumptions:

- It does not allow for longitudinal slip at the wheels, which is important when tyres are approaching their limits of adhesion.
- Tyres are disc-like, which may be an over-simplification when large camber angles are encountered.

For these reasons, a multibody motorcycle model was developed.

3.4.4 Multibody Model

To investigate the effect of torque vectoring in two-wheeled vehicles, another SimMechanics multibody model was created. Because there can be large changes in the geometry of the bike and rider combination due to rider actuations and vehicle state, it is difficult to derive mathematical equations of motion that include all of these effects; therefore, the multibody modelling approach was used again. A similar technique was employed by Sharp and Limebeer [66] for modelling a motorcycle in Autosim [39].

The motorcycle model was created in SimMechanics using a model developed by Meijaard and Popov [40]. Also useful is an example included in the SimMechanics package [76] that uses Sharp and Limebeer's motorcycle model as a basis.

The motorcycle has a rider whose body is inclined at a specified angle and can lean side-to-side about the seat, a steering system that steers and twists[1] about specified axes, telescopic front suspension, and a rear swingarm with monoshock-type suspension. The wheels each have different dimensions and mass and inertia properties, and to which different drive torques can be applied. Separate front and rear tyre models are used for the calculation of tyre forces and aligning moments.

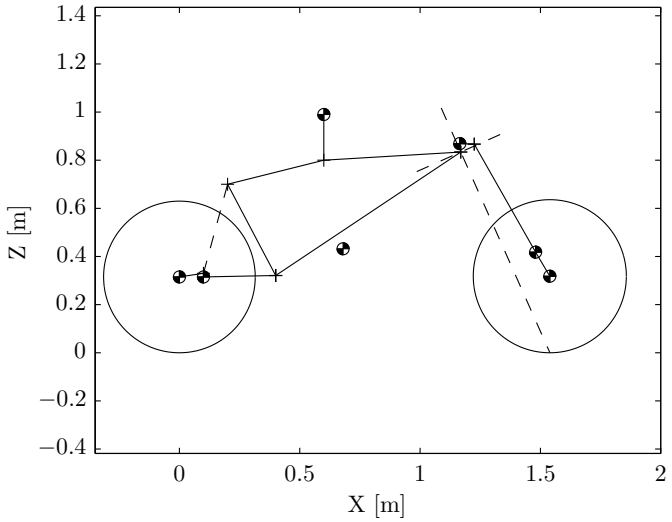

Figure 3.13: Initial location of the centres of mass and joints of the motorcycle

The model consists of seven connected bodies, as shown in Figure 3.13, each with an associated mass and rotary inertia. There are 13 degrees of freedom specified to describe the motion of the bodies: the system can move with six degrees of freedom, the rider can lean, the front frame can steer and twist, there is suspension at the front and rear, and both wheels roll aobut their axle.

Mainframe

As for the automobile model, in SimMechanics gravity and an origin in space are defined, then the main motorcycle frame is connected to the origin with a joint that allows it to move with six degrees of freedom. In the *body* block for the vehicle mainframe, the mass and inertia of the mainframe are defined, along with CSs at the centre of mass, the areodynamic centre of pressure, the intersection of the steer and twist axes, the seat, and the attachment points of the swingarm and rear suspension. Parameters are given in Appendix C.2

[1]Twist is a rotation of the steering system about an axis perpendicular to the steer axis, which results in a lateral deflection of the front wheel.

Rider

The rider upper body is connected to a CS at the location of the seat, with a joint that allows the upper body to lean from side to side. The angle of inclination of the rider's body about the rider's y-axis is also specified. A lean torque can be applied between the rider and the mainframe. A rotational spring and damper represents the rider's efforts to remain upright in the seat.

Steering and Front Wheel

A *body* representing the handlebars is connected to the frame with a joint at the centre of the headtube. It allows steer and twist degrees of freedom at specified angles to the vertical; they are perpendicular to each other, as shown by dashed lines in Figure 3.13. Each of the axes have associated spring and damping parameters, and a steering torque can be applied to the handlebars about the steer axis, with an associated reaction on the frame. Twist has a small effect on handling and stability: lateral flexibility between the mainframe and the front tyre contact patch reduces the damping of the weave mode at high speed, though the high stiffness of contemporary motorcycles means that the sensitivity is low [62].

The handlebar *body* is connected, through a *prismatic* joint with a linear suspension model, to a *body* representing the unsupended forks. A CS is specified at the centre of the front axle, where the front wheel *body* is attached to the forks with a *revolute* joint. Front wheel drive torque is applied to the wheel and has a reaction on lower forks.

Swingarm and Rear Wheel

At the rear, the swing arm is connected to the main frame with a *revolute* joint, and a linear spring–damper suspension acts between two specified CSs on the frame and swing arm. A further CS is specified for the centre of the rear axle, where, finally, the rear wheel is connected with another *revolute* joint. A drive torque is applied about its axis, with an associated reaction on the mainframe.

Suspension

The motorcycle has front and rear suspension, both of which have linear springs and dampers. The front suspension is of the telescopic type, which acts along the line of the front forks and can be described using the SimMechanics joint spring–damper.

The rear suspension has a linear spring and damper acting between specified points on the mainframe and rear swingarm: this results in non-linear rear suspension characteristics. Using the same technique as [76], the following equation is used to

find the suspension forces applied at the two CSs,

$$\pm \boldsymbol{F} = \frac{\boldsymbol{s}}{\|\boldsymbol{s}\|}\left[F_{\text{preload}} - \left(\|\boldsymbol{s}\| - s_{\text{nominal}}\right)K - \left(\frac{\boldsymbol{s}}{\|\boldsymbol{s}\|}\boldsymbol{v}\right)C\right], \tag{3.44}$$

where $\boldsymbol{s} = \boldsymbol{s}_1 - \boldsymbol{s}_2$ is the distance between the two coordinate systems and $\boldsymbol{v} = \boldsymbol{v}_1 - \boldsymbol{v}_2$, the relative velocity, when the global CS is used. s_{nominal} is the distance between the two points in the initial configuration. K and C are the spring and damping coefficients, respectively. ($\|\boldsymbol{s}\| = \sqrt{s_X^2 + s_Y^2 + s_Z^2}$, and thus $\frac{\boldsymbol{s}}{\|\boldsymbol{s}\|}$ represents a unit vector in the direction between the two connected points.)

Aerodynamics

Aerodynamic lift and drag forces for the combined motorcycle and rider are calculated for the current vehicle speed, v_{xv}, and applied at a point specified on the motorcycle mainframe corresponding to the Centre of Pressure (CoP). The forces are then transformed from the *vehicle intermediate* CS to the *global* CS using the rotation matrix, $\mathbf{R}$, of the mainframe,

$$\boldsymbol{F}_{\text{aero}\,xyzv} = \begin{bmatrix} -0.5\rho_{\text{air}}C_{\text{drag}}v_{xv}^2 \\ 0 \\ 0.5\rho_{\text{air}}C_{\text{lift}}v_{xv}^2 \end{bmatrix} \tag{3.45}$$

$$\boldsymbol{F}_{\text{aero}\,XYZ} = \mathbf{R}_v\boldsymbol{F}_{\text{aero}\,xyzv}. \tag{3.46}$$

The rotation matrix is described in Appendix A.

Motorcycle Multibody Model Summary

Further parameters and initial conditions are specified by the user. Steer torque, lean torque and drive torques can be specified or controlled during simulation, depending on the required manoeuvre. SimMechanics can display an animation of the simulation, and data from the bodies and tyre models can be logged for post-processing.

3.4.5 Motorcycle Modelling Summary

This section has described how a motorcycle can be modelled for dynamic analysis. Models of increasing complexity were introduced to capture necessary characteristics of the system. The models described were:

- the geometric description of a motorcycle cornering with camber;
- a steady-state model developed from the *bicycle model* for automobiles;

- a mathematical dynamic model with four degrees of freedom, viz., lateral and rotational velocities, and lean and steer angles;
- a multibody model suitable for torque vectoring investigations.

Developing the models in this way allows the models to be verified with each other and the results they predict used with confidence. The resulting multibody model can be used for a wide range of dynamical studies and can easily be modified for other motorcycles, and even bicycles.

3.5 Wheel Model

This section concerns the calculation and application of the forces and moments to the wheel *body*, given the position and velocity of its centre of mass. The wheel model contains parameters for the size and shape of the wheel, and thus, the kinematics of the contact patch can be determined, which are required for the tyre model. The wheel model is identical in both the motorcycle and automobile models but the tyre model, and other parameters, do change.

In the SimMechanics multibody models, for each wheel, a *body* is defined that is allowed to rotate about its y-axis, the location and orientation of which is determined by its connection to the model. The mass is acted upon by the drive torque and by the tyre forces and moments. The various tyre models themselves are considered in Section 3.6, while this section describes the calculation of the variables required by the tyre model, and the application of the forces and moments to the body.

3.5.1 Undeformed Wheel Radius Accounting for Camber

The position of the centre of the contact path varies more with camber for motorcycle tyres than for automobile tyres, as shown in Figure 3.14. To maintain similarity between the models, this is dealt with by setting the tyre toroidal radius, r_t, to zero for the automobile wheel model; thus, the magnitude of the wheel radius does not change with camber but the rest of the equations in this section can still be used.

The motorcycle tyre model includes the effect of contact patch migration as the wheel cambers, and the influence it has on wheel radius—a characteristic that was not captured by the original SimMechanics model [76] and which was thought to be important to this investigation.

To allow the vertical deflection of the cambered wheel to be calculated, the radius of the undeformed, yet cambered, wheel is required, as shown in Figure 3.15. The position of the undeformed tyre surface at the point where it is tangent to the horizontal plane, is calculated from the camber angle and tyre dimensions in the *tyre*

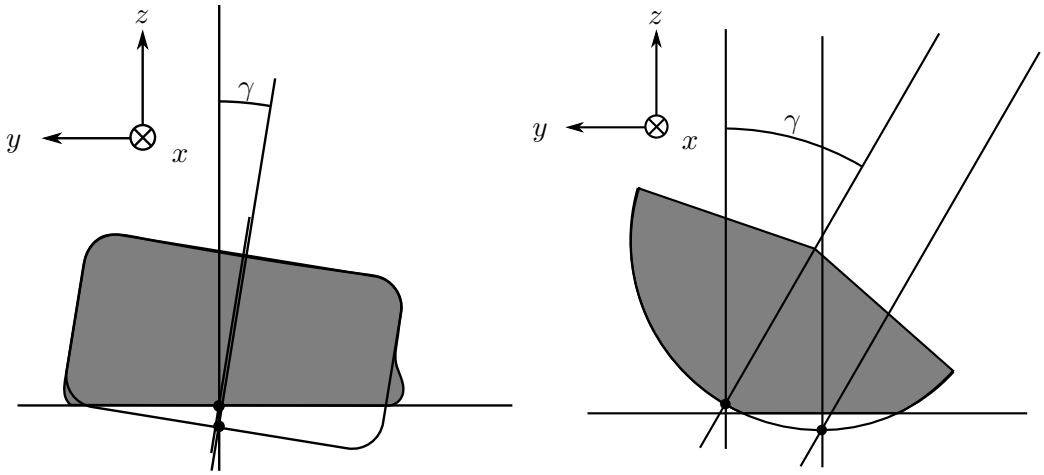

(a) Car tyre **(b)** Motorcycle tyre

Figure 3.14: Location of centre of contact patch with camber

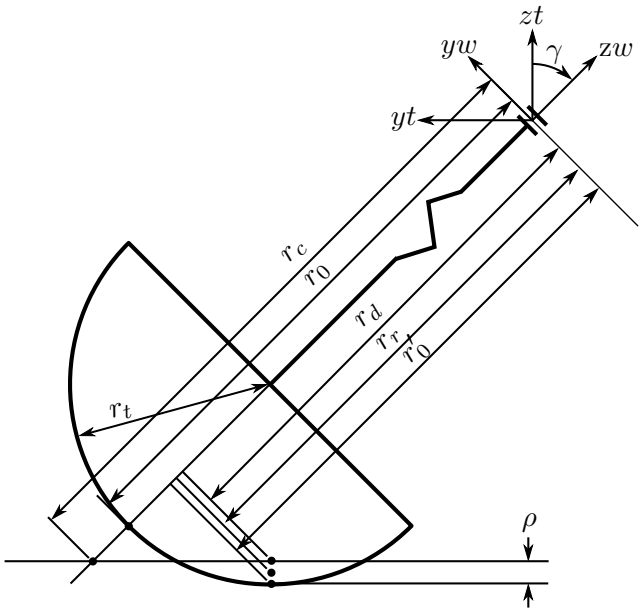

Figure 3.15: The various radii of a cambered motorcycle wheel

CS as follows,

$$\boldsymbol{r}'_{0,xyzt} = \begin{bmatrix} 0 \\ (r_0 - r_t)\sin\gamma \\ -\left((r_0 - r_t)\cos\gamma + r_t\right) \end{bmatrix}, \tag{3.47}$$

where r_0 is the undeformed radius of the wheel when vertical, and r_t is the radius of the tyre toroid. Since the position of the wheel centre is known in the *global* CS, the radius vector must be transformed from a *wheel* CS to the *global* CS using a rotation matrix, $\mathbf{R}_{\psi t}$, which represents an anticlockwise rotation about the global Z-axis equal to the yaw angle, ψ, of the tyre (see Appendix A). The displacement vectors representing the wheel centre location, $\boldsymbol{s}$, and the undeformed cambered radius, $\boldsymbol{r}'_0$, can then be simply added together to find the position of the undeformed wheel in the *global* CS,

$$\boldsymbol{r}'_{0,XYZ} = \mathbf{R}_{\psi t}\boldsymbol{r}'_{0,xyzt} \tag{3.48}$$

$$\boldsymbol{s}'_{0,XYZ} = \boldsymbol{s}_{\text{wheel centre},XYZ} + \boldsymbol{r}'_{0,XYZ}. \tag{3.49}$$

Normally, this point will be below the road surface.

3.5.2 Deformed Wheel Radius

The location of the undeformed tyre described above will be directly below the centre of the contact patch at the road surface. The vertical deflection of the tyre, ρ_z, required for the tyre model, is therefore the Z-component of the position vector of the undeformed tyre, $\boldsymbol{s}'_0$, which will be negative in normal situations. The location of the centre of the contact patch, s_{CP}, is found by replacing the Z-component with zero.

The positions of the wheel centre and contact patch (on the ground) are now known in the *global* CS, and, thus, the distance between them can be calculated. To transform the distance vector into the *tyre* CS, the inverse of $\mathbf{R}_{\psi t}$ is used

$$\boldsymbol{r}_{d,XYZ} = \boldsymbol{s}_{\text{wheel centre},XYZ} - \boldsymbol{s}_{CP,XYZ} \tag{3.50}$$

$$\boldsymbol{r}_{d,xyzt} = \text{inv}\left(\mathbf{R}_{\psi t}\right)\boldsymbol{r}_{d,XYZ}. \tag{3.51}$$

3.5.3 Wheel Rolling Radius

The linear speed of rolling of the tyre is calculated using $v = r\omega$ and, thus, the radius is of critical importance. A definition of rolling radius is chosen such that in free-rolling conditions, the wheel maintains a constant speed without the application

of an external torque. Its value will change with vertical load and camber angle, but not with longitudinal slip.

Its value must be between the wheels undeformed and deformed radii ($r'_{0,zw}$ and $r_{d,zw}$ in Figure 3.13, between which the difference is $\rho\cos(\gamma)$). It is smaller than the undeformed radius because compression of the tyre circumference has taken place, but it is larger than the deformed radius because the tyre is more stiff circumferentially than it is radially. As the deformed radius reduces with vertical load, the rolling radius also reduces but at a slower rate.

In the model, using a value from [40], the rolling radius is modelled as being $0.33\rho_z$ below the surface of the road, where ρ_z is the vertical distance between the undeformed radius, $\boldsymbol{r}'_0$, and deformed radius, $\boldsymbol{r}_d$, at that instant.

3.5.4 Effective Wheel Radius

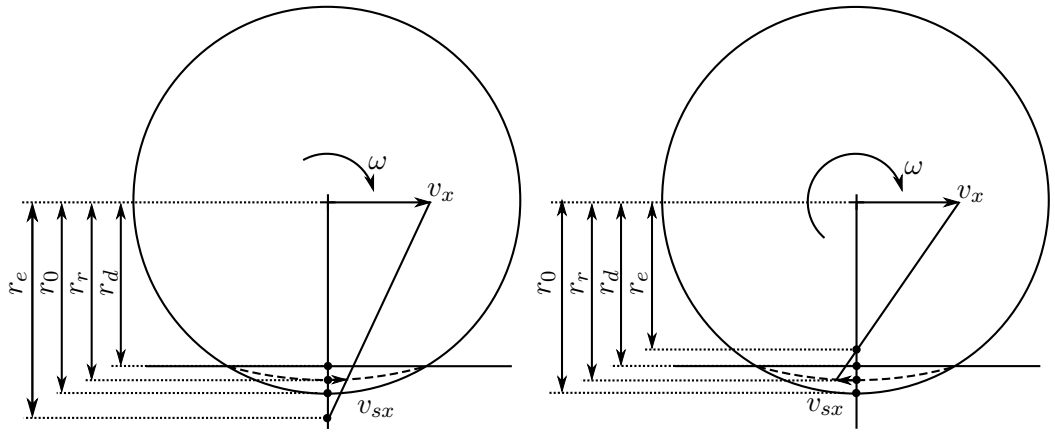

(a) During braking **(b)** During acceleration

Figure 3.16: Effective wheel radius variation

The effective wheel radius is the (imaginary) point at which the tyre velocity is zero: it is the point about which the tyre appears to rotate at that instant to an observer whose position is fixed in space.

In the case of zero longitudinal slip, the effective radius is equal to the rolling radius, but when slip is present, the effective wheel radius will move up or down (for accelerating and braking, respectively) as shown in Figure 3.16. This definition means that no force is generated when the wheel is in free-rolling. An alternative definition (with an associated shift in the longitudinal slip vs. force graph) would need a small negative slip speed, and therefore positive tyre force, to maintain a constant speed. The presence of rolling resistance is separate from this effect and will still act to slow the vehicle.

The effective wheel radius can be calculated using

$$r_e = \frac{v_{xt}}{\omega_{yw}}, \tag{3.52}$$

where v_{xt} is the longitudinal velocity of the tyre and ω_{yw} is the angular velocity about the local yw-axis. Note: this definition differs from some other texts where the effective wheel radius is defined only at zero slip.

3.5.5 Calculation of the Tyre Forces and Moments

The tyre forces and moments generated at the contact patch in the *tyre* CS can be calculated using values of longitudinal slip, κ, lateral slip, $\alpha^\star$, camber angle, γ, and the vertical deflection, ρ, along with parameters that specify the tyre characteristics taken from [40] or [46] for the motorcycle and automobile, respectively. Calculation takes place in a Simulink subsystem with parameters for the tyres specified in MATLAB. For more details about the tyre models see Section 3.6.

3.5.6 Application of the Tyre Forces and Moments

The tyre models calculate forces and moments to be applied at the contact patch; however, in SimMechanics, forces and moments have to be applied at a CS attached to, and moving with, a body. No suitable CS exists at the contact patch location; therefore, the forces and moments are first transposed to the wheel centre and then rotated into the *global* CS before application to the body.

Shifting the application point of the tyre forces to the wheel centre means an additional moment, caused by the tyre forces acting at a distance, must be applied. This is calculated using the cross product of the forces and the translation, using the deformed radius, $\boldsymbol{r}_d$, calculated in Section 3.5.2,

$$\boldsymbol{M}'_{xyzt} = \boldsymbol{M}_{xyzt} + \left(\boldsymbol{r}_{d,xyzt} \times \boldsymbol{F}_{xyzt}\right). \tag{3.53}$$

Both the forces and moments are applied in the *global* CS. To achieve this, the rotation matrix is used again

$$\boldsymbol{F}_{XYZ} = \mathbf{R}_{\psi t}\boldsymbol{F}_{xyzt} \tag{3.54}$$

$$\boldsymbol{M}_{XYZ} = \mathbf{R}_{\psi t}\boldsymbol{M}'_{xyzt}. \tag{3.55}$$

3.5.7 Wheel Modelling Summary

This section has described how the forces and moments generated at the tyre–road contact patch can be calculated and applied, given the position and velocity of the

wheel centre of mass and details of the wheel's geometry. The same model is used for both motorcycles and automobiles; only the parameters and tyre models change. Details of the tyre models themselves are given in the next section.

3.6 Tyre Models

In the case of vehicle dynamics simulation, it is not practical to calculate tyre forces from first principles, i.e., by using the friction coefficient of the tyre–road interaction and knowledge of the tyre's deflection; nor is it practical to use finite element models, which are computationally too expensive for use in simulations. Thus, *semi-empirical* models are used, which fit experimental data to mathematical approximations in order to give a realistic representation of the tyre.

Tyre models for both two- and four-wheeled vehicles will be described in this section because, while their characteristics can be very different, the modelling approach is similar.

3.6.1 Calculation of Slip Input Quantities

The longitudinal and lateral slip velocities, $v_{\text{slip},xt}$ and $v_{\text{slip},yt}$ respectively, parallel to the road plane and in the *tyre* CS, are made non-dimensional using the longitudinal velocity v_{xt} of the wheel centre. The lateral slip velocity is the equal to the lateral velocity of the contact patch, $v_{\text{slip},yt} = v_{yt}$. The slip ratios are calculated using the equations

$$\kappa = -\frac{v_{\text{slip},xt}}{v_{xt}} \tag{3.56}$$

$$\alpha^\star = \frac{v_{yt}}{v_{xt}}, \tag{3.57}$$

where κ is the longitudinal slip ratio and $\alpha^\star$ is the lateral slip ratio. The * differentiates the value from the commonly used slip angle, $\alpha = \tan(\alpha^\star)$, though at small angles the difference is negligible.

To find the required values in SimMechanics, the velocity of the wheel centre is transformed from the *global* CS into the yaw-rotated *tyre* CS with the use of a rotation matrix, as described in Appendix A. SimMechanics can give local velocities in the directions of the priciple axes of the body, but since the body is rotating, the directions of the axes are also rotating, meaning that the *local* velocities of the body are not in the same CS as the *tyre* CS. The longitudinal slip velocity is calculated

using,

$$\begin{aligned} v_{\text{slip},xt} &= v_{xt} - v_r \\ &= v_{xt} - \omega r_{r,zw}, \end{aligned} \tag{3.58}$$

in which v_r is the rolling velocity and $r_{r,zw}$ is the rolling radius in the *wheel* CS, defined in Section 3.5.3 and shown in Figure 3.15. The angular velocity, ω, is taken about the wheel's local yw-axis (in the *wheel* CS).

The camber angle, γ, is the angle of inclination of the wheels plane of symmetry, which can be obtained from the rotation matrix of the wheel body, as described in Appendix A.

Having obtained a value for the vertical deflection of the tyre, ρ_z, as described in Section 3.5.2, along with the longitudinal and lateral slip ratios, κ and $\alpha^\star$, and the camber angle, γ, the situation is fully defined for the tyre models to estimate the resulting tyre forces and moments.

3.6.2 Car Tyres

Linear Model

When the magnitude of the wheel slip is small, the tyre forces generated by the wheel are roughly proportional to the slip:

$$F_x = K_x \kappa \tag{3.59}$$

$$F_y = -K_y \alpha, \tag{3.60}$$

where K_x and K_y are the longitudinal and lateral stiffnesses of the tyre, which can be calculated from experimental data. For further information, see the *brush model* [46]. The linear tyre model will be used for verification purposes, and is useful for checking that simulation models will compile and run.

As the slip magnitude increases, there is more relative motion between the tread material and the road surface. Heat is generated in the contact patch, and the response of the tyre force to the slip becomes non-linear; thus, the above equations are no longer valid. Since ATD needs to be investigated in high-speed situations close to the limit of friction, a tyre model that is valid for larger slip magnitudes is required.

Simple *Magic Formula* Model

Prof. Pacejka, along with others at TU-Delft, developed the *Magic Formula* tyre model [46] to address the large deviations observed in experimental results from

analytical models such as the *brush model*. The semi-empirical model is a set of equations that relate tyre load, lateral and longitudinal slips, and camber angle to lateral and longitudinal forces. Many versions, differing in complexity and range of validity, are widely used in computer simulations.

The general form of the equations for lateral and longitudinal tyre force are

$$F_x = D_x \sin(C_x \arctan[B_x\kappa - E_x(B_x\kappa - \arctan[B_x\kappa])]) \tag{3.61}$$

$$F_y = D_y \sin(C_y \arctan[B_y\alpha - E_y(B_y\alpha - \arctan[B_y\alpha])]), \tag{3.62}$$

where the model parameters have the following nomenclature:

B stiffness factor

C shape factor

D peak value

E curvature factor

in which D varies with vertical load. For simplicity, to keep the number of parameters to a minimum, the variation is assumed to be proportional: $D = F_z D'$. In this work, the sign conventions used by Pacejka [46] have been updated to match ISO8855 [27].

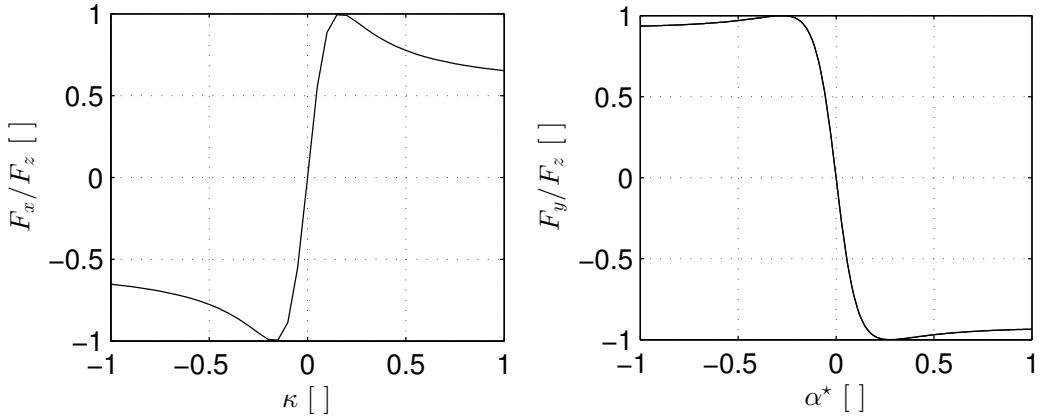

(a) Longitudinal **(b)** Lateral

Figure 3.17: Simple *Magic Formula* tyre model characteristics

The resulting plots of tyre force are shown in Figure 3.17, which show that tyre force peaks and subsequently falls away with increasing slip.

The above equations are designed for use when slip is principally in one direction only, either lateral or longitudinal. Using the above equations in situations of combined slip can give a resultant force very much greater than the magnitude of the vertical load. In an attempt to increase the range of validity of the model to include

these situations, the concept of the *friction circle* is introduced. If the resultant force is greater than the magnitude of the vertical load, then lateral and longitudinal forces are scaled to be within the maximum, as shown in the MATLAB code in Appendix B.3. This changes the tyre forces as shown in Figure 3.18.

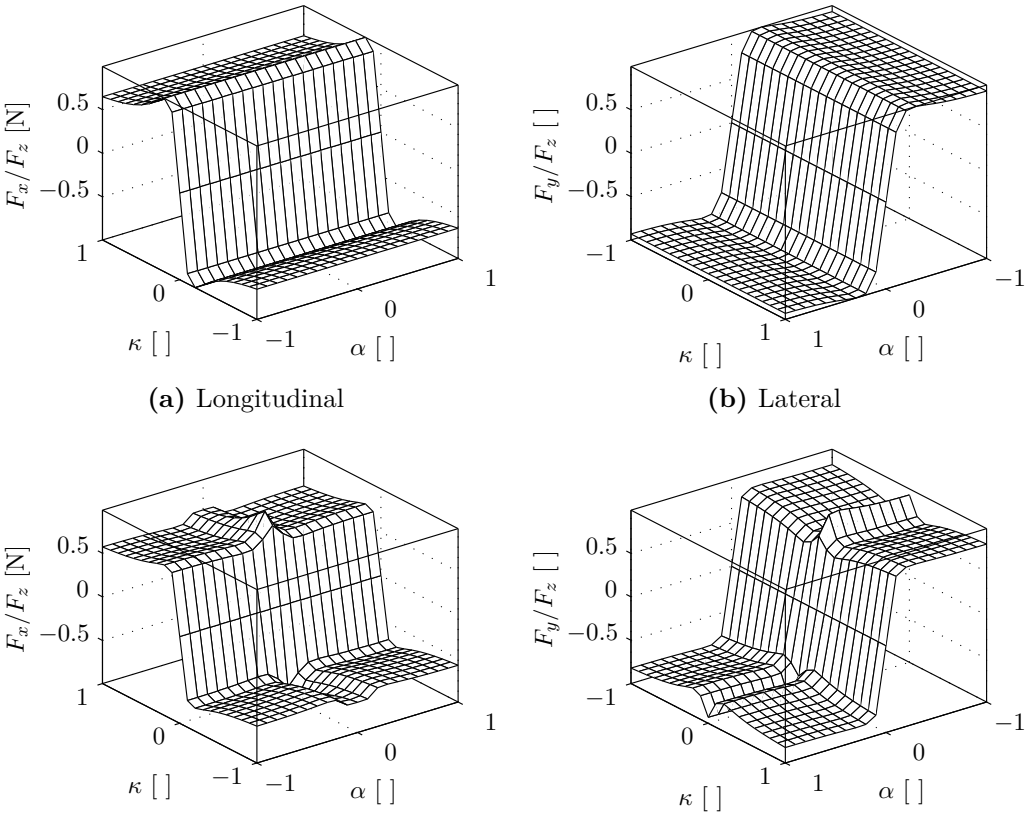

(a) Longitudinal

(b) Lateral

(c) Longitudinal (with friction circle)

(d) Lateral (with friction circle)

Figure 3.18: Simple *Magic Formula* in combined slip conditi

Despite the friction circle, this eight-parameter model is limited for use with the multibody vehicle model, where camber angles are not necessarily zero, and where moments generated by the tyres are important. Also, horizontal forces cannot be assumed to vary linearly with vertical load. For a tyre model that gives more realistic predictions, the complete set of *Magic Formula* equations is required.

Complete *Magic Formula* Model

The full set of *Magic Formula* equations [46] is coded in Simulink, allowing a more complete model of the tyre to be used in simulation. A more realistic vertical load model is used, with subsequent effect on the generation of horizontal forces. The model also includes the effect of camber, and calculates moments in the three principle directions of the tyre, viz., aligning moment, rolling resistance and the overturning

couple. Moments are generated about the origin at the centre of the contact patch because the force resulting from the pressure distribution over the contact patch is offset.

Figure 3.19 shows plots generated with the full *Magic Formula* tyre model and demonstrate its complexity. Figure 3.19b shows that lateral force is affected by the camber angle: a positive camber angle means that a negative lateral force is generated at low lateral slip ratios. Figures 3.19c and 3.19d show how the lateral and longitudinal tyre forces vary under combined slip situations. Figures 3.19e and 3.19f show the effect of vertical load on lateral and longitudinal forces for a range of slip magnitudes. The area enclosed by the lines in Figure 3.19g is the friction circle for the simulated tyre: the maximum magnitude of tyre force that can be produced. Finally, Figure 3.19h shows the effect of lateral slip ratio on aligning moment.

Fitting Tyre Model Parameters

To maintain comparability between the different car tyre models, the parameters need to be chosen such that the models give similar results for the same specified inputs. For this the simple *Magic Formula* and linear tyre models were fitted to the more complex *Magic Formula* model. The result is shown in Figure 3.20 for a vertical load of 3000 N, and the fitted parameters are given in Tables 3.1 and 3.2.

Table 3.1: Fitted parameter values for the simple *Magic Formula* tyre model

Parameter	Value
B_x	4.7
C_x	2.6
D_x	1.0
E_x	0.99
B_y	4.5
C_y	2.2
D_y	1.0
E_y	1.04

3.6.3 Motorcycle Tyres

Motorcycle tyres generate lateral forces in a different way from car tyres, in that the cambering of the wheel causes forces to be generated geometrically, i.e., slip is

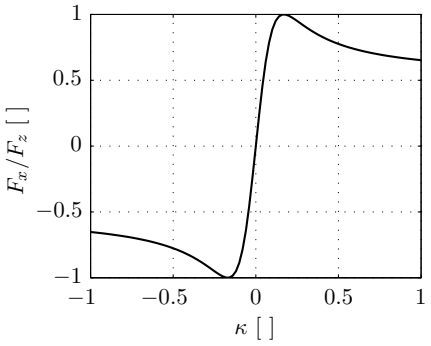

(a) Longitudinal

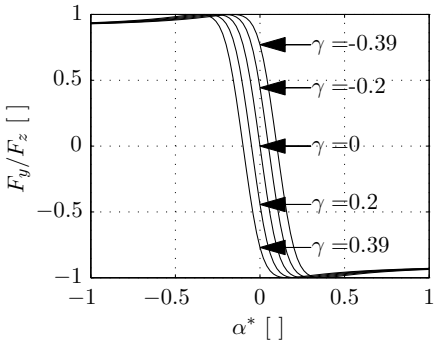

(b) Lateral, for various camber angles

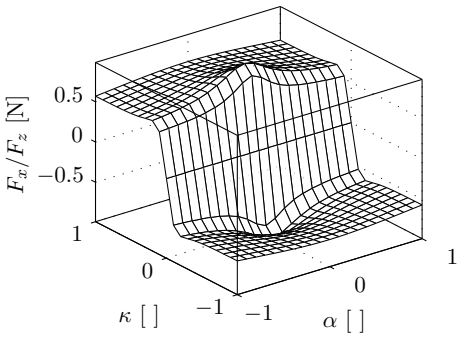

(c) Longitudinal, combined slip

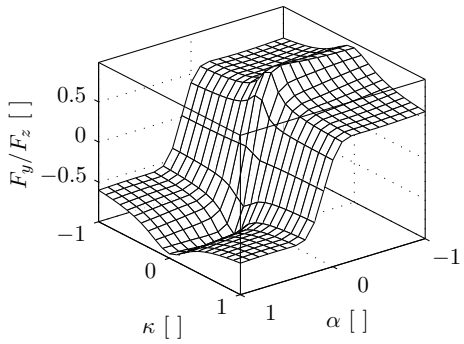

(d) Lateral, combined slip

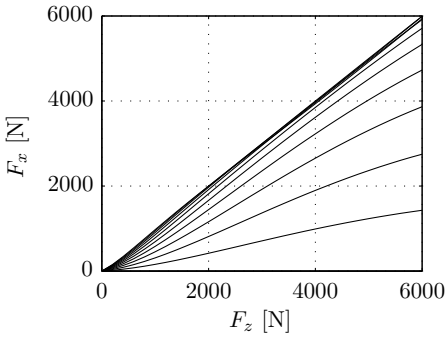

(e) F_x load dependence, $\kappa = 0 : 0.02 : 0.2$

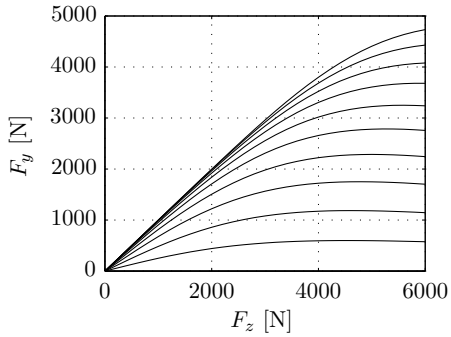

(f) F_y load dependence, $\alpha^\star = |0 : 0.02 : 0.2|$

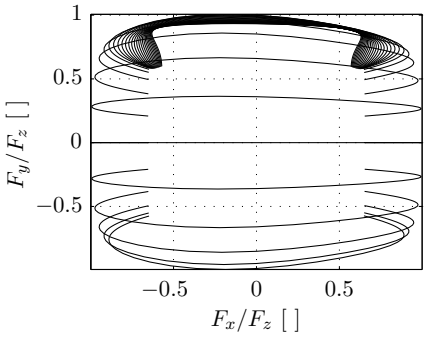

(g) The friction circle, $\alpha^\star = -1 : 0.04 : 0.20$

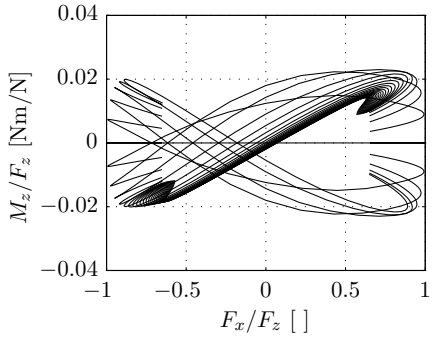

(h) Aligning moments, $\alpha^\star = -1 : 0.04 : 0.20$

Figure 3.19: Complete *Magic Formula* tyre model plots

Table 3.2: Fitted parameter values for the linear tyre model

Parameter	Value
K_x	12.22 N
K_y	9.9 N

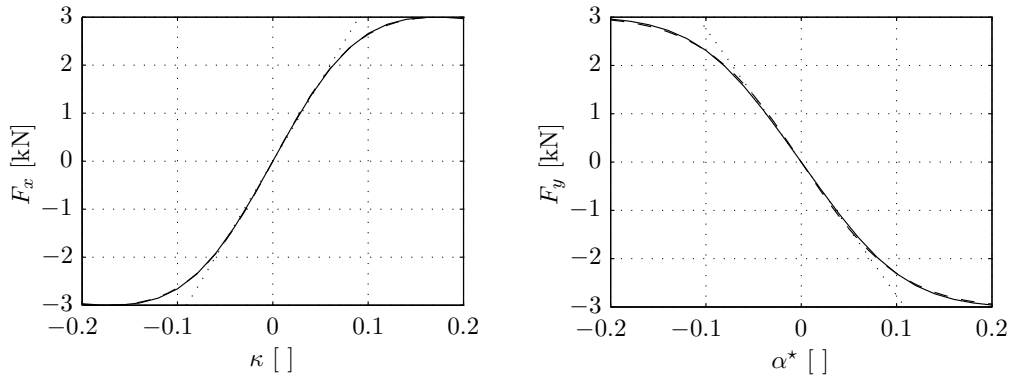

(a) Longitudinal **(b)** Lateral

Figure 3.20: Tyre model fitting. · · · ·linear model; – – –simple *Magic Formula* model; ——full *Magic Formula* model.

not required. Lateral and longitudinal slip are, in general, still present and must be taken into account. Two motorcycle tyre models have been used and are commented upon here.

The *Magic Formula* Model

The *Magic Formula* was extended to model motorcycle tyres by Pacejka [46]; however, parameter values are not widely available. A paper by Sharp *et al.* [65] presents various improvements on the Autosim model in [66], and includes the fitting of parameters to the *Magic formula*. Parameter values are presented for two different rear wheels, and one front wheel, including the effect of combined slip. The tyre models were coded in Simulink, and have a complexity between the simple and full versions of the *Magic Formula* for car tyres. Plots of the calculated tyre forces are shown in Figure 3.21.

The Meijaard–Popov Model

A tyre model created by Meijaard and Popov [40] is used for the calculation of lateral, longitudinal and vertical forces, along with the aligning moments. The inputs from the vehicle model are similar to those of the *Magic Formula* models. The model

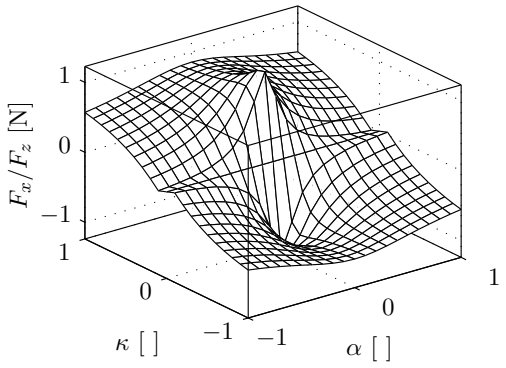

(a) Longitudinal force

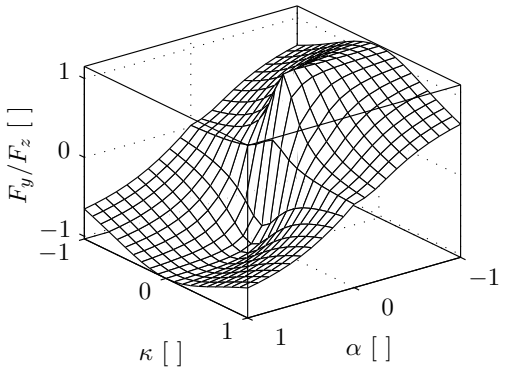

(b) Lateral force

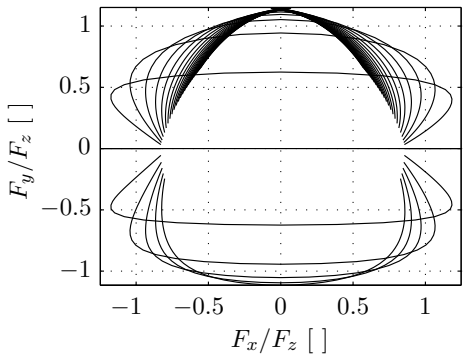

(c) Friction circle $\alpha^\star = -1 : 0.04 : 0.20$

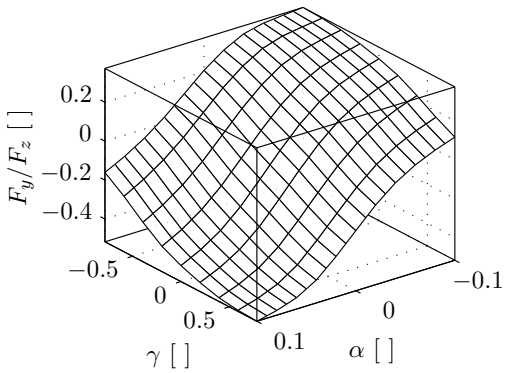

(d) Camber thrust

Figure 3.21: Magic formula motorcycle tyre model plots

assumes a toroidal tyre, and forces and moments are calculated at a point at the centre of the contact patch. The influence of tyre relaxation length is also included to allow transient manoeuvres to be analysed. Because the point of application is at the centre of the contact patch, which moves laterally with camber, the overturning moment is accounted for.

The Meijaard–Popov model was chosen for the investigations into torque vectoring because it requires fewer parameters and allows faster simulation, while still allowing for large camber angles, and calculation of aligning moments.

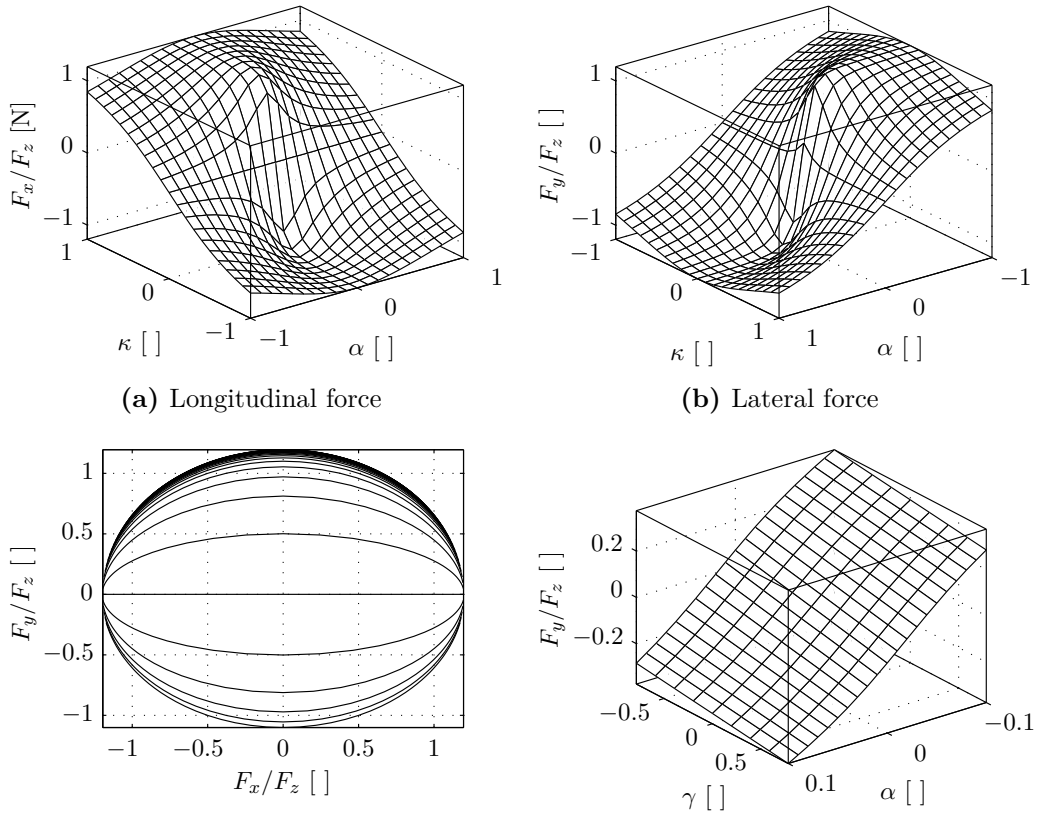

(a) Longitudinal force

(b) Lateral force

(c) Friction circle $\alpha^\star = -1 : 0.04 : 0.20$

(d) Camber thrust

Figure 3.22: Meijaard–Popov motorcycle tyre model plots

Figure 3.22 shows plots of the lateral and longitudinal tyre forces generated in conditions of combined lateral and longitudinal slip, as calculated with the tyre model. It is clear that when the tyre is generating large forces in one direction, its ability to generate them in the other is diminished. Figure 3.22c shows the friction circle for the Meijaard–Popov motorcycle tyre model, and Figure 3.22d shows how lateral slip and camber angle combine to generate lateral force.

3.6.4 Tyre Modelling Summary

This section has described various tyre models that can be used with the vehicle models described in Sections 3.3 and 3.4. They range from simple linear models suitable for basic simulations where vertical load does not change, to complex models suitable for conditions of combined slip and large camber angles. The tyre models are interchangeable in the wheel model described in Section 3.5, depending on the simulation.

3.7 Simple Controllers and Driver Models

To allow comparisons to be made between vehicles with different torque distribution strategies, the vehicles must be capable of completing the same manoeuvre at the same speed; for example, when comparing the power consumption of various vehicles negotiating the same constant radius corner. This requires a driver model, with inputs including speed and positional feedback, that controls steering and drive torque inputs to the vehicle model. As mentioned at the start of the chapter, the addition of a driver model that monitors the states of the vehicle and adjusts the inputs can closes the feedback loop, as shown diagrammatically in Figure 3.1.

3.7.1 Speed Control

In the cases of both the motorcycle and automobile models, the speed controller works in the same way: the total amount of drive torque to be delivered to the wheels is controlled. There are two options open to the user: firstly, specifying the amount of torque directly, regardless of the vehicle's motion. This method can be used to determine maximum tractive performance in conditions of limited friction.

Secondly, controlling the amount of torque to bring the vehicle's speed to a target speed for comparative purposes. The total amount of drive torque is determined using Proportional–Integral (PI) control of the vehicle speed relative to a reference speed, v_{ref}, with the following equations and equivalent Simulink blocks:

$$e_{\text{speed}} = v_{\text{ref}} - v_v \tag{3.63}$$

$$\tau_{\text{drive}} = G_p e_{\text{speed}} + G_i \int_0^t e_{\text{speed}} \, \mathrm{d}t \tag{3.64}$$

where v_v is the resultant vehicle velocity, τ is drive torque, G_p and G_i are the proportional and integral gains, set by hand for the car and motorcycle models. The resultant vehicle velocity is used so that vehicles can follow the same path with different amounts of sideslip, but still travel at the same resultant velocity. Suitable gains for steady speed simulations are given in Table 3.3.

Table 3.3: Speed controller gains

Parameter	Value
G_i	1000
G_p	200

PI control is used for its simplicity—a good result can be achieved by tuning only two parameters—and because, after a small amount of trial-and-error, the error in the vehicle speed quickly drops to zero.

3.7.2 Driveline Control

The total amount of drive torque is split between the wheels according to ratios specified by the user before simulation. For automobiles, the equations governing the amount of torque, τ, received by the front-left, front-right, back-left and back-right wheels are

$$\tau_{fl} = T_f T_l \tau_{\text{drive}} \tag{3.65}$$

$$\tau_{fr} = T_f \left(1 - T_l\right) \tau_{\text{drive}} \tag{3.66}$$

$$\tau_{bl} = \Big(1 - T_f\Big) T_l \tau_{\text{drive}} \tag{3.67}$$

$$\tau_{br} = \Big(1 - T_f\Big) \left(1 - T_l\right) \tau_{\text{drive}}, \tag{3.68}$$

where T_f and T_l are ratios that specify the proportion of torque to go to the front and left wheels respectively. For any value of T_f and T_l, the sum of all the wheel torques is equal to the total drive torque, τ_{drive}. For motorcycles, the equations are similar but for only two wheels; in this case, only the front–rear ratio is required.

The above equations can be used to describe any ideal driveline layout with open diferential(s) or distributed drive; for example, four-wheeled vehicles that are Front Wheel Drive (FWD), Four Wheel Drive (4WD) and Rear Wheel Drive (RWD) are specified with T_f equal to 1, 0.5, and 0, respectively and $T_l = 0.5$ in each case. By varying T_f and T_l, the influence of ATD can then be investigated.

The torque distribution ratios are usually specified between 0 and 1; however, there are special cases where the values can be greater than 1, or less than zero. These include when braking one or more wheels is considered through the use of a value less than zero, in which case, a regenerative motor or overdriven differential could be used to supply extra power to another. Similarly, a theoretical through-the-road hybrid (see Section 2.2.3) could be specified by using $T_f > 1$, with the rear wheels having a negative, regenerative torque.

An ideal driveline model was used to avoid the physical limitations of ATD systems currently available and focus on the potential impact that the systems could have. As part of preliminary research, an engine–gearbox–differential model was created for a four-wheeled vehicle to investigate the effect of this on the vehicle handling and efficiency. SimDriveline was used, which is a modelling environment specifically for one-dimensional rotating systems and is similar to, and can interface with, SimMechanics; however, simulations were slow and the results of the ATD investigation were obscured by the added complexity. For this reason, an ideal driveline system was used for the rest of the research.

3.7.3 Steer Control

The way in which drivers control the steering systems of motorcycles and automobiles differs, calling for different steering controllers for the models.

Automobile Steer Control

Automobiles are generally directionally controlled by specifying the steering wheel angle [2, 18]; the torque feedback through the steering system to the driver will have an impact on the driving experience, but is not essential for control of the vehicle. Thus, the automobile model is controlled by a driver model that specifies the steer angle.

There are various options available for calculating the required the steer angle. Open loop methods include setting a value for the entire simulation, or a sinusoidal or step input can be programmed to occur at a given time. Closed loop methods incorporating feedback include minimising the heading angle error or yaw rate error using PI control. The former is calculated using the equation

$$e_\theta = \left(\frac{1}{R_{\text{ref}}} \int_0^t |\boldsymbol{v}_v| \, \mathrm{d}t \right) - \theta, \tag{3.69}$$

where θ is the heading angle, which is calculated as the sum of the yaw angle, ψ, and sideslip angle of the vehicle, β. The heading angle, which is the direction of the velocity vector, is used so that vehicles can travel with different amounts of sideslip along the same path. R_{ref} is the reference cornering radius, which can be infinity for a straight line. The first term on the right-hand side is the target heading angle of the vehicle at time t; when $R_{\text{ref}} = \infty$, the term equals zero. Minimising the heading angle error will result in a vehicle that follows a defined circular, or straight, path. The steer angle is calculated using PI control with an equation of the same form as Equation (3.64).

The yaw rate error, $e_{\dot{\psi}}$, is calculated using

$$e_{\dot{\psi}} = \frac{|\boldsymbol{v}_v|}{R_{\text{ref}}} - \dot{\psi}_v, \tag{3.70}$$

where the symbols have the same meaning as above, and a straight line is achieved by setting $R_{\text{ref}} = \infty$. This method of control is simpler than heading angle control as it does not involve an integral. Minimising the yaw rate error, again using Equation (3.64), results in vehicles that are cornering at the correct yaw rate, but are not necessarily cornering on the same path. In a steady state, the rate of change of yaw angle and heading angle are the same. Suitable controller gains are given in Table 3.4.

Table 3.4: Automobile steer controller gains

Parameter	Value
G_i	10
G_p	10

Motorcycle Steer Control

Contrary to the driver of an automobile, the rider of a motorcycle controls its directional response with a mixture of steering torque and lean torque inputs [33]. The angle of the handlebars relative to the frame is of less importance to the rider than the sense of the torque reaction. Steer torque is applied through the rider's hands and arms to the handlebars, and has a reaction through the rider's seat on the mainframe. This causes the handlebars, forks and front-wheel to rotate relative to the frame. The direction of the applied torque is opposite to the direction in which the
which turns the motorcycle. The rider can also apply a lean torque to the mainframe by modifying the force applied to the footpegs, seat and handlebars.

Various motorcycle models in the literature are controlled by just one and, in some cases, both of the inputs. In this model, the rider is assumed to try to stay in the plane of symmetry of the motorcycle mainframe: a rotational spring–damper acting about the longitudinal axis at the location of the seat is used to model the rider's effort.

The steering torque is controlled, again using the PI technique, so that the vehicle obtains its target yaw rate. The error is calculated as in Equation (3.70), but the

steer torque τ_{steer}, in this case is determined by

$$\tau_{\text{steer}} = -\left(G_p e_{\dot{\psi}} + G_i \int_0^t e_{\dot{\psi}} \, \mathrm{d}t\right). \tag{3.71}$$

Tuning of the gains is slightly harder because of the motorcycle's tendency to capsize with large steer inputs; however, suitable parameters are shown in Table 3.5.

Table 3.5: Motorcycle steer controller gains

Parameter	Value
G_i	20
G_p	2

3.8 Chapter Summary

This chapter has covered the evolution of the vehicle models, including the wheel and tyre models, and the simple driver models used to control them. Firstly, mathematical models of a motorcycle and automobile were created, which are suitable for simple handling investigations. Then, models of a motorcycle and vehicle were created in SimMechanics, a multibody modelling environment.

The automobile model has 14 degrees of freedom, and the drive torques of the wheels can be actuated indivudially to simulate torque vectoring. The vehicle can pitch and roll with the accelerations of the vehicle, and simple suspension models are included at the connections between the wheels and the vehicle. The effects of aerodynamic lift and drag acts on a point specified at the centre of pressure.

The motorcycle model has 13 degrees of freedom, and, again, the individual drive torques on the wheels can be specified. The rider can apply a steer torque to the handlebars and a lean torque to the mainframe. The handlebars can rotate about the steer axis, and twist of the steering system is allowed with specified spring and damping properties. A linear spring–damper simulates suspension at the front wheel, while a spring–damper acting between points on the mainframe and swingarm simulates the non-linear suspension characteristics of monoshock rear suspension.

The wheels of the motorcycle model are assumed to be toroidal, with an associated shift of the contact patch with camber. Because of the peculiarities of SimMechanics, tyre forces are applied at the centre of mass of the wheels, and the shift in the point of application of the forces is accounted for.

Various tyre models were covered for both the motorcycle and the vehicle, ranging from linear models for the calculation of the horizontal forces, to complex tyre models for the calculation of all tyre forces and moments. These include the effects of reduced horizontal forces at high vertical loads, camber angle, and combined longitudinal and lateral slip.

Finally, driver models capable of controlling the vehicles to maintain a specified path and speed were described. In the automobile model, the driver model adjusts the steer angle to acheive a desired yaw angle or yaw rate, which can vary with time. In the motorcycle model, the rider applies a steer torque to the handlebars to induce a camber angle and turn the vehicle. In both cases, the total drive torque is controlled so that the vehicle achieves a desired speed.

Together, these components form advanced models that are suitable for investigations into the effects of torque distribution. The next chapter will describe how the models are verified to guarantee their accuarcy, before the handling and efficiency of vehicles with active torque distribution is described in Chapters 5 and 6, respectively.

Chapter 4

Model Verification

Active Torque Distribution (ATD)—the process of varying the drive torque distribution between the wheels of a vehicle—influences handling characteristics and energy efficiency. The multibody vehicle models of the automobile and the motorcycle, decribed in Chapter 3, were created with the purpose of investigating and quantifying those effects; however, before the models can be used to predict the influence that torque vectoring could have on handling and efficiency, they must first be verified to ensure their accuracy.

The methods used to verify the models will be described in this section. Verification is a two stage process: firstly, the mathematical models of the automobile and the motorcycle are used to verify the multibody simulations, and secondly, the forces and moments applied to the system are checked against the motion that they cause, with a final check that energy is conserved.

The mathematical and multibody models of the automobile and the motorcycle will be summarized in Sections 4.1.1 and 4.2.1, respectively.

4.1 Four-Wheeled Vehicle Model Verification

Chapter 3 introduced various models that can be used for the study of the dynamics of four-wheeled vehicles. In this section these models will be compared against each other to ensure the results are comparable.

4.1.1 Introduction

The models introduced in Section 3.3 were:

1. the geometric description of a vehicle turning at a very low speed. When the wheels roll without slipping, the radius of turn, R, can be calculated using the

equation

$$\delta = \frac{l}{R}, \tag{3.1 revisited}$$

where δ is the average steer angle of the front wheels, and l is the wheelbase of the vehicle.

2. the *bicycle model*, which has two degrees of freedom: the lateral velocity, v_y, and the yaw rate, $\dot{\psi}$. The equations of motion are

$$m\left(\dot{v}_y + \dot{\psi} v_x\right) = 2F_{y\,f} + 2F_{y\,b} \tag{3.6 revisited}$$

$$I\ddot{\psi} = 2l_f F_{y\,f} - 2l_b F_{y\,b}, \tag{3.7 revisited}$$

where m is the vehicle mass, I is the inertia about the Z-axis, and l_f and l_b are the distances from the centre of mass to the front and back axles, respectively. The F_y terms are the lateral tyre forces.

3. a seven-degree-of-freedom model with lateral, longitudinal and yaw velocity freedoms, plus four rotational freedoms for the wheels. The equations of motion are

$$\begin{aligned} &m\left(\dot{v}_x - \dot{\psi} v_y\right) = \\ &\left(F_{x\,fl} + F_{x\,fr}\right)\cos\delta - \left(F_{y\,fl} + F_{y\,fr}\right)\sin\delta + F_{x\,bl} + F_{x\,br} + F_{\text{aero}} \end{aligned} \tag{3.13 revisited}$$

$$\begin{aligned} &m\left(\dot{v}_y + \dot{\psi} v_x\right) = \\ &\left(F_{x\,fl} + F_{x\,fr}\right)\sin\delta + \left(F_{y\,fl} + F_{y\,fr}\right)\cos\delta \quad + F_{y\,bl} + F_{y\,br} \end{aligned} \tag{3.14 revisited}$$

$$\begin{aligned} &I\ddot{\psi} = \\ &\left[\left(F_{x\,fr} - F_{x\,fl}\right)\cos\delta + \left(F_{y\,fr} - F_{y\,fl}\right)\sin\delta\right]\frac{t_f}{2} + \left[F_{x\,br} - F_{x\,bl}\right]\frac{t_b}{2} \\ &+ \left[\left(F_{y\,fl} + F_{y\,fr}\right)\cos\delta + \left(F_{x\,fl} + F_{x\,fr}\right)\sin\delta\right] l_f + \left[F_{y\,bl} + F_{y\,br}\right] l_b, \end{aligned} \tag{3.15 rev.}$$

where t_f and t_b are the track widths of the front and back axles, respectively.

4. a multibody model with 13 degrees of freedom. Modelled in SimMechanics, it has the seven degrees of freedom of Item 3, plus vertical, pitch and roll freedoms, and linear suspension models at each of the wheels. Tyre models in the multibody model are interchangeable, and include, as discussed in Section 3.6:

(a) a linear tyre model, in which lateral and longitudinal tyre forces vary linearly with slip

$$F_x = K_x \kappa \qquad \text{(3.59 revisited)}$$
$$F_y = -K_y \alpha. \qquad \text{(3.60 revisited)}$$

where κ and α are the longitudinal and lateral slip ratios, and K_x and K_y are the longitudinal and lateral tyre stiffnesses. The horizontal forces do not vary with vertical load.

(b) a four parameter *Magic Formula* model [46] with equations

$$F_x = D_x \sin(C_x \arctan[B_x\kappa - E_x(B_x\kappa - \arctan[B_x\kappa])]) \qquad \text{(3.61 rev.)}$$
$$F_y = D_y \sin(C_y \arctan[B_y\alpha - E_y(B_y\alpha - \arctan[B_y\alpha])]), \qquad \text{(3.62 rev.)}$$

where B, C, D and E are scaling factors based on the tyre properties, derived from experimental results. Horizontal forces are assumed to vary linearly with vertical load.

(c) the full set of *Magic Formula* equations [46], which account for speed, camber, the combined slip situation and the varying effect of vertical load on the horizontal forces, amongst other things.

The models have different ranges of validity; for example, the geometric description of a vehicle in Item 1 is only valid at very low speeds. However, the more complex models should also be valid at very low speeds and hence, the models should produce similar results in this situation. This section will verify the models by comparing them in scenarios where their results should be the same.

4.1.2 Low Speed

At very low speeds, the forces required to turn the vehicle are small; therefore the magnitude of the slip experienced is also small and all the vehicle models should corner according to the geometrical constraints described in Item 1, regardless of the weight distribution or tyre properties.

Figure 4.1 shows position plots, in the *global* Coordinate System (CS), for the centres of gravity of the four vehicle models described in Section 3.3 and with the parameters specified in Appendix C.1. The simulation parameters are shown in Table 4.1. The dotted line shows the path defined by the geometric description of a cornering vehicle, from which the turning radius for the specified parameters is calculated at 47.75 m.

Table 4.1: Parameter values for simulation results shown in Figure 4.1

Parameter	Symbol	Value
wheelbase length	l	$2.5\,\mathrm{m}$
steer angle	δ	$3°$
vehicle speed	v	$1\,\mathrm{m\,s^{-1}}$
simulation length	t	$300\,\mathrm{s}$

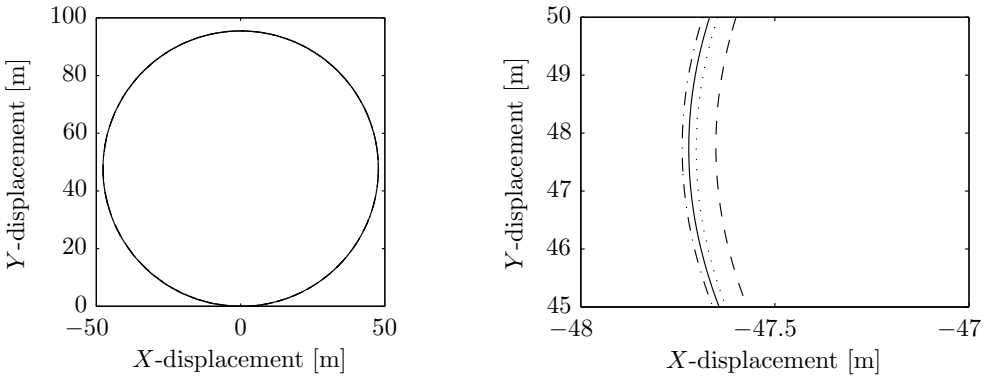

(a) Overview **(b)** Detail

Figure 4.1: Low speed vehicle position plots. · · · Geometrically defined path; – · – Bicycle model; – – – 7-Degree-of-Freedom (DoF) model; —— Multibody model.

Figure 4.1b shows the small differences between the models. The reason the 7-DoF model has a smaller turning radius than the *bicycle model* and multibody model is because the front wheels are assumed to have the same steering angle but follow different paths, thus leading to different slip angles. The multibody model steering system accounts for this through the implementation of Ackermann steering geometry, as described in Section 3.3.4. Other differences in path are accountable to small amounts of slip that do occur at low speed.

Overall, through these simulations, a level of confidence is gained in the models, and further verification can take place at higher speeds.

4.1.3 Moderate Speed

At a moderate speed, the assumptions made at each modelling stage begin to affect the results. Firstly, by using a linear tyre model in all vehicle models, and then introducing more representative tyre models and other complexities, the different models can be used together to increase confidence in their results.

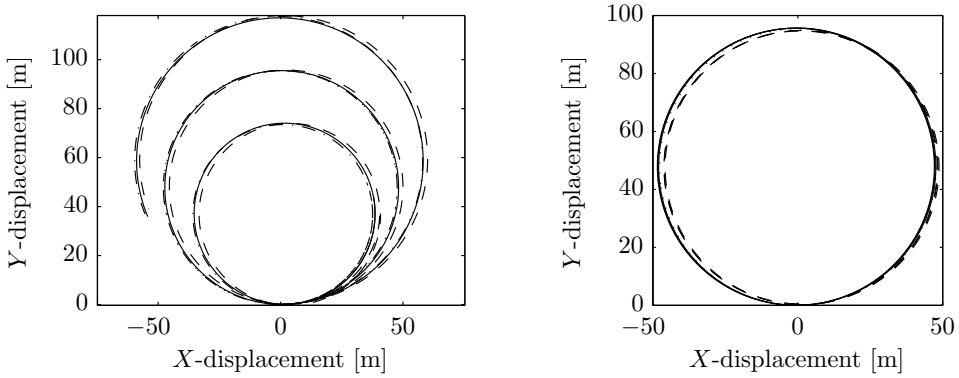

(a) Linear tyre model **(b)** Simple *Magic Formula* tyre model

Figure 4.2: Moderate speed vehicle position plots. · · · ·Geometrically defined path; – · – · Bicycle model; – – – 7-DoF ; —— Multibody model.

Table 4.2: Parameter values for simulation results shown in Figure 4.2

Parameter	Symbol	Value
steer angle	δ	3°
vehicle speed	v	$10\,\mathrm{m\,s^{-1}}$
simulation length	t	30 s

Table 4.3: Parameter values for *Vehicles A, B* and *C*

Parameter	Symbol	Value		
		Vehicle A	*Vehicle B*	*Vehicle C*
Front axle to CoG	l_f	1.0 m	1.25 m	1.5 m
Back axle to CoG	l_b	1.5 m	1.25 m	1.0 m

Linear Tyre Model

Figure 4.2 shows the results of simulating three vehicles with different weight distributions, as specified in Table 4.3, with the parameters given in Table 4.2. The three different weight distributions specified for *Vehicle A*, *Vehicle B* and *Vehicle C*, define vehicles whose static handling characteristics are Understeer (US), Neutral Steer (NS) and Oversteer (OS), respectively. These terms will be addressed in detail in Chapter 5, but for now, the different vehicles merely provide a range of values over which the models can be verified.

Figure 4.2a shows the results from using a linear tyre model (where horizontal tyre forces do not depend on the vertical load), in the *bicycle model*, 7-DoF and multibody models. Reassuringly, the three models predict very similar results: the three vehicles follow different paths with *Vehicle A* having the largest radius paths, and *Vehicle C* having the smallest radius paths. *Vehicle B* closely follows the geometrically defined path.

Simple *Magic Formula* Tyre Model

If, however, a tyre model is used in which the horizontal tyre forces do vary with vertical load, as a real tyre does, then the results are very different. Figure 4.2b shows the results of using the simple *Magic Formula* tyre model in the three different vehicle models. The horizontal forces in this tyre model are assumed to vary linearly with vertical load. Simulation results are presented for the three different weight distributions as described above, for each of the three vehicle models.

When the horizontal tyre forces vary linearly with vertical load, any changes in weight distribution (static or dynamic) is effectively cancelled out and all vehicles follow the same path.

The fact that the multibody model matches the predictions of the mathematically derived *bicycle model* and 7-DoF model gives confidence that the multibody simulation environment, SimMechanics, is producing valid equations of motion from the block diagrams. Small differences seen between position plots in Figure 4.2b are caused by

the lack of Ackermann steering geometry in the 7-DoF model, and by the wheels of the multibody model due to their mass, inertia and gyroscopic effects influencing the motion.

While the use of the simple *Magic Formula* tyre model with a linear relationship between horizontal and vertical forces does not allow the study of handling characteristics, it can still be useful for investigating the impact of torque vectoring by looking at the changes that can be made; however, it is evident that the more detailed tyre model is required for a full investigation to take place.

Complete *Magic Formula* Tyre Model

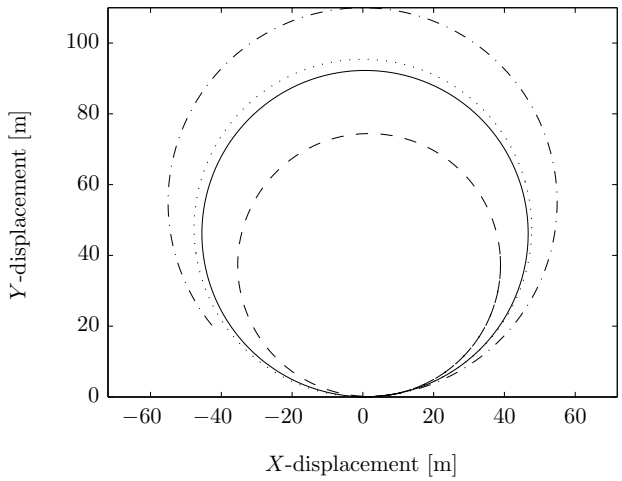

Figure 4.3: Position plots with complete *Magic Formula* tyre model. · · · ·Geometrically defined path; −·−·− *Vehicle A*; − − − *Vehicle B*; —— *Vehicle C*.

Figure 4.3 shows position plots for the multibody model with the complete *Magic Formula* tyre model, again for the three vehicles specified in Table 4.3, with the parameters in Table 4.2. The path the vehicles follow now depends on the specified weight distribution, with front heavy *Vehicle A* having the largest turn radius and rear-heavy *Vehicle C* having the smallest turn radius. This corresponds with the vehicles being Understeer (US) and Oversteer (OS), respectively, with *Vehicle B* having a Neutral Steer (NS) characteristic. The difference between these results and the simple *Magic Formula* tyre model results is due to the varying influence of vertical load on horizontal force generation in the complete *Magic Formula* model, as shown in Figures 3.19e and 3.19f.

For more information about automobile handling characteristics please refer to Section 5.1.

4.1.4 Radius of Curvature Check

In a steady state cornering situation, to check that the multibody model is performing correctly, the radius of curvature of the vehicle's position plot can be checked against the radius expected of a particle travelling in circular motion with a known speed and yaw rate, and also with that expected of a vehicle travelling with known steer and sideslip angles.

Instantaneous Radius of Curvature

The instantaneous radius of curvature of the vehicle path, R, is given by

$$R = \frac{\left[1 + \left(\frac{\mathrm{d}X}{\mathrm{d}Y}\right)^2\right]^{3/2}}{\left|\frac{\mathrm{d}^2X}{\mathrm{d}Y^2}\right|} \tag{4.1}$$

where X and Y are the displacements in the *global* CS, and $\frac{\mathrm{d}X}{\mathrm{d}Y}$ and $\frac{\mathrm{d}^2X}{\mathrm{d}Y^2}$ are the first and second derivatives.

Circular Motion of a Particle

The radius of curvature of a particle moving in circular motion at velocity, v, is given by

$$R = \frac{v}{\dot{\psi}} \tag{4.2}$$

where $\dot{\psi}$ is the yaw rate.

Steer and Sideslip Angle

Figure 4.4 shows that for a large radius, the relationship between steer angle and sideslip angles, and turning radius is

$$R = \frac{l}{\delta + \alpha_b - \alpha_f}, \tag{4.3}$$

for a vehicle with sideslip angles, α_f and α_b, at the front and rear wheels respectively, which is valid for non-linear tyres and in the presence of external forces.

Comparison of Radii

A vehicle was controlled to corner with a radius of 50 m, and the resulting radii were calculated for comparison. Figure 4.5 shows that similar radii are obtained for the three methods mentioned above.

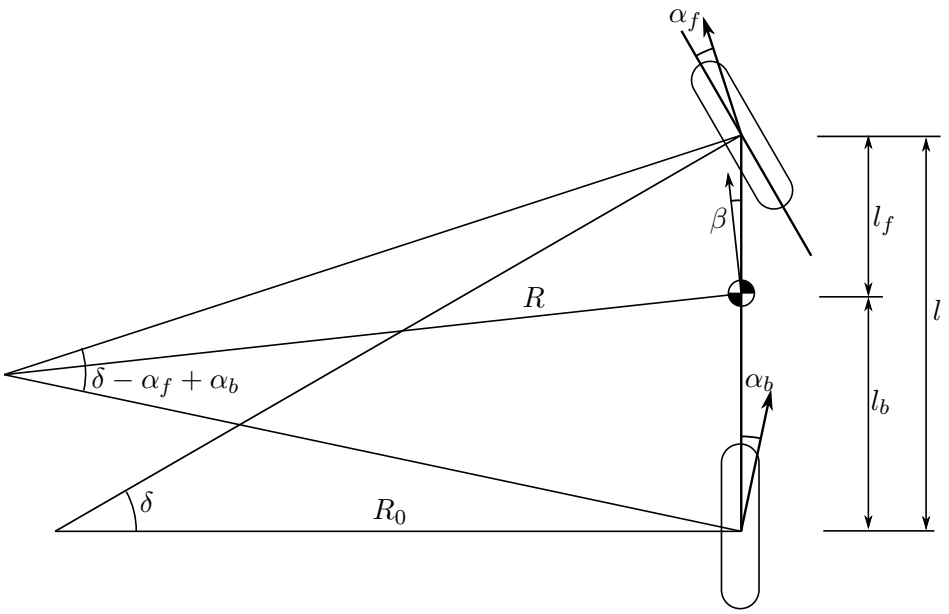

Figure 4.4: Sideslip angles of a cornering vehicle

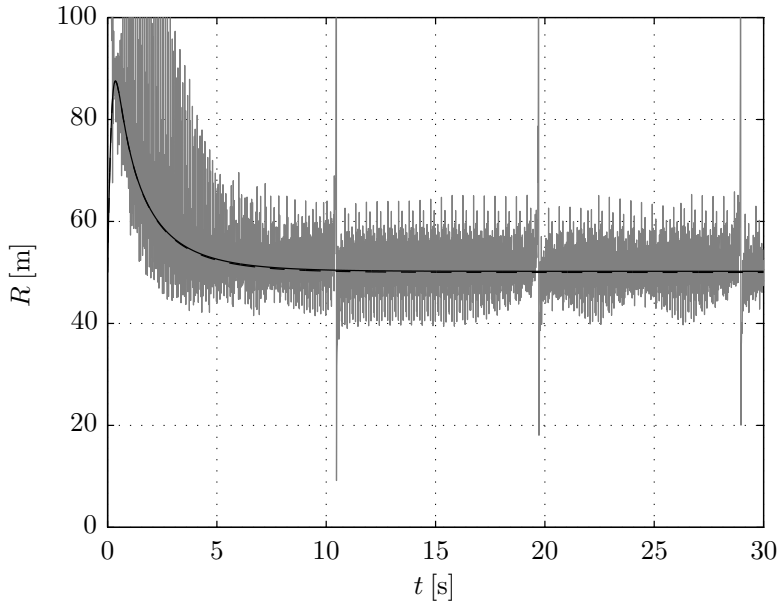

Figure 4.5: Instantaneous Radius Check Using Various Methods. —— Path curvature; —— Slip angle calculation; – – – Particle motion.

The radius of curvature calculated from the vehicle's path contains numerical error because it is calculated using differentials of numerical data. Error is especially prevalent at times when the vehicle's x-axis and the global X-axis are parallel leading to a division by zero; however, the mean value appears to be consistent with radii calculated by other methods.

4.1.5 Convergence

Finally, it is prudent to check that the Ordinary Differential Equation (ODE) solver has converged on a correct solution to the equations of motion generated by SimMechanics according to the block diagram of the automobile model. A numerical solution has *converged* when it approaches the exact solution. In most of the simulations presented herein, the MATLAB solver `ode45` is used to solve the resulting ODEs; however, if the motion calculated by this solver is different from the motion calculated by other solvers, it is indicative that the solution has not converged on the exact solution.

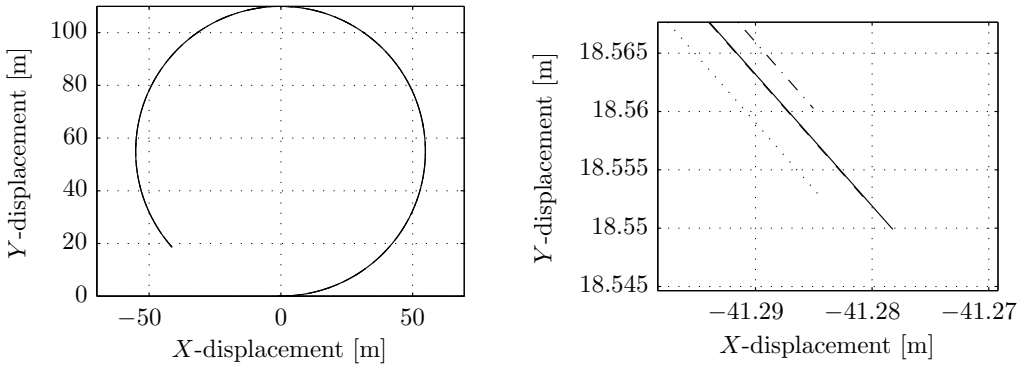

(a) Overview **(b)** Detail

Figure 4.6: Convergence of various solvers. · · · `ode23tb`; −·−·`ode23t`; − − −`ode23`; —— `ode45`.

Figure 4.6 shows similar results for position plots of *Vehicle A* simulated with parameters from Table 4.2 with the variable step ODE solvers shown in Table 4.4. Figure 4.6b shows the position after 30 s, where it can be seen the the predicted positions with the different solvers are with a few millimetres of each other, suggesting converged solutions. Indeed, the result from `ode23` is barely distinguishable from that of `ode45`.

Table 4.4: ODE solvers

Solver	Problem Tyre	Method
`ode45`	Non-stiff	Fifth-order Runge-Kutta
`ode23`	Non-stiff	Third-order Runge-Kutta
`ode23t`	Moderately stiff	Trapezoidal rule
`ode23tb`	Stiff	Trapezoidal rule with the second order backward difference formula

4.2 Two-Wheeled Vehicle Model Verification

Chapter 3 also covered the modelling of a motorcycle for dynamic investigations. This section will verify the multibody model with the mathematical calculations to ensure confidence in the results.

4.2.1 Introduction

The motorcycle models discussed in Section 3.4 increased in complexity as attempts were made to more realistically represent the motorcycle. The models introduced were:

1. the geometric description of a motorcycle cornering with camber in a steady state, for which the equation is

$$\gamma \approx \tan\gamma = \frac{\cancel{m}a_y}{\cancel{m}g} = \frac{v_x^2}{gR}, \qquad \text{(3.36 revisited)}$$

   where γ is the camber angle, a_y is the lateral acceleration and g is the gravitational acceleration.

2. a steady-state, two-degree-of-freedom model based on the *bicycle model*. The model assumes the camber angle of both wheels varies according to Equation (3.36), and substitutes this into the vehicle modelling equations, to arrive

at the equations

$$m\dot{\psi}v_x = \left(K_{\alpha f} + K_{\alpha b}\right)\beta + \left(\frac{l_f K_{\alpha f} - l_b K_{\alpha b}}{v_x} + \frac{\left(K_{\gamma f} + K_{\gamma b}\right)v_x}{g}\right)\dot{\psi} - K_{\alpha f}\delta \qquad \text{(3.41 revisited)}$$

$$0 = \left(l_f K_{\alpha f} - l_b K_{\alpha b}\right)\beta + \left(\frac{l_f^2 K_{\alpha f} + l_b^2 K_{\alpha b}}{v_x} + \frac{\left(l_f K_{\gamma f} - l_b K_{\gamma b}\right)v_x}{g}\right)\dot{\psi} - l_f K_{\alpha f}\delta. \qquad \text{(3.42 revisited)}$$

where K_α and K_γ are lateral and camber tyre stiffesses, and β is the sideslip angle at the centre of mass of the motorcycle. The steer input is steer angle, rather than steer torque, which is more commonly used for motorcycle modelling; however, it is assumed that in steady-state cornering, the steer angle is proportional to the steer torque.

3. a four-degree-of-freedom, with equations of motion of the form

$$\mathbf{M}\begin{bmatrix}\ddot{y}\\ \ddot{\psi}\\ \ddot{\delta}\\ \ddot{\gamma}\end{bmatrix} + \mathbf{N}\begin{bmatrix}\dot{y}\\ \dot{\psi}\\ \dot{\delta}\\ \dot{\gamma}\end{bmatrix} + \mathbf{P}\begin{bmatrix}\delta\\ \gamma\end{bmatrix} + \mathbf{G}\left[\tau_s\right] = 0, \qquad \text{(3.43 revisited)}$$

where τ is the torque applied to the handlebars by the rider. The motorcycle is free to move with lateral and yaw motions, and can steer and camber, with notation y, ψ, δ and γ, respectively.

4. a 13-degree-of-freedom multibody model specified in SimMechanics, including the effects of front and rear suspension, steer and twist motions of the steering system, aerodynamic lift and drag, and toroidal tyres. The available tyre models include:

   (a) a simple lateral tyre model where tyre force varies linearly with sideslip angle and camber angle, for example,

   $$F_{yf} = K_{\alpha f}\alpha_f + K_{\gamma f}\gamma_f; \qquad \text{(3.39 revisited)}$$

   (b) a *Magic Formula*-based approach [46] with parameters for motorcycle tyres fitted by Sharp *et al.* [65];

(c) a simple tyre model, created by Meijaard and Popov [40], that nevertheless includes the effect of combined slip, toroidal tyres and the large magnitudes of camber that can be experienced by motorcycles.

4.2.2 Verification of the Cornering Motorcycle

Verification of the motorcycle model is more difficult than the automobile model because of the various assumptions made for the different models, and because the possible inputs to the system include steer angle, steer torque, and lean torque. In this section, the multibody model is checked against various methods of estimating the radius of a cornering motorcycle.

Table 4.5: Motorcycle model parameters for verification

Parameter	Symbol	Value
target vehicle speed	v_{ref}	$15\,\mathrm{m\,s^{-1}}$
target cornering radius	R_{ref}	$100\,\mathrm{m}$
simulation length	t	$60\,\mathrm{s}$
total mass	m	$285.7\,\mathrm{kg}$
centre of gravity height	h	$0.5796\,\mathrm{m}$
wheelbase length	l	$1.539\,\mathrm{m}$
average tyre toroidal radius	r_t	$0.9\,\mathrm{m}$

Table 4.6: Motorcycle model results for verification

Parameter	Symbol	Value
steer angle	δ	$0.0122\,\mathrm{rad}$
camber angle	γ	$0.2592\,\mathrm{rad}$

The multibody motorcycle model, with parameters specified in Appendix C.2, was controlled to turn at $15\,\mathrm{m\,s^{-1}}$ with a cornering radius of 100 m. The simulation parameters are given in Table 4.5 and the resulting values are shown in Table 4.6. In this steady-state situation, the lean angle of the rear frame is 0.2592 rad. The yaw angle of the front wheel, relative to the rear, is 0.0122 rad, which includes the effect of the inclination of the steer axis from vertical, ϵ. To maintain comparability with the vehicle model, this will be referred to as the steer angle, δ, which, assuming twist

is negligable, is related to the angle of rotation of the handlebars about the steer axis, δ', with the equation

$$\delta = \delta' \cos \epsilon. \tag{4.4}$$

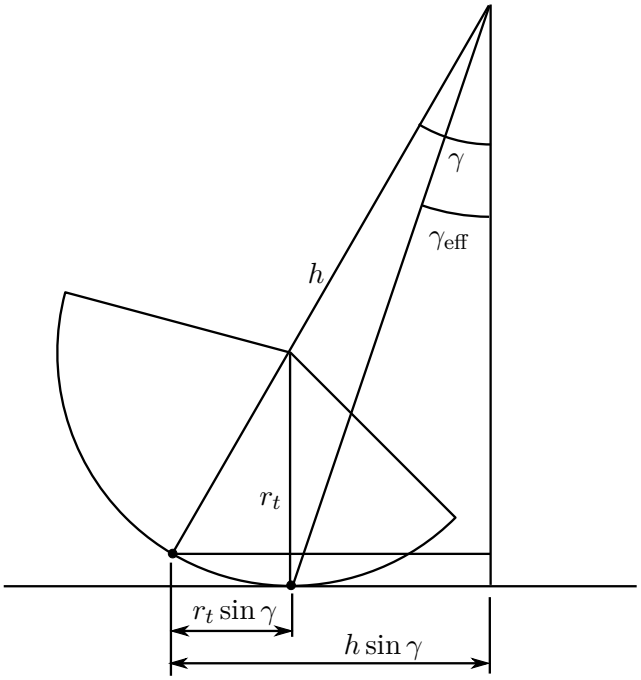

Figure 4.7: Effective camber angle of a motorcycle

The geometric description predicts a camber angle of

$$\gamma = \arctan \frac{v_x^2}{gR} = 0.2255\,\text{rad}; \tag{4.5}$$

however, when the tyres are assumed to be toroidal, rather than disk-like, the effective camber angle is less than the lean angle of the rear frame, as shown in Figure 4.7. When $h \gg r_t$, the measured camber angle is approximately related to the effective camber angle with the equation,

$$\sin \gamma_{\text{eff}} \approx \left(1 - \frac{r_t}{h}\right) \sin \gamma; \tag{4.6}$$

thus, after correction for toroidal tyres, the camber angle required to make a 100 m at turn at $15\,\text{m}\,\text{s}^{-1}$ is 0.2679 rad.

The fact that this is a slight (3.3 %) over-estimation of the camber angle from the SimMechanics simulation is because of factors that affect the radius of turn of the multibody model, including the camber thrust of the tyres, which will tend to

reduce the radius for a given camber angle. The camber angles of the front and rear tyres will differ because of the rake and steer angles. The twist of the front frame relative to the rear will have an effect, though the impact will be small because of the high stiffness of modern motorcycles [62]. Also, different sideslip angles at the wheels mean that the motorcycle can be thought of as US or OS, which affects the radius of turn. Aerodynamic lift and tyre aligning moments will also have a small effect.

Similar results are obtained for different cornering radii and speeds, giving confidence in the multibody model.

Cossalter [11] suggests that the cornering radius of a cambered motorcycle can be estimated using the equation

$$R \approx \frac{l}{\delta} \cos \gamma, \tag{4.7}$$

which estimates a radius of 121.9 m. The actual radius is likely to be smaller for the reasons mentioned above.

4.2.3 Radius of Curvature Check

Using the same method as for the automobile, the instantaneous radius of curvature of the path predicted by the multibody motorcycle model can be checked with that of a particle in circular motion, and with that predicted from the sideslip angles of the vehicle and tyres using Equation (4.3), as shown in Figure 4.4.

Figure 4.8 shows that all radii mentioned are the same in steady-state. The noise in the radius of curvature of the path is caused by numerical error in the results; the points at which it tends to infinity are when the motorcycle has a yaw angle equal to zero or π, thus leading to a division by zero.

4.3 Power Balance

It is possible to check that the forces and moments applied to the vehicle are having the effect that is expected of them, according to Newton's laws of motion. Similarly, conservation of energy can be checked by comparing the power applied to the system with the power dissipated in it [16]. These checks are applicable to both the two- and four-wheeled vehicle, and, in fact, any other multibody system.

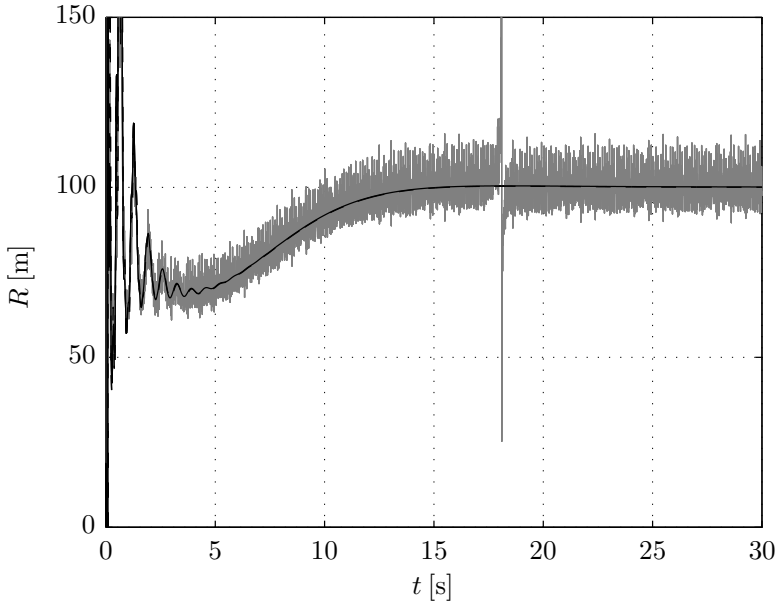

Figure 4.8: Instantaneous radius of curvature of the motorcycle using various methods. Path curvature; Slip angle calculation; Particle motion.

4.3.1 Force Balance

It is necessary to check that the sum of the tyres forces is equal to the sum of the aerodynamic, inertial and gravitational forces,

$$\boldsymbol{F}_{\text{error}} = \sum_{i=1}^{n_w} \boldsymbol{F}_{i\text{tyre}} + \boldsymbol{F}_{\text{aero}} + \sum_{j=1}^{n_m} m_j \left(\boldsymbol{\omega} \times \boldsymbol{v} + \boldsymbol{g}\right) \tag{4.8}$$

for $i = 1, \ldots, n_w$ wheels and $j = 1, \ldots, n_m$ masses. $\boldsymbol{F}_{\text{tyre}}$ is the vector of tyre forces, and $\boldsymbol{F}_{\text{aero}}$ is the vector of aerodynamic lift and drag forces acting on the vehicle. $\sum_j m_j$ represents the sum of all the machine's constituent masses, $\boldsymbol{v}$ is the velocity vector of the main body and $\boldsymbol{\omega}$ is its angular velocity vector, such that $\boldsymbol{\omega} \times \boldsymbol{v}$ gives the inertial acceleration vector. $\boldsymbol{g}$ is the gravitational acceleration vector, which in this case is $\begin{bmatrix} 0 & 0 & -9.81 \end{bmatrix}$.

Care must be taken that all of the force and velocity vectors are transformed into the same CS for the balance: in this case, the *vehicle intermediate* CS is used, which moves and rolls with the vehicle.

Figure 4.9 shows a typical result of the force error calculation. The errors are small in steady-state, relative to the forces present in the system, which may be tens of kilo-newtons.

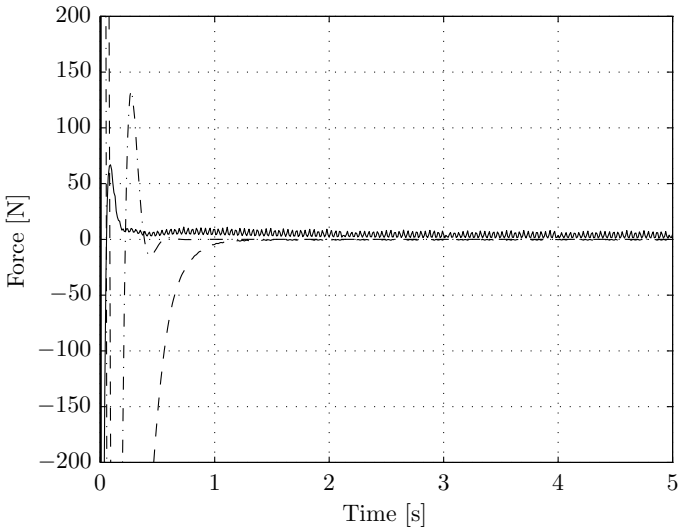

Figure 4.9: Typical force balance. —— $F_{\text{error}\,x}$; − − − $F_{\text{error}\,y}$; − · − · $F_{\text{error}\,z}$.

4.3.2 Moment Balance

The moments applied to the system should also sum to zero in steady state motion. A reference point is chosen and the effect of the forces acting at a distance from this reference point create the moments used in the balance. The reference point can be any point in space, but for simplicity, the centre of mass of the mainframe is chosen. Again, the *vehicle intermediate* CS is used.

$$\begin{aligned}\boldsymbol{M}_{\text{error}} = &\sum_{i=1}^{n_w} \left(\boldsymbol{M}_{i\text{tyre forces}} + \boldsymbol{M}_{i\text{tyre moments}} + \boldsymbol{M}_{i\text{gyroscopic}} \right) \\ &+ \sum_{j=1}^{n_m} \left(\boldsymbol{M}_{j\text{inertial}} + \boldsymbol{M}_{j\text{gravitational}} \right) + \boldsymbol{M}_{\text{aerodynamic}}\end{aligned} \tag{4.9}$$

for $i = 1, \ldots, n_w$ wheels and $j = 1, \ldots, n_m$ masses. Where the moments are generated by forces acting at a distance from the reference point, which is the case for the tyre forces, and the aerodynamic, inertial and gravitational forces, the moments are calculated using

$$\boldsymbol{M} = (\boldsymbol{s} - \boldsymbol{s}_{\text{ref}}) \times \boldsymbol{F}, \tag{4.10}$$

where $\boldsymbol{s}$ is the position of the body in the *global* CS. The moments arising from the tyre moments and the gyroscopic moments are summed directly. Since the applied driving torques to the front and rear wheels each have equal and opposite reactions on the forks and mainframe respectively, they are not included in the moment balance.

A typical result for the force error calculation is shown in Figure 4.9. The

steady-state errors are small relative to the moments in the system, which may be hundreds of newton-meters.

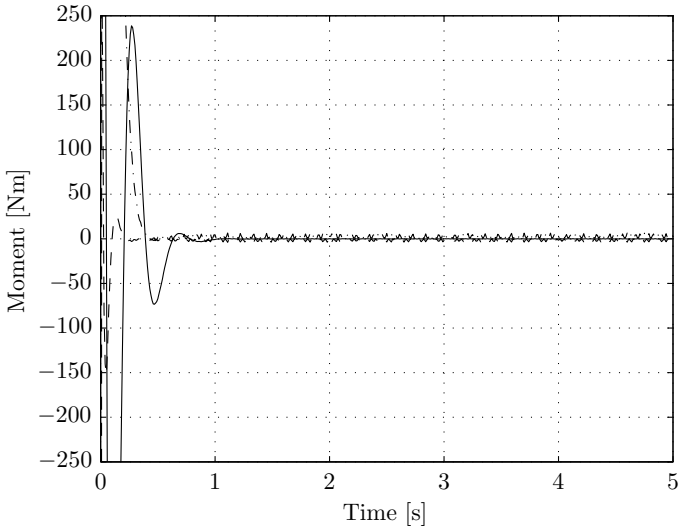

Figure 4.10: Typical moment balance. —— $M_{\text{error}\,x}$; – – – $M_{\text{error}\,y}$; – · – · $M_{\text{error}\,z}$.

Calculation of Gyroscopic Moments

The moments generated through gyroscopic precession of the rotating wheels are calculated for each of the wheels using

$$\boldsymbol{M} = \dot{\boldsymbol{H}} + \boldsymbol{\Omega} \times \boldsymbol{H}, \tag{4.11}$$

where $\boldsymbol{H}$ is the angular momentum of the gyroscope and $\boldsymbol{\Omega}$ is the angular velocity of the reference frame [41]. In a steady state, the time rate of change of angular momentum $\dot{\boldsymbol{H}}$ is zero. Here again, one must be careful with the coordinate systems.

Angular momentum is calculated in the yaw-rotated and inclined *wheel* CS using

$$\boldsymbol{H}' = \mathbf{I}\boldsymbol{\omega}, \tag{4.12}$$

where $\mathbf{I}$ is the 3×3 inertia matrix of the body and $\boldsymbol{\omega}$ is the angular velocity in the *wheel* CS mentioned above. The angular momentum is transformed into the yaw-rotated but not inclined*tyre* CS, which has only a yaw rotation, through the use of a rotation matrix for a camber rotation:

$$\boldsymbol{H} = \mathbf{R}_\gamma \boldsymbol{H}'. \tag{4.13}$$

Gyroscopic moments can now be calculated for each of the rotating bodies in their own yaw-rotated *tyre* CS, all that remains is to transform them from that into the CS of the chosen reference point, i.e., the *vehicle intermediate*. This is achieved through the use of a yaw rotation matrix where the yaw angle used is the relative yaw angle between the body and the reference frame

$$\psi_{\text{rel}} = \psi - \psi_{\text{ref}} \tag{4.14}$$

$$\boldsymbol{M}_{\text{gyro}} = \mathbf{R}_{\psi_{\text{rel}}} \left(\boldsymbol{\omega}_v \times \boldsymbol{H} \right). \tag{4.15}$$

4.3.3 Power Balance

Finally, the amount of power supplied by the SimMechanics *actuators* can be checked against the dissipaters in the model:

$$P_{\text{error}} = \sum_{i=1}^{n_w} \left(P_{i\text{drive}} + P_{i\text{slip}} + P_{i\text{moments}} \right) + P_{\text{aero}}, \tag{4.16}$$

for $i = 1, \ldots, n_w$ wheels.

The amount of drive power provided by the engine and/or motor(s) is calculated at the wheels, neglecting transmission losses, as follows:

$$P_{\text{drive}} = \sum_{i=1}^{n_w} \tau_i \omega_i \tag{4.17}$$

for $i = 1, \ldots, n_w$ wheels, where τ is torque about the wheel's axle, and ω is a wheel's angular velocity about its axle.

The amount of power consumed as slip at the wheel–road contact can be calculated as

$$P_{\text{slip}} = \sum_{i=1}^{n_w} \left(F_{i\,xt} v_{i\,s,xt} + F_{i\,yt} v_{i\,yt} \right), \tag{4.18}$$

where F_{xt} and F_{yt} are the longitudinal and lateral tyre forces, and $v_{s,xt}$ and v_{yt} are the longitudinal and lateral slip velocities in the *tyre* CS. The equations are similar to those given in [1, 35] and [3, p. 70]. Since the forces and velocities are opposite in sign, this is always negative.

The amount of power consumed through the tyre aligning moment is

$$P_{\text{moments}} = \sum_{i=1}^{n_w} M_{i\,zt} \omega_{i\,zt}, \tag{4.19}$$

where M_{zt} is the tyre aligning moment, and ω_{zt} is its angular velocity about the vertical axis.

Finally, the amount of power consumed overcoming aerodynamics is

$$P_{\text{aero}} = \sum \boldsymbol{F}_{\text{aero}} \boldsymbol{v}_{xyzv}, \tag{4.20}$$

where $\boldsymbol{F}_{\text{aero}}$ is the vector of aerodynamic forces and $\boldsymbol{v}_{xyzv}$ is the vector of velocities of the mainframe.

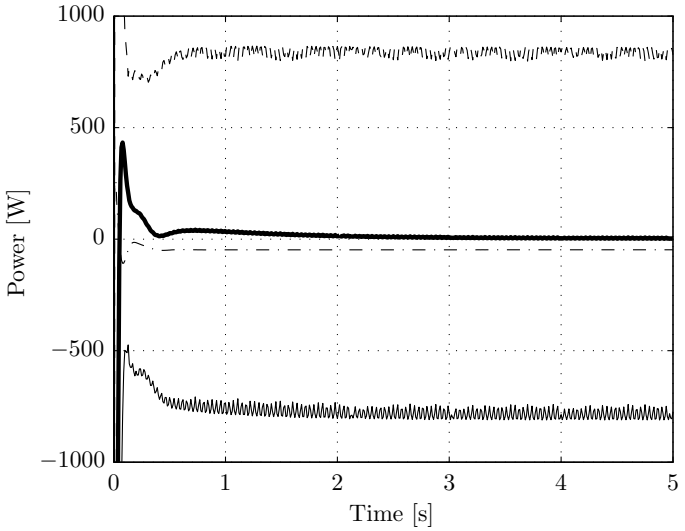

Figure 4.11: Typical power balance. —— $P_{\text{error}\,x}$; – – – $P_{\text{error}\,y}$; – · – · $P_{\text{error}\,z}$; —— P_{sum}.

A typical power balance plot is shown in Figure 4.11, where the sum of the x, y and z errors is approximately zero. The reason that there are apparent errors in the principle directions is because, for example, power is applied about the y-axis, but is balanced by the tyre force in the x-axis.

4.4 Chapter Summary

This chapter has used the geometric descriptions of turning two- and four-wheeled vehicles to verify the multibody models, and thus give confidence in the results they predict. Using the radius of an automobile taking a large radius corner at very low speed, the bicycle model and 7-DoF model were verified, then by using three tyre models (viz. linear, simple *Magic Formula* and complete *Magic Formula*), the vehicle models were proven to give similar results at low and moderate speeds.

At high speeds and lateral accelerations, important differences between the tyre models were demonstrated. Most notably, differences are due to the effect of vertical load on the handling characteristics. The effect of combined slip at high speed will

also affect the results of the multibody model, which is an important characteristic for torque vectoring studies and is ignored by the simpler models.

The multibody motorcycle model was verified with the geometric description of a bicycle cornering with camber with reasonable accuracy. Again, differences arise because of the inclusion of effects that are ignored by the simpler models. In the motorcycle models, the main causes of the discrepancies are toroidal tyres and gyroscopic effects of rotating bodies.

In both the motorcycle and automobile cases, the radii calculated from the steer and slip angles at the wheels matched the expected results, which gives confidence in the kinematics of the system.

Finally, the forces and moments applied to the systema were balanced against the effect that they had on the motion with good accuracy, and the energy applied to the system matched closely the amount dissipated.

The multibody models have a larger range of validity than the mathematical models, for example, at high slip ratios and with dynamic load transfer. The remaining sections of the thesis will use the multibody models for handling and efficiency studies where the mathematical models would not be valid.

Chapter 5

Vehicle Handling

Handling and stability improvements in automobiles have been achieved through augmentation of their drivelines with electronically controlled components, as described in Chapter 2. Traditionally, these were achieved by either limiting the total power of the engine, or by applying the brake at one, or more, of the wheels, with systems such as an Electronic Stability Program (ESP) [71]. Both of these methods mean that the controller might interfere with the driver's request of the vehicle and reduce the vehicle's speed; its intervention may thus prove an annoyance. To avoid this, such systems only become active when the controller detects a dangerous situation, meaning the systems are not being utilised most of the time. Active Torque Distribution (ATD), or torque vectoring, offers the opportunity to actively influence the handling of the vehicle at all times, without interfering with the driver's demand.

Mechanical systems that can vary the distribution of torque in automobiles exist [54, 57], and a small number of motorcycle manufacturers have developed motorcycles that can apply some of their torque at the front wheel [10, 28]. The effect of torque distribution has been studied with mathematical models of automobiles [21, 45], but research into motorcycles with front-wheel drive is lacking.

Mathematical and multibody models of an automobile and a motorcycle were presented in Chapter 3, and were verified to ensure their accuracy in Chapter 4. This chapter uses those models to investigate the influence that varying the distribution of drive torque has on the handling of the vehicles. The mathematical models described in earlier chapters will be used for initial studies, to investigate the effect that changes in, for example, weight distribution and tyre stiffness have on the handling characteristics of the vehicles. The multibody models will then be used to demonstrate the influence of torque vectoring.

5.1 Steady-State Handling

The cornering behaviour of a vehicle is an important performance characteristic for a driver, and one which a vehicle designer has to consider. The steady-state handling characteristics of a vehicle determine, to some extent, how a vehicle feels to drive. They are also important in determining what happens as the vehicle approaches its limit of adhesion. Racing drivers often prefer race cars to exhibit oversteer characteristics as they require less effort to turn at high speed, while it is common for road vehicles to be slightly understeer as the characteristics are more predictable for novice drivers, thus making them safer.

The steady-state handling characteristics of automobiles have been studied by many [2, 18] and are well understood. A method for quantifying them using linear approximations is presented in this section, with the purpose of applying it to the full multibody simulation. A similar approach with application to motorcycle dynamics [30] is less common and is also presented in this section.

5.1.1 Automobiles

Linear Investigation

In automobiles, the most commonly used measure of directional response is the *understeer gradient* [18], which is a measure of handling performance under steady-state conditions. It is derived mathematically from the *bicycle model* with linear tyre characteristics assumed, as follows. The equations of motions given in Equations (3.11) and (3.12) can be rearranged to give

$$m\dot{v}_y + \left(2K_{\alpha f} + 2K_{\alpha b}\right)\frac{v_y}{v_x} + \left(2K_{\alpha f}l_f - 2K_{\alpha b}l_b + mv_x^2\right)\frac{\dot{\psi}}{v_x} = 2K_{\alpha f}\delta \tag{5.1}$$

$$I\ddot{\psi} + \left(2K_{\alpha f}l_f - 2K_{\alpha b}l_b\right)\frac{v_y}{v_x} + \left(2K_{\alpha f}l_f^2 + 2K_{\alpha b}l_b^2\right)\frac{\dot{\psi}}{v_x} = 2K_{\alpha f}l_f\delta. \tag{5.2}$$

where $K_{\alpha f}$ and $K_{\alpha b}$ are the linear lateral tyre stiffnesses.

In steady state conditions, $\ddot{\psi} = \dot{v}_y = 0$, thus, using the substitution $\beta = {}^{v_y}/_{v_x}$, Equations (5.1) and (5.2) can be written in matrix form

$$\begin{bmatrix} 2\left(K_{\alpha f} + K_{\alpha b}\right) & \frac{2}{v_x}\left(K_{\alpha f}l_f - 2K_{\alpha b}l_b\right) + mv_x \\ 2\left(K_{\alpha f}l_f - K_{\alpha b}l_b\right) & \frac{2}{v_x}\left(K_{\alpha f}l_f^2 + 2K_{\alpha b}l_b^2\right) \end{bmatrix} \begin{Bmatrix} \beta \\ \dot{\psi} \end{Bmatrix} = \begin{Bmatrix} 2K_{\alpha f}\delta \\ 2K_{\alpha f}l_f\delta \end{Bmatrix}. \tag{5.3}$$

Through inversion of the matrix and subsequent simplification, expressions for the sideslip angle, β, and the yaw rate, $\dot{\psi}$, in terms of the steer angle, δ, and velocity,

v_x, of the vehicle are

$$\beta = \left(\frac{1 - \frac{m}{2l} \frac{l_f}{l_b K_{\alpha r}} v_x^2}{1 - \frac{m}{2l^2} \frac{K_{\alpha f} l_f - K_{\alpha r} l_b}{K_{\alpha f} K_{\alpha r}} v_x^2} \right) \frac{l_b}{l} \delta \tag{5.4}$$

$$\dot{\psi} = \left(\frac{1}{1 - \frac{m}{2l^2} \frac{K_{\alpha f} l_f - K_{\alpha r} l_b}{K_{\alpha f} K_{\alpha r}} v_x^2} \right) \frac{v_x}{l} \delta. \tag{5.5}$$

In steady-state cornering, the radius of turn, $R = {}^{v_x}/_{\dot{\psi}}$, and Equation (5.5) can be rearranged to give

$$\delta = \frac{l}{R} \left(1 - \frac{m}{2l^2} \frac{K_{\alpha f} l_f - K_{\alpha b} l_b}{K_{\alpha f} K_{\alpha b}} v_x^2 \right). \tag{5.6}$$

By noting that the lateral acceleration is $a_y = {}^{v_x^2}/_{R}$,

$$\begin{aligned} \delta &= \frac{l}{R} - \frac{m}{2l} \frac{K_{\alpha f} l_f - K_{\alpha b} l_b}{K_{\alpha f} K_{\alpha b}} a_y \\ &= \frac{l}{R} + K a_y, \end{aligned} \tag{5.7}$$

where K is the *understeer gradient* [2, 18, 75]. It describes how the steer angle of the vehicle must be changed to achieve a certain cornering radius, R, at a given speed. Further simplification of K can be achieved by noting that the vertical loads at the front and rear tyres are given by

$$F_{z\,f} = \frac{mgl_b}{2l} \tag{5.8}$$

$$F_{z\,b} = \frac{mgl_f}{2l}, \tag{5.9}$$

thus,

$$K = \frac{1}{g} \left(\frac{F_{zf}}{K_{\alpha f}} - \frac{F_{zb}}{K_{\alpha b}} \right). \tag{5.10}$$

Application to Real Automobiles

Although the understeer gradient is derived for linear vehicles, the concept is useful in the analysis of real vehicles. For a vehicle with a small steer angle, δ, and small sideslip angles, α_f and α_r at the front and rear respectively, the radius of turn is

$$R = \frac{l}{\delta + \alpha_b - \alpha_f}, \tag{4.3 revisited}$$

which is valid in the presence of camber and external forces. By rearranging Equation (4.3) for δ and equating it with Equation (5.7), one obtains

$$\alpha_f - \alpha_b = \frac{l}{R} K v_x^2, \tag{5.11}$$

which shows that the sign of the left-hand side must determine the sign of the understeer gradient, K, in a steady-state turn. In other words, the understeer gradient of any vehicle, with linear or non-linear tyres assumed, can be calculated using

$$K = \frac{R}{l v_x^2} \left(\alpha_f - \alpha_b \right). \tag{5.12}$$

The sign of the understeer gradient is, therefore, positive when the slip angle at the front wheels is greater than the slip angle at the rear wheels, and vice versa. A qualitative description, based on the sign of the understeer gradient, allows a vehicle to be put into one of three categories:

1. **Understeer (US)** When the lateral slip speeds at the front wheels are greater than at the rear wheels, $\alpha_f > \alpha_b$, the understeer gradient is positive, $K > 0$. The vehicle is described as understeer, and Equation (4.3) shows that the radius of turn will be larger than a vehicle with no sideslip at the wheels ($v_x \approx 0$). In other words, the steer angle required to maintain a constant radius turn must be increased as vehicle speed increases.

2. **Neutral Steer (NS)** When the lateral slip speeds at the front and rear wheels are equal, $\alpha_f = \alpha_b$, the understeer gradient is zero, $K = 0$. The vehicle is described as neutral steer, and no change in steer angle is required to maintain a constant radius turn, regardless speed. In this case, the steer angle required is defined by the Ackermann angle,

$$\tan \delta = \frac{l}{R}. \tag{3.1 revisited}$$

3. **Oversteer (OS)** When the lateral slip speeds at the front wheels are smaller than at the rear wheels, $\alpha_f < \alpha_b$, the understeer gradient is negative, $K < 0$. The vehicle is described as oversteer, and the turn radius will be smaller at high speeds than lower speeds. A smaller steer angle is required to maintain a constant radius turn with increasing vehicle speed.

In this section, three different weight distributions are considered for the comparison of handling characteristics, as defined in Table 5.1. With reference to

Equation (5.10), when the tyres are assumed to be identical and linear, and all other parameters remain the same, the understeer gradients of *Vehicles A, B* and *C* are positive, zero and negative, respectively; thus, *Vehicle A* can be described as Understeer (US), *Vehicle B* as Neutral Steer (NS) and *Vehicle C* as Oversteer (OS).

Table 5.1: Parameter values for *Vehicles A, B* and *C*.

Parameter	Symbol	Value		
		Vehicle A	*Vehicle B*	*Vehicle C*
Front axle to CoG	l_f	1.0 m	1.25 m	1.5 m
Back axle to CoG	l_b	1.5 m	1.25 m	1.0 m

While the derivation of the understeer gradient is obtained using the *bicycle model* and linear approximations, the analysis can be applied to the non-linear multibody model developed in Section 3.3, in the same way that it can be applied to real vehicles.

The understeer gradient, and other handling properties, can be obtained with an appropriately instrumented vehicle [18]; for example, by driving a vehicle around a circle of known constant radius, whilst recording steer angle and speed, Equation (5.7) can be solved from the gradient of a plot of steer angle, δ, against lateral acceleration, a_y. Various test methods are defined in ISO4138:2004 "Passenger Cars – Steady-state circular driving behaviour – Open-loop test methods" [26], for the determination of handling parameters of real four-wheeled road vehicles.

Standard Automobile Handling Results

The multibody model of the automobile, as described in Section 3.3, is used to find the handling properties of the simulated vehicles. 'Method One' of [26] is used: a constant radius manoeuvre with a constant rate of increase in longitudinal speed of $0.1\,\mathrm{m\,s^{-2}}$. The steady increase in speed means the vehicle is in a quasi-steady-state, where transient behaviour is insignificant. This testing method means that the speed can be increased until the vehicle can no longer follow the requested path.

It is useful to simulate the vehicle in a way that closely represents the real world tests. Ideal road, tyre and weather conditions mean that subtle changes in handling can be analysed; however, certain aspects of real vehicles are not accounted for, such as compliance of the steering system. Ultimately, the success of a torque vectoring system will be determined by how it feels to a driver.

With the benefit of complete data for the vehicle motion from the multibody model, various other graphs can be plotted, which give a dynamicist the opportunity

to graphically compare the handling characteristics of the vehicles. Figure 5.1 shows various plots of data generated with the SimMechanics multibody model, for the three vehicles defined in Table 5.1, with common parameters from Appendix C.1. The simulation parameters are given in Table 5.2 and all vehicles have an ideal driveline that distributes torque evenly between all four wheels.

Table 5.2: Parameters for handling comparison simulations

Parameter	Symbol	Value
initial vehicle speed	v_0	$1\,\mathrm{m\,s^{-1}}$
rate of increase in speed	a_x	$0.1\,\mathrm{m\,s^{-2}}$
turn radius	R	$50\,\mathrm{m}$

Steer Angle Figure 5.1a shows how the steer angle must be changed to maintain the radius of turn as vehicle speed increases. At low speeds, all vehicles require a steer angle of 0.05 rad, which corresponds to the Ackermann Angle. As speed increases, *Vehicle A* must have its steer angle increased considerably, whilst the steer angle of *Vehicle C* can be reduced. This corresponds to the linear predictions that *Vehicle A* and *Vehicle C* would be US and OS respectively. The required steer angle for *Vehicle B* remains fairly constant at low speeds, in accordance with a NS vehicle, but must be increased slightly at higher speeds as the vehicle starts to exhibit understeer tendencies.

Sideslip Angle Figure 5.1b shows plots of the sideslip angle, $\beta = {}^{v_y}/_{v_x}$, at the centre of mass of the vehicle. At low speeds, with little or no lateral slip velocity at the tyres, all vehicles exhibit a positive slip angle. This is due to the fact that the rear wheels corner with a smaller radius than the front, meaning that the centre of gravity has a small positive lateral velocity. The sideslip angle of the vehicle centre of mass becomes negative for all vehicles as speeds increase and the sideslip of the wheels becomes dominant. In comparison to each other, for all speeds, the sideslip angle of *Vehicle C* is more negative than *Vehicle B*, which in turn is more negative than *Vehicle A*.

Lateral Acceleration Gain One of two reasons for applying a steer input to a vehicle is to produce a lateral acceleration, for example, to change lanes on a motorway. Thus, the ratio of lateral acceleration to steer input is an important handling quantity, and is known as the lateral acceleration gain [18]. Returning to

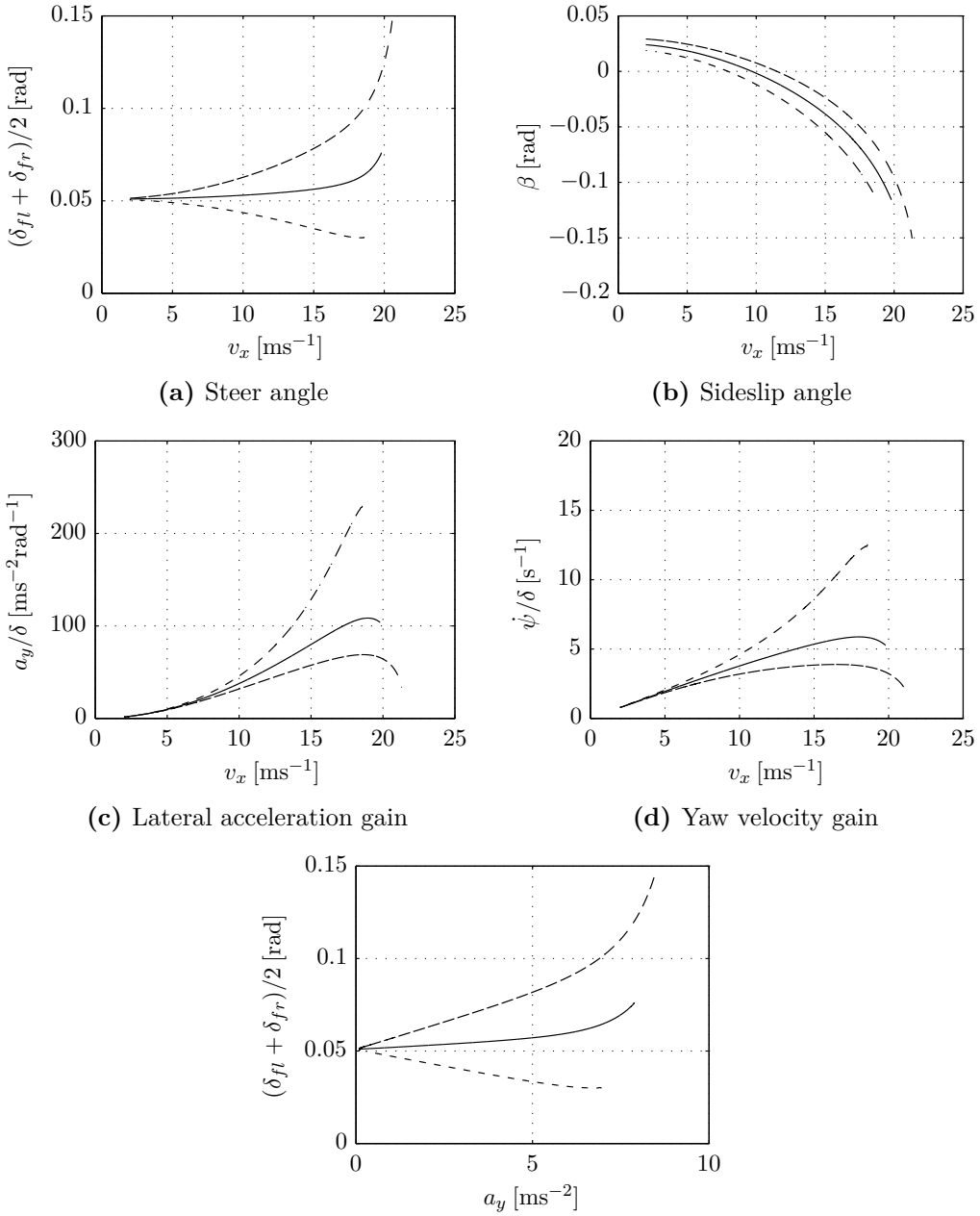

(a) Steer angle

(b) Sideslip angle

(c) Lateral acceleration gain

(d) Yaw velocity gain

(e) Understeer gradient

Figure 5.1: Handling characteristics. – – – *Vehicle A*; —— *Vehicle B*; – · – · *Vehicle C*.

the linear definition, which is valid at low speed, rearranging Equation (5.7) and noting that $R = v_x^2/a_y$, the lateral acceleration gain is shown to be

$$\frac{a_y}{\delta} = \frac{v_x^2}{l + Kv_x^2}. \tag{5.13}$$

This handling property is dominant at high speeds because v_x^2 appears in the numerator. For a neutrally steered vehicle with $K = 0$, the lateral acceleration gain is linearly dependent on the square of vehicle speed. An US vehicle with $K > 0$ will have a lateral acceleration less than the NS vehicle, and vice versa for an OS vehicle with $K < 0$. In the case of an oversteer vehicle, there is a speed at which the denominator is equal to zero, which means an infinite gain. This is known as the *critical speed* and is the speed above which the vehicle exhibits an oscillatory instability.

Considering the lateral acceleration results from the multibody model, Figure 5.1c shows results that broadly correspond to the linear analysis. With a constant steer angle, the lateral acceleration of *Vehicle C*, which is OS, increases with speed, and keeps increasing until the vehicle can no longer maintain the desired path. *Vehicle A*'s lateral acceleration rises slower than *Vehicle C*, then peaks and subsequently falls away, for no more lateral acceleration can be gained through an increase of the steer angle. At high speed, *Vehicle B* also exhibits some understeer tendency.

Yaw Rate Gain The second reason for a driver to apply a steer input to a vehicle is to cause a change in the yaw angle of the vehicle by introducing a yaw velocity. Thus, the rate at which a steer input causes a yaw velocity is also an important handling quality of a vehicle, and is known as the yaw velocity gain, or yaw rate gain. Again, the linear definition will be used to quantify the gain for low speeds. Rearranging Equation (5.7) and noting that $a_y = v_x^2/R$ and $R = v_x/\dot{\psi}$, thus $a_y = v_x\dot{\psi}$, the yaw rate gain is shown to be

$$\frac{\dot{\psi}}{\delta} = \frac{v}{l + Kv_x^2}. \tag{5.14}$$

For a NS vehicle, the yaw rate gain is linear and proportional to velocity, v. For an OS vehicle with $K < 0$, the denominator reduces in magnitude with increasing speed until the gain becomes infinite at the *critical speed*, whilst for an US vehicle, the reaches a maximum at the *characteristic speed* and subsequently falls away.

Figure 5.1d shows the yaw rate gain from the simulation results of the multibody model. *Vehicle B* does indeed have a linear yaw rate response for much of its speed range, but the response reduces at it nears its limit of adhesion. *Vehicles A* and *C* exhibit typical understeer and oversteer characteristics, respectively.

Understeer Gradient Finally, using Equation (5.7), the understeer gradient of any vehicle can be calculated from the gradient of a plot of steer angle against lateral acceleration. Figure 5.1e shows this plot for the multibody models of *Vehicles A, B* and *C*. The vehicles appear to have approximately linear characteristics when the lateral acceleration is below $6\,\mathrm{m\,s^{-2}}$ ($\approx 0.6\,\mathrm{g}$), which occurs at a speed of $17\,\mathrm{m\,s^{-1}}$ in this case. At moderate speeds, the understeer gradients are 3.94×10^{-3}, -9.89×10^{-4} and -5.74×10^{-3} for *Vehicles A, B* and *C*, respectively.

It is interesting to see what happens as the speeds increase further: *Vehicles A* and *B* become *more* understeer, and the steer angle is increased to try and maintain the path, while *Vehicle C* becomes slightly *less* oversteer. The vehicle does not reach the *critical speed* predicted from the linear derivation, where the steer angle would be zero, instead deviating from the path before this point.

The speed at which each of the vehicles become uncontrollable in this situation—the maximum speed plotted on the graphs—is higher for *Vehicle A* than for the *Vehicles B* and *C*. This is because as the rear tyres of *Vehicle C* begin to saturate, the vehicle starts to spin and, thus, approaches an infinite yaw rate gain. A vehicle with a higher *understeer gradient* suffers less and remains controllable.

Standard Vehicle Model Summary In summary, at moderate speeds the multibody model predicts similar handling characteristics as the linear models; however, in all cases, the vehicles are slightly more understeer than their linear counterparts, especially at higher speed. This is due to the effect of aligning moments and combined lateral and longitudinal slip at the tyres.

Front–Rear Torque Vectoring (4WD)

The same three vehicles, with the weight distributions described in Table 5.1, are used to investigate the effect that front–rear torque distribution has on automobiles handling. An ideal torque vectoring driveline would be able to split torque in any ratio between the front and rear wheels. The extreme case is where 100 % of the drive torque can be sent to the wheels of the front or rear axles; thus, comparing a Front Wheel Drive (FWD) vehicle and a Rear Wheel Drive (RWD) vehicle, with all other parameters held constant, will give the range of handling characteristic that can be achieved for that vehicle. The three vehicles specified in Table 5.1 perform the same 50 m constant radius turn at a steadily increasing speed, as specified in Table 5.2. Common vehicle parameters are given in Appendix C.1. For comparison, the vehicles with equal distribution are also plotted.

Figure 5.2 shows handling characteristics plots for *Vehicles A, B* and *C*, with a range for each vehicle shown as a shaded area. In these cases, at moderate speeds of up to $13\,\mathrm{m\,s^{-1}}$, the range of handling characteristics made available through varying

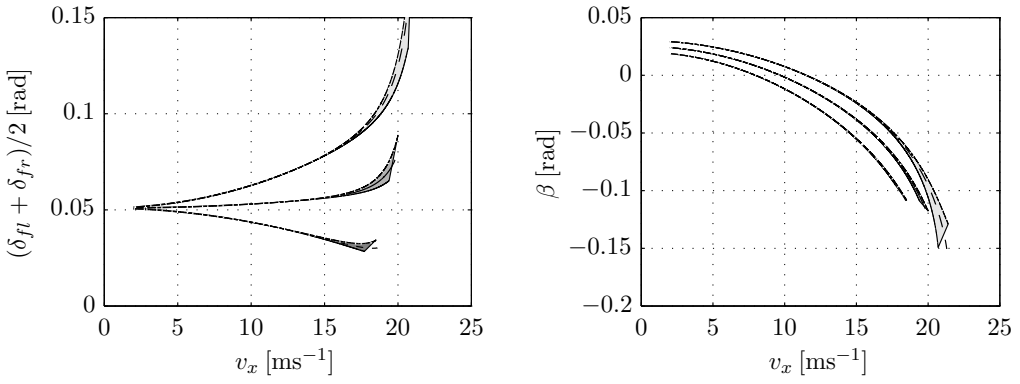

(a) Steer angle

(b) Sideslip angle

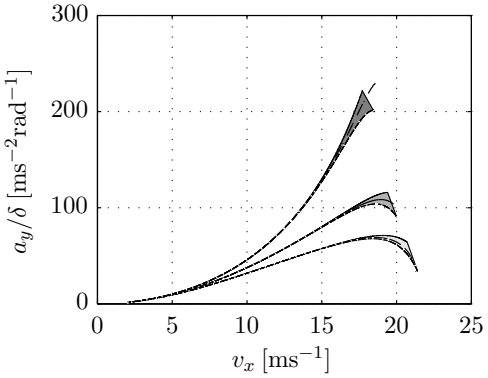

(c) Lateral acceleration gain

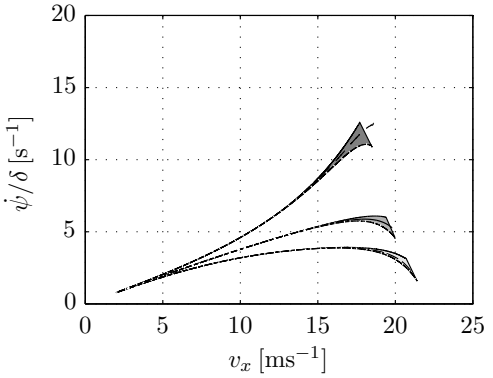

(d) Yaw velocity gain

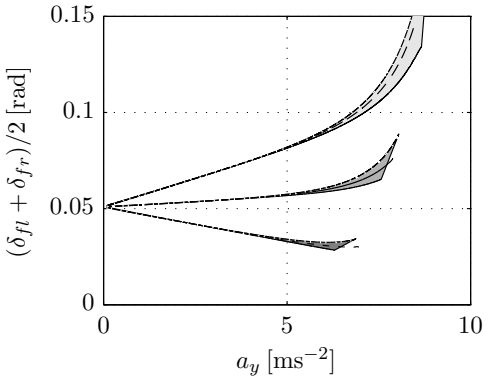

(e) Understeer gradient

Figure 5.2: Handling characteristics with varying front–rear torque distribution. – – – *Vehicle A*; ——— *Vehicle B*; –·–·– *Vehicle C*; ------ 100 % front torque bias in each case.

the front–rear torque distribution is negligible: FWD, Four Wheel Drive (4WD) and RWD vehicles exhibit the same characteristics for each weight distribution.

Above this speed, the torque distribution has a small effect: for each weight distribution, the FWD vehicle for is *more* understeer than the four-wheel drive vehicle, while the RWD vehicle is *more* oversteer. This has associated effects on the lateral acceleration gains and yaw rate gains, as shown in Figures 5.2c and 5.2d. At these higher speeds, the tyres need to generate higher forces to maintain the desired radius. In this manoeuvre, the maximum speed is reached when the lateral tyre forces have saturated and the radius of curvature is no longer achieved. The torque distribution affects the longitudinal slip at the wheel, which, in turn, affects the maximum lateral tyre force because of the combined slip situation.

For *Vehicle A*, which has US static handling characteristics, the sideslip angle, and therefore tyre forces, at the front wheels are greater than at the rear. Putting the drive torque through the front wheels increases the longitudinal slip, further reducing the capacity of the tyres to generate lateral force and making the vehicle *more* understeer. Conversely, transferring torque away from the front wheels increases their capacity to generate lateral force, reducing the understeer tendency. Similarly, *Vehicle C*, which is OS naturally, has greater sideslip angles at the rear; transferring power away from these wheel increases their capacity to generate lateral force and reduces the oversteer.

The change in steady-state vehicle handling characteristics with front–rear torque distribution is, however, small, in comparison with the effect of weight distribution.

Left–Right Torque Vectoring (4WD)

Again, *Vehicles A, B* and *C* from Table 5.1 are used in simulations of the same 50 m constant radius manoeuvre; however, this time the drive torque is varied between the left and right wheels, assuming that the drive torque is distributed equally between the front and rear wheels, i.e., an ideal 4WD torque vectoring driveline. Plots for vehicles with 100 % of the drive torque at the inside and outside wheels are shown with that of the standard equally-distributed 4WD vehicle.

Comparison of Figure 5.3 with Figure 5.2 shows how the effect of varying the torque distribution between the left and right wheels is much greater than for front–rear torque distribution. In general, transferring the torque to the inside wheel makes a vehicle *more* understeer than the standard vehicle, and vice versa for transferring torque to the outside wheel. Interestingly, the effect can be seen at moderate speeds as it is not solely dependent on the combined slip situation.

By considering Figures 5.3c and 5.3d, left–right torque vectoring is shown to be able to bring the lateral acceleration gain and yaw rate gain of *Vehicles A* and *C* much closer to the plots for the NS *Vehicle B*. This is achieved for the understeer *Vehicle A*

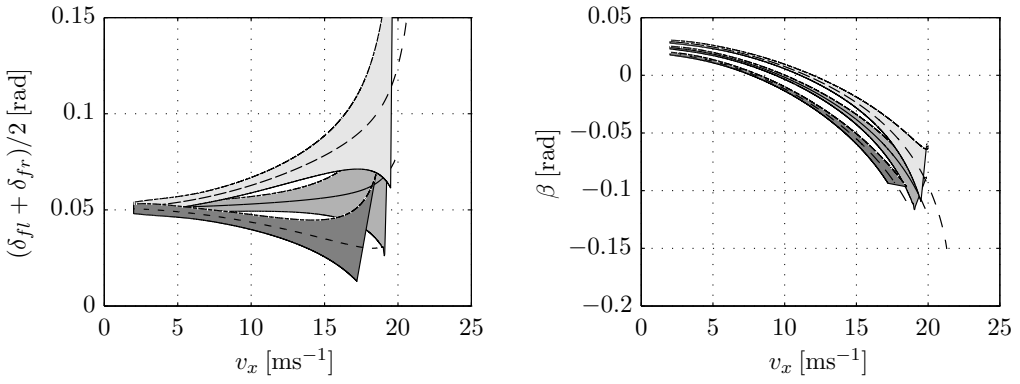

(a) Steer angle

(b) Sideslip angle

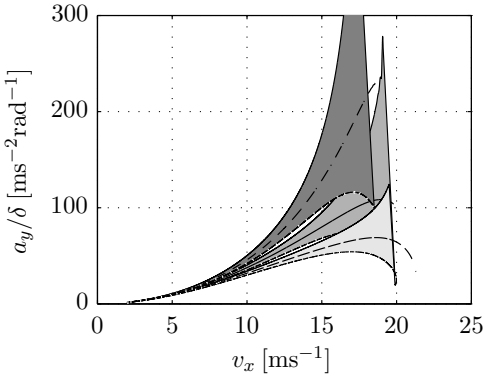

(c) Lateral acceleration gain

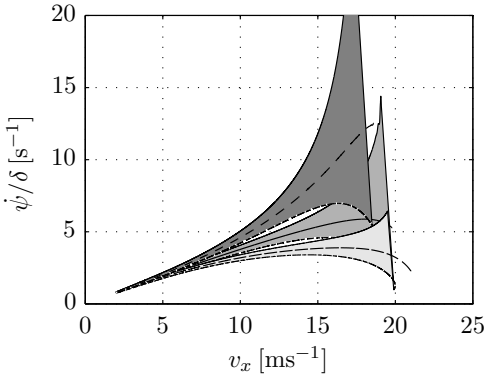

(d) Yaw velocity gain

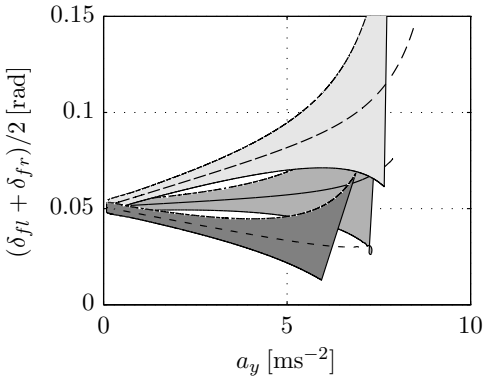

(e) Understeer gradient

Figure 5.3: Handling characteristics with varying left–right torque distribution (4WD). – – – *Vehicle A*; ——— *Vehicle B*; –·–·– *Vehicle C*; ------ 100 % inside wheel torque bias in each case.

by biasing the torque to the outside wheels, where the yaw moment generated by the difference in longitudinal tyre forces acts to assist in the yawing of the vehicle. Although, by considering the gradient of the steer angle against lateral acceleration plot in Figure 5.3e for the vehicle with torque at the inside wheels, one can see that the understeer gradient of *Vehicle A* becomes negative at $4.5\,\mathrm{m\,s^{-2}}$, meaning that the vehicle is demonstrating oversteer tendency. This contributes the vehicle becoming unstable at a lower speed than its counterparts with equal or outside wheel torque biasing.

Transferring torque to the inside wheels of *Vehicle A* results in the US characteristic being exacerbated, and the effect increases with speed.

For *Vehicle C*, which is naturally OS, varying the torque distribution between the left and right wheels again has a large effect on handling, as shown by the dark grey ranges of Figures 5.3c and 5.3d. The vehicle with 100 % of the drive torque applied at the inside wheels has lateral acceleration and yaw rate gains approaching those of the NS vehicle. The gradient in Figure 5.3e for *Vehicle C* with drive torque to only the inside wheels shows that the *understeer gradient* of this vehicle is zero at $5\,\mathrm{m\,s^{-2}}$.

Transferring the drive torque to the outside wheels of *Vehicle C* makes its oversteer characteristic worse, and reduces the speed at which it becomes unstable as the torque at the outside wheel acts to increase the yaw moment generated by the loading situation about the centre of mass.

Vehicle B offers good potential for altering the handling characteristics through varying the distribution of torque. An US or OS handling characteristic could be chosen according to the driver's preference in a given situation.

Left–Right Torque Vectoring (FWD and RWD)

As described in Chapter 2, some vehicles that are solely FWD have torque vectoring differentials for controlling the torque distribution between the left and right wheels. Figure 5.4 shows the handling characteristics for an ideal vehicle of that description. A corresponding RWD vehicle with left–right torque vectoring is shown in Figure 5.5. In each case, the FWD or RWD vehicle with equal torque distribution is shown for comparison.

The plots in Figures 5.4 and 5.5 are very similar, especially at low speed, which is corroborated by the fact that varying the front–rear distribution has little effect at low speed (Figure 5.2). At higher speeds, the FWD vehicles have slightly higher understeer gradients than the 4WD vehicles, and the RWD vehicles slightly lower understeer gradients.

In both cases, however, the range of handling values made available by torque vectoring is similar to that of the 4WD vehicle (Figure 5.3), but the maximum speed

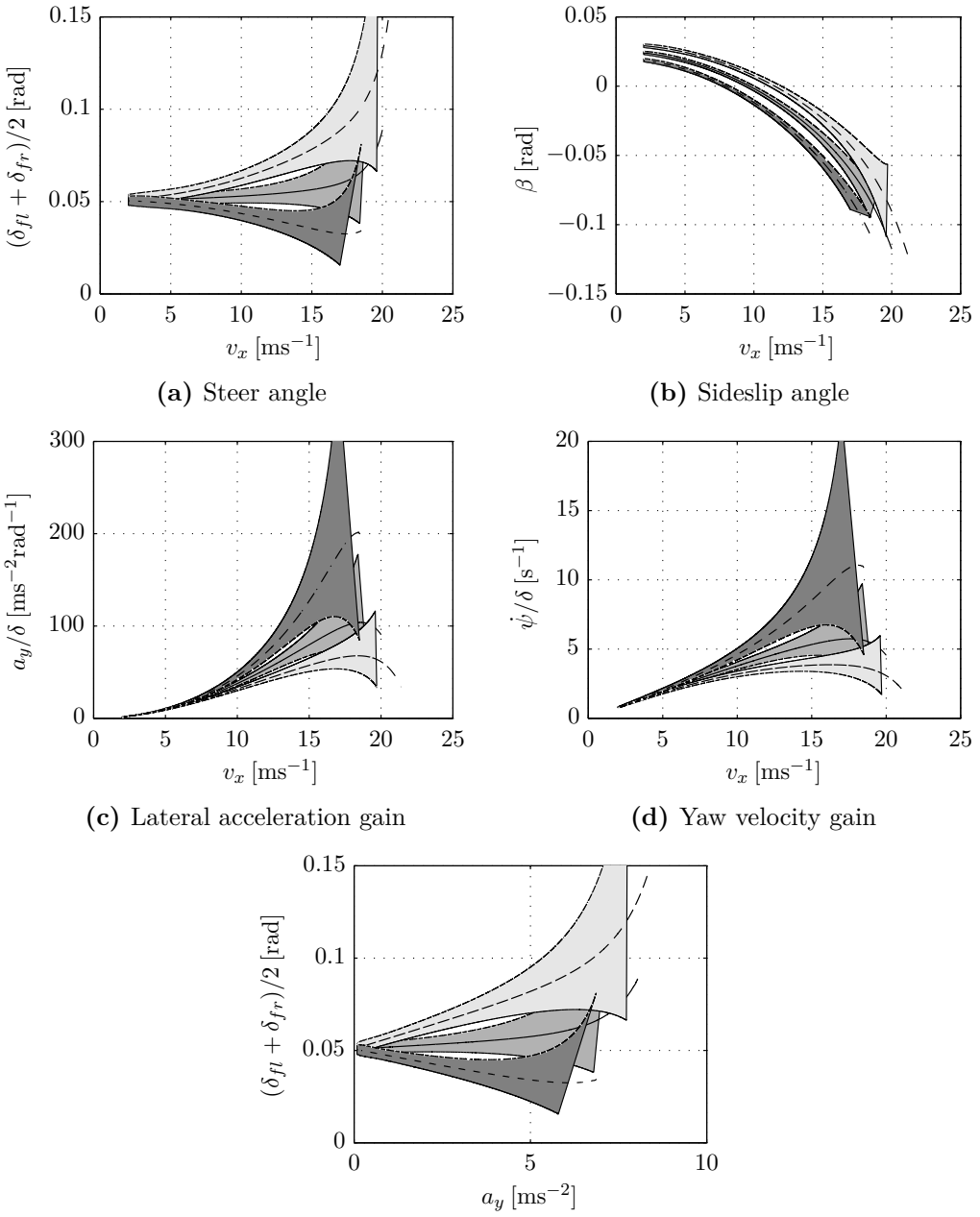

(a) Steer angle

(b) Sideslip angle

(c) Lateral acceleration gain

(d) Yaw velocity gain

(e) Understeer gradient

Figure 5.4: Handling characteristics with varying left–right torque distribution (FWD). – – – *Vehicle A*; ——— *Vehicle B*; –·–·– *Vehicle C*; ------ 100 % inside wheel torque bias in each case.

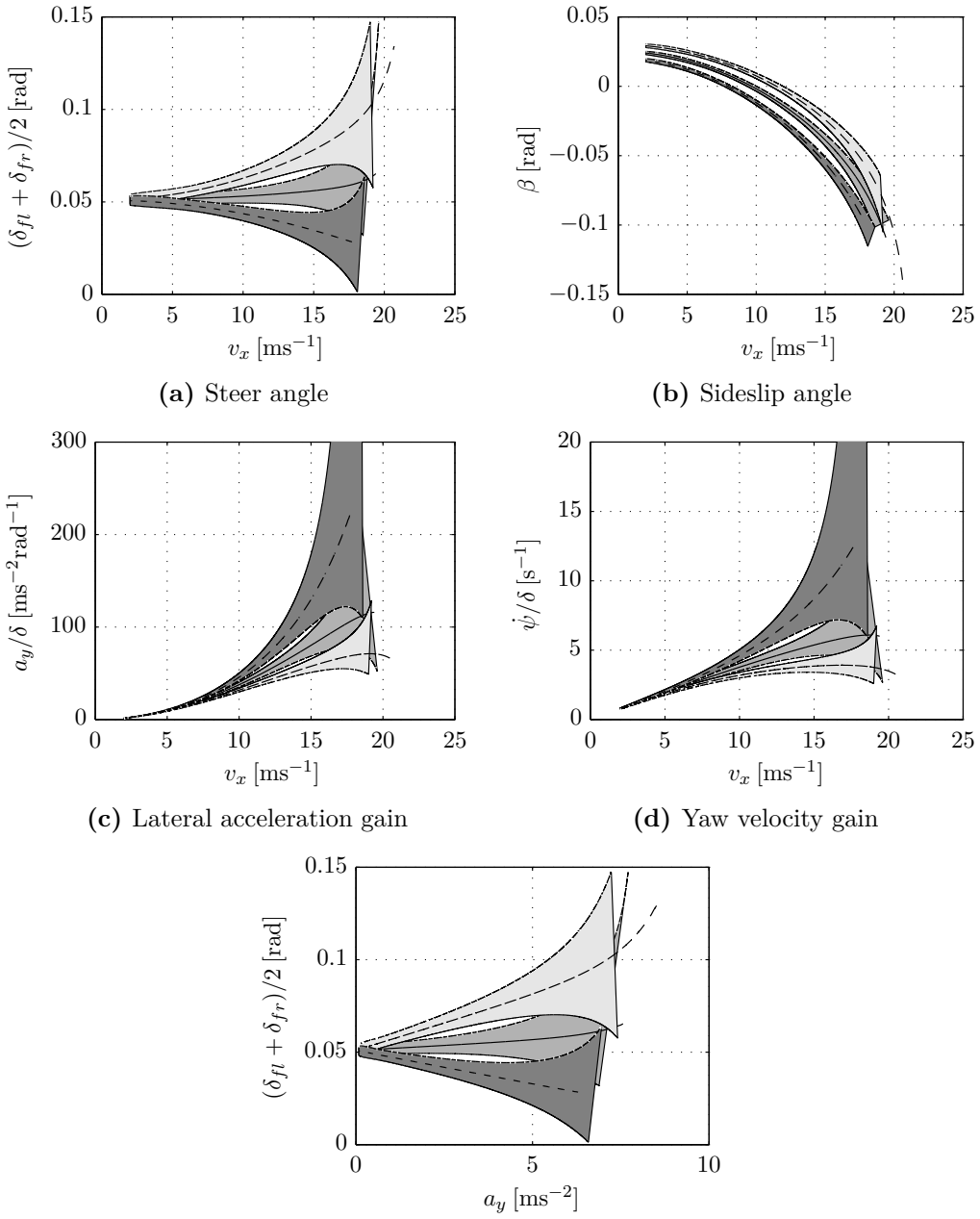

(a) Steer angle

(b) Sideslip angle

(c) Lateral acceleration gain

(d) Yaw velocity gain

(e) Understeer gradient

Figure 5.5: Handling characteristics with varying left–right torque distribution (RWD). – – – *Vehicle A*; ——— *Vehicle B*; –·–·– *Vehicle C*; ------ 100 % inside wheel torque bias in each case.

reached before the vehicle becomes uncontrollable is slightly lower. This is due to saturation of the tyre forces of the single driving wheel.

Automobile Steady-State Handling Investigation Summary

This section has presented the results of an investigation into the steady-state handling of four-wheeled vehicles, with the effect of front–rear and left–right torque distribution demonstrated. Equations were presented for the handling characteristics derived from the linear *bicycle model*, and their application to real vehicles commented upon. The multibody model was used to simulate standard handling tests and the results used to draw conclusions about their handling properties. The effect of front–rear torque vectoring was shown to be negligible at low speeds and small at high speed, because it depends on the combined slip situation at the tyres. Left–right torque vectoring has much more effect throughout the moderate speed range because a yaw moment can be generated by the difference in tractive forces.

5.1.2 Motorcycles

This section will present the results of an investigation into the steady-state handling of motorcycles. Firstly, a four-Degree-of-Freedom (DoF) dynamic model will be used to analyse the effect of a steer torque input on the motorcycle steering system, then equations are derived to calculate the steady-state response. Finally, the multibody model is used to further the handling investigation to include the effect of varying torque distribution.

Steady-State Handling Results

A four-degree-of-freedom dynamic motorcycle model was developed by Seffen *et al.* [59] after Sharp [63], with equations of motion of the form

$$\mathbf{M}\begin{bmatrix}\ddot{y}\\ \ddot{\psi}\\ \ddot{\delta}\\ \ddot{\gamma}\end{bmatrix} + \mathbf{N}\begin{bmatrix}\dot{y}\\ \dot{\psi}\\ \dot{\delta}\\ \dot{\gamma}\end{bmatrix} + \mathbf{P}\begin{bmatrix}\delta\\ \gamma\end{bmatrix} + \mathbf{G}\left[\tau_s\right] = 0, \qquad \text{(3.43 revisited)}$$

where the input to the system is τ, the torque applied to the handlebars by the rider. The MATLAB code, including parameters, is given in Appendix B.5. A motorcycle is simulated at various speeds ranging from 1 to $25\,\mathrm{m\,s^{-1}}$ and steer torques from 0 to $1\,\mathrm{N\,m}$. In each case, the model is allowed 60 s to reach a steady state.

Steady-state results obtained from the given parameters are shown in Figure 5.6. Figure 5.6a shows that the steer angle reduces with speed for a given steer torque,

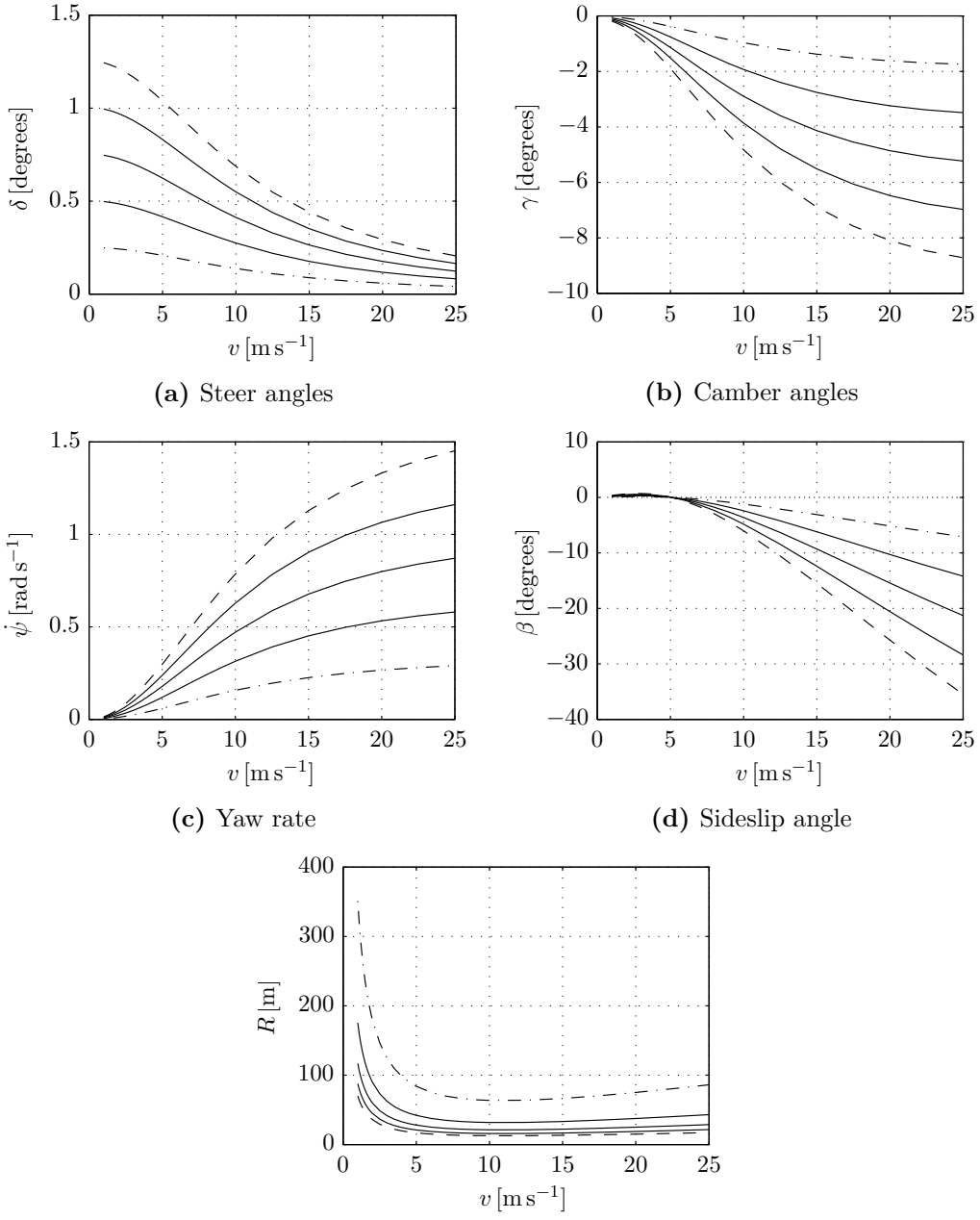

(a) Steer angles

(b) Camber angles

(c) Yaw rate

(d) Sideslip angle

(e) Turn Radius

Figure 5.6: Steady-state results of the four-DoF motorcycle model for various steer torques, τ_s [N m]. $\cdots\cdot$0; $-\cdot-\cdot$0.2; ——0.4; ——0.6; ——0.8; $-\,-\,-$1.

but steer angle is proportional to steer torque at all speeds. Camber angle increases with speed for a given steer torque, and is also proportional to steer torque, as shown in Figure 5.6b. Similar increases are seen in yaw rate and sideslip angle in Figures 5.6c and 5.6d, again with proportionality to steer torque. The sideslip angle is positive at low speed when the rear wheel corners with a smaller radius than the front, leading to a small lateral velocity of the centre of mass. At high speeds, the sideslip of the wheels becomes dominant and the sideslip angle at the centre of mass becomes negative.

With the parameters and code given, results for sideslip angle and radius (Figures 5.6d and 5.6e) do not appear to be sensible; however, the fact that the model predicts that the outputs are proportional to steer torque and, therefore, steer angle means that it is reasonable to consider gains for yaw rate, sideslip angle and lateral acceleration in a way that is analogous to the automobile.

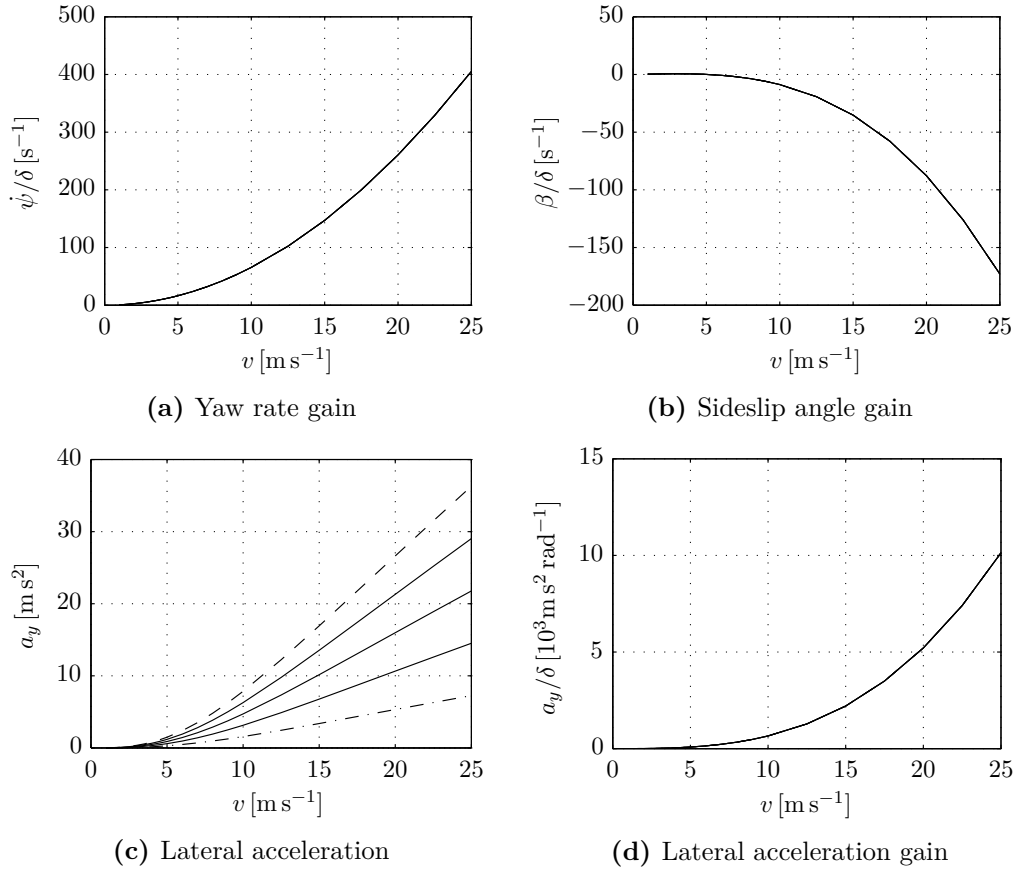

(a) Yaw rate gain **(b)** Sideslip angle gain

(c) Lateral acceleration **(d)** Lateral acceleration gain

Figure 5.7: Steady-state results of the four-DoF motorcycle modelfor various steer torques, $\tau_s\,[\mathrm{N\,m}]$. · · · ·0; – · – · 0.2; —— 0.4; —— 0.6; —— 0.8; – – – 1.

Yaw rate gain and sideslip angle gain are found by dividing the quantities by the steer angle, δ, plots of which are shown in Figures 5.7a and 5.7b. Figure 5.7c

shows the lateral acceleration of the motorcycles, and Figure 5.7d shows the lateral acceleration gain after division by the steer angle.

Linear Investigation

Using a similar approach to the automobile model, handling characteristics for the linear motorcycle model are obtained, and used for comparison with the multibody motorcycle model for torque vectoring investigations.

The tyre lateral forces are assumed to vary linearly with sideslip angle and camber angle with the stiffnesses, K_α and K_γ, respectively. In this linear model, the motorcycle is assumed to have two degrees of freedom: the yaw angle, ψ, and the sideslip angle, β, which is equivalent to the lateral velocity. In steady-state cornering, $\dot{v}_y = \dot{\beta} = \ddot{\psi} = 0$, and the equations of motion for a cornering motorcycle are

$$\begin{aligned} m\dot{\psi}v_x &= \left(K_{\alpha f} + K_{\alpha b}\right)\beta + \\ &\left(\frac{l_f K_{\alpha f} - l_b K_{\alpha b}}{v_x} + \frac{\left(K_{\gamma f} + K_{\gamma b}\right)v_x}{g}\right)\dot{\psi} - K_{\alpha f}\delta \qquad \text{(3.41 revisited)} \\ 0 &= \left(l_f K_{\alpha f} - l_b K_{\alpha b}\right)\beta + \\ &\left(\frac{l_f^2 K_{\alpha f} + l_b^2 K_{\alpha b}}{v_x} + \frac{\left(l_f K_{\gamma f} - l_b K_{\gamma b}\right)v_x}{g}\right)\dot{\psi} - l_f K_{\alpha f}\delta, \qquad \text{(3.42 revisited)} \end{aligned}$$

which can be written in matrix form

$$\begin{bmatrix} K_{\alpha f} + K_{\alpha b} & \frac{l_f K_{\alpha f} - l_b K_{\alpha b}}{v_x} + \frac{(K_{\gamma f} + K_{\gamma b})v_x}{g} + m v_x \\ l_f K_{\alpha f} - l_b K_{\alpha b} & \frac{l_f^2 K_{\alpha f} + l_b^2 K_{\alpha b}}{v_x} + \frac{(l_f K_{\gamma f} - l_b K_{\gamma b})v_x}{g} \end{bmatrix} \begin{Bmatrix} \beta \\ \dot{\psi} \end{Bmatrix} = \begin{Bmatrix} K_{\alpha f}\delta \\ K_{\alpha f} l_f \delta \end{Bmatrix}. \quad (5.15)$$

Following inversion of the matrix and simplification, the equations for calculating the steady-state sideslip angle and yaw rate of the motorcycle are

$$\beta = \left(\frac{1 - \left(\frac{m}{l}\frac{l_f}{l_b K_{\alpha b}} + \frac{1}{g}\frac{K_{\gamma b}}{l_b K_{\alpha b}}\right)v_x^2}{1 - \left(\frac{m}{l^2}\frac{K_{\alpha f} l_f - K_{\alpha b} l_b}{K_{\alpha f} K_{\alpha b}} + \frac{1}{gl}\frac{K_{\gamma f} K_{\alpha b} - K_{\gamma b} K_{\alpha f}}{K_{\alpha f} K_{\alpha b}}\right)v_x^2}\right)\frac{l_b}{l}\delta \quad (5.16)$$

$$\dot{\psi} = \left(\frac{1}{1 - \left(\frac{m}{l^2}\frac{K_{\alpha f} l_f - K_{\alpha b} l_b}{K_{\alpha f} K_{\alpha b}} + \frac{1}{gl}\frac{K_{\gamma f} K_{\alpha b} - K_{\gamma b} K_{\alpha f}}{K_{\alpha f} K_{\alpha b}}\right)v_x^2}\right)\frac{v_x}{l}\delta. \quad (5.17)$$

By comparison with the equivalent equations for the vehicle model in Equations (5.4) and (5.5), it is clear that the terms introduced by the effect of camber are those

beginning with $1/gl$. Notice that sideslip angle and yaw rate are still proportional to steer angle. Through the substitution of $R = v_x/\dot{\psi}$ and $a_y = v_x^2/R$ into Equation (5.17), an equation for the *understeer gradient* of the motorcycle, K_{MC}, can be obtained:

$$\begin{aligned}\delta &= \frac{l}{R}\left(1 - \left(\frac{m}{l^2}\frac{K_{\alpha f}l_f - K_{\alpha b}l_b}{K_{\alpha f}K_{\alpha b}} + \frac{1}{gl}\frac{K_{\gamma f}K_{\alpha b} - K_{\gamma b}K_{\alpha f}}{K_{\alpha f}K_{\alpha b}}\right)v_x^2\right) \\ &= \frac{l}{R} - \left(\frac{m}{l^2}\frac{K_{\alpha f}l_f - K_{\alpha b}l_b}{K_{\alpha f}K_{\alpha b}} + \frac{1}{gl}\frac{K_{\gamma f}K_{\alpha b} - K_{\gamma b}K_{\alpha f}}{K_{\alpha f}K_{\alpha b}}\right)a_y \\ &= \frac{l}{R} + K_{\mathrm{MC}}a_y.\end{aligned} \tag{5.18}$$

The handling characteristic equation for the motorcycle can be compared with that of the automobile model to investigate how the camber stiffnesses of the tyres affect the cornering radius of a motorcycle. The second term of the motorcycle understeer gradient adds to the first term, which is the understeer gradient without camber influences; thus when the second term is positive, the motorcycle will be *more* understeer than the standard vehicle, and vice versa. Increasing the camber stiffness of the front tyre, $K_{\gamma f}$ or decreasing the rear camber stiffness, $K_{\gamma b}$, would make the motorcycle *more* understeer, and the radius of turn would reduce for a given steer angle. Decreasing the camber stiffness of the front tyre, $K_{\gamma f}$, or increasing the camber stiffness of the rear tyre, $K_{\gamma b}$, would have the opposite effect.

Weight Distribution Effects In order to investigate the effect of weight-distribution on the handling of motorcycle, simulations of the two-DoF model were made with the weight distributions in Table 5.3 and other parameters in Table 5.4. Results are plotted in Figure 5.8 for a steer angle, δ, of 0.02 rad and speeds ranging from 1 to 20 $\mathrm{m\,s^{-1}}$.

Table 5.3: Parameter values for *Motorcycles A, B* and *C*

Parameter	Symbol	Value		
		Motorcycle A	*Motorcycle B*	*Motorcycle C*
Front axle to CoG	l_f	0.576 m	0.770 m	0.964 m
Back axle to CoG	l_b	0.964 m	0.770 m	0.576 m

There is a large variation in the predicted radii of the motorcycles, especially at higher speeds. The motorcycle with equal weight distribution, *Motorcycle B*, is understeer in this case, as Figure 5.8a shows a radius that increases with speed. This is because of the relative lateral and camber stiffnesses of the tyres. Compared to

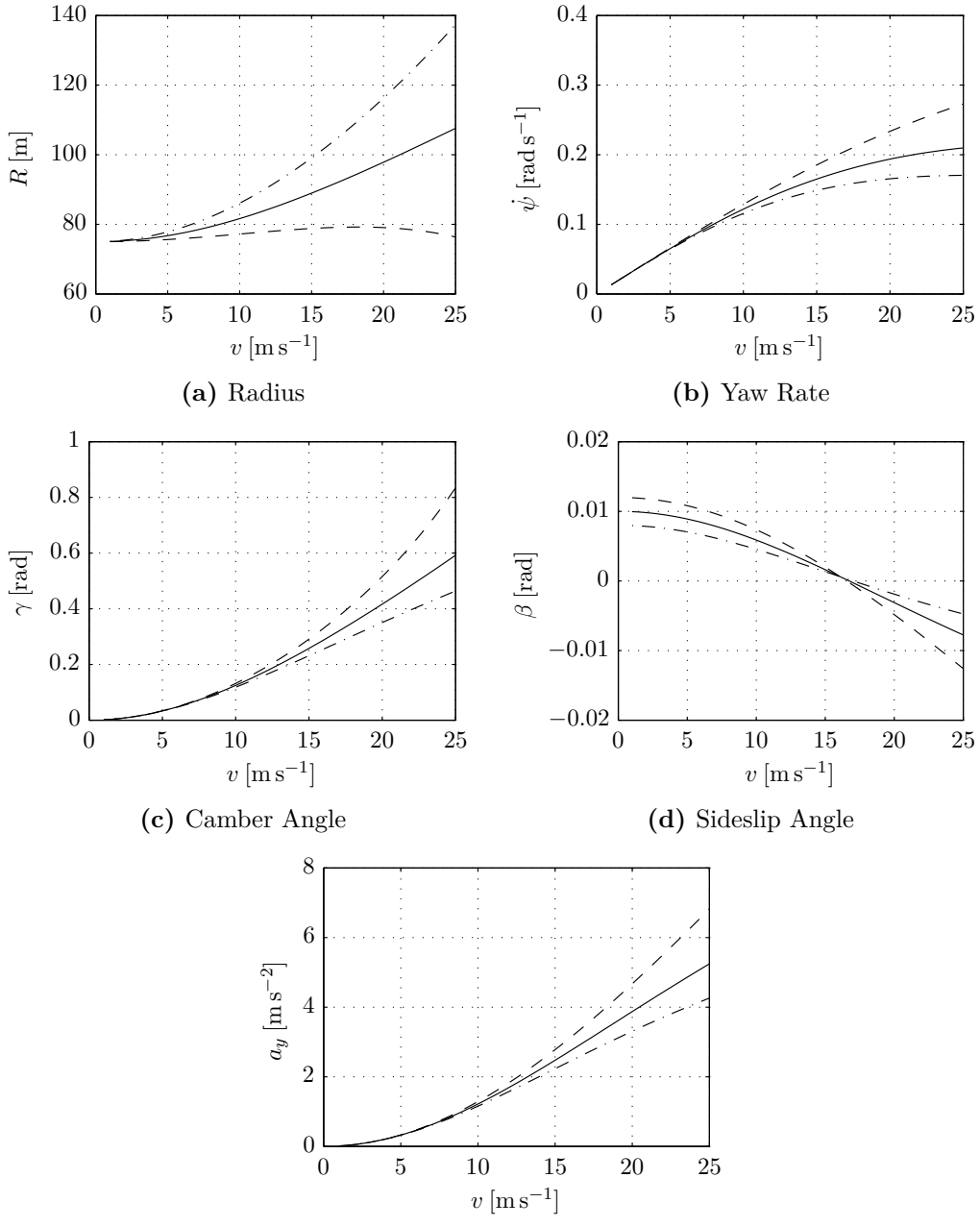

(a) Radius

(b) Yaw Rate

(c) Camber Angle

(d) Sideslip Angle

(e) Lateral Acceleration

Figure 5.8: Effect of weight-distribution on linear motorcycle model handling characteristics with a steer angle of 0.02 rad. – – – *Motorcycle A*; —— *Motorcycle B*; – · – · *Motorcycle C*.

Table 5.4: Parameter values for steady-state motorcycle simulations

Parameter	Symbol	Value
total mass	m	$150\,\mathrm{kg}$
wheelbase length	l	$1.54\,\mathrm{m}$
graviational acceleraion	g	$9.81\,\mathrm{m\,s^{-2}}$
front tyre lateral stiffness	$K_{\alpha f}$	$54575\,\mathrm{N\,rad^{-1}}$
front tyre camber stiffness	$K_{\gamma f}$	$24725\,\mathrm{N\,rad^{-1}}$
rear tyre lateral stiffness	$K_{\alpha r}$	$2927.1\,\mathrm{N\,rad^{-1}}$
rear tyre camber stiffness	$K_{\gamma r}$	$1385.7\,\mathrm{N\,rad^{-1}}$

this, *Motorcycles A* and *C* are more oversteer and more understeer respectively. Here, the relative lateral and camber stiffnesses of the tyres are significantly influencing the handling characteristics meaning the vehicle with the rear-heavy weight distribution is actually more understeer, and vice versa.

The side slip angle, which is positive at low speed, becomes negative at high speed as shown in Figure 5.8d. Interestingly, in this case, the sideslip angle plots cross each other as both camber and lateral stiffnesses affect the results; this is not the case for the four-wheeled vehicle.

Tyre Parameter Effects The next set of simulations looks at the influence of tyre lateral and camber stiffnesses on the motorcycle handling properties. *Motorcycle C*, which most closely represents the motorcycle used in the multibody simulations, is simulated for an increase in each of the four possible tyre parameters, viz., front camber stiffness, rear camber stiffness, front lateral stiffness and rear lateral stiffness. Results for a steer angle of $0.02\,\mathrm{rad}$ are shown in Figure 5.9.

For a given steer angle, the motorcycle in question has a smaller turn radius, and therefore a higher yaw rate, when either the front camber stiffness is increased or the rear lateral stiffness is increased. The turn radius is larger following an increase in either the rear camber stiffness or the front lateral stiffness. The results are not as intuitive as the vehicle model because of the interaction between the camber thrust and lateral slip tyre forces.

Concerning the sideslip angle, shown in Figure 5.9d, it appears that the changes made at the front wheel affect the magnitude of the sideslip, whereas changes made at the rear add to, or subtract from, the sideslip angle regardless of its sign.

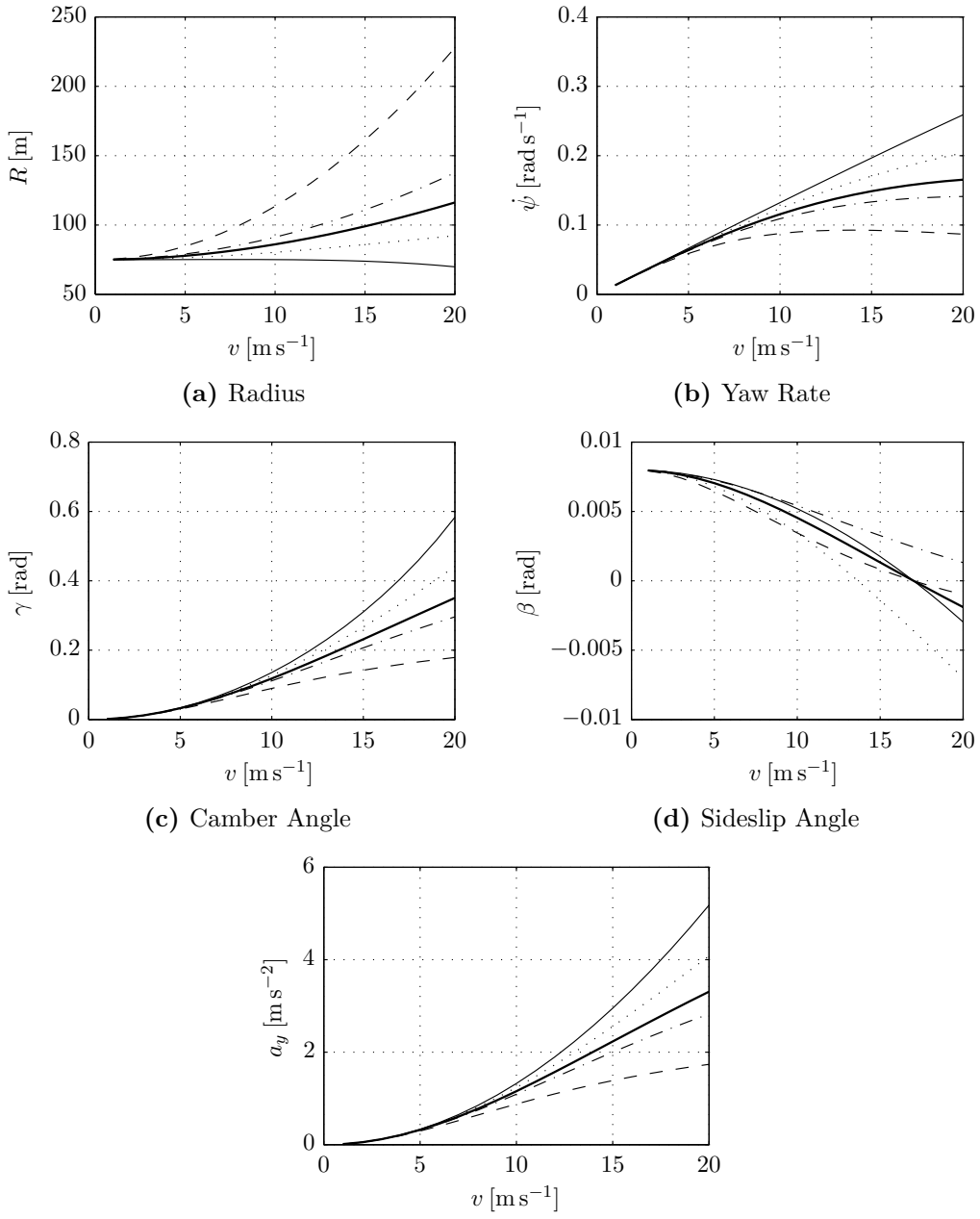

(a) Radius **(b)** Yaw Rate

(c) Camber Angle **(d)** Sideslip Angle

(e) Lateral Acceleration

Figure 5.9: Effects of tyre characteristics on linear motorcycle model handling characteristics with a steer angle of 0.02 rad. ——— Standard; —— $2K_{\alpha f}$; $-\cdot-\cdot$ $2K_{\alpha r}$; $- - -$ $2K_{\gamma f}$; $\cdots$ $1.2K_{\gamma r}$.

Application to Real Motorcycles

The multibody model defined in Section 3.4.4, with parameters specified in Appendix C.2, was controlled to take corners at three different speeds, as defined in Table 5.5.

Table 5.5: Parameter values for simulations

Parameter	Symbol	Value		
		Simulation 1	Simulation 2	Simulation 3
speed	v_x	$12.5\,\mathrm{m\,s^{-1}}$	$15\,\mathrm{m\,s^{-1}}$	$17.5\,\mathrm{m\,s^{-1}}$
radius	R	$50\,\mathrm{m}$	$100\,\mathrm{m}$	$150\,\mathrm{m}$

Although the results in Figure 5.10 do not match exactly those of the linear model, they are, at least, qualitatively similar. They do not match exactly for reasons including the effects of aligning moments, gyroscopic moments, tyre toroidal radii, and aerodynamic lift and drag. This demonstrates the importance of including these effects in a simulation that attempts to investigate subtle changes in handling characteristic.

Torque Vectoring in Motorcycles

Finally, the effect of torque vectoring is demonstrated using the multibody motorcycle model. In this situation, the motorcycle is controlled to corner at a specified yaw rate at a specific speed, and therefore achieves a constant radius turn. The speed is controlled to $12.5\,\mathrm{m\,s^{-1}}$. This situation is similar to 'Method One' of ISO4138 [26] for automobiles.

The torque distribution ratio, T_f, determines the amount of torque delivered to the front wheel. By varying the ratio from 0 to 1 in increments of 0.1, the effect of transferring power from the rear wheel to the front can be analysed.

Figure 5.11a shows the effect of torque distribution on the steer angle required to make a turn of constant radius. It is clear that as more torque is transferred to the front wheel, less steer angle is required. This has an associated reduction in steer torque. The magnitude of the change is small, however, at around 0.5 %. The motorcycle, which, according the the linear model, is oversteer, becomes less oversteer as more torque is transferred to the front wheel.

There is also a slight reduction of around 0.5 % in sideslip angle as the front wheel receives more power. The sideslip angle gain, shown in Figure 5.11b shows only a small change over the range, and has a maximum at $T_f = 0.2$. Yaw rate gain

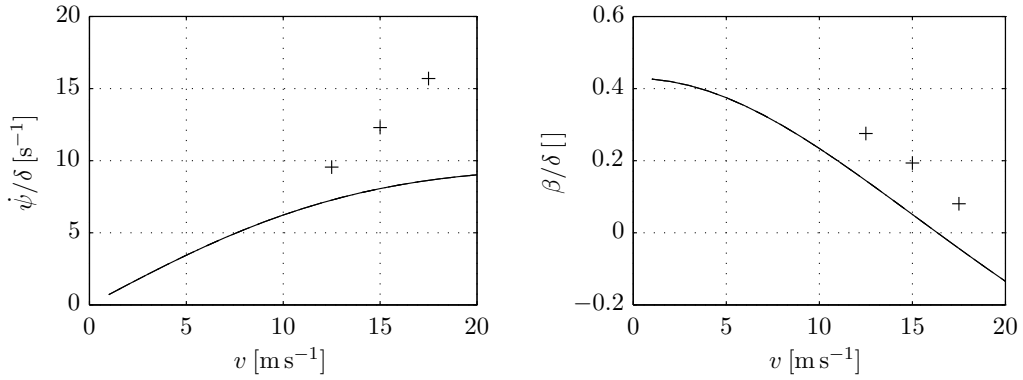

(a) Yaw Rate Gain

(b) Sideslip Angle Gain

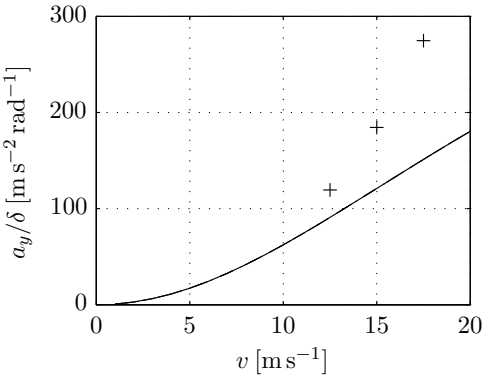

(c) Lateral Acceleration Gain

Figure 5.10: Multibody motorcycle handling diagrams. ——Linear Model; +++ Multibody Model.

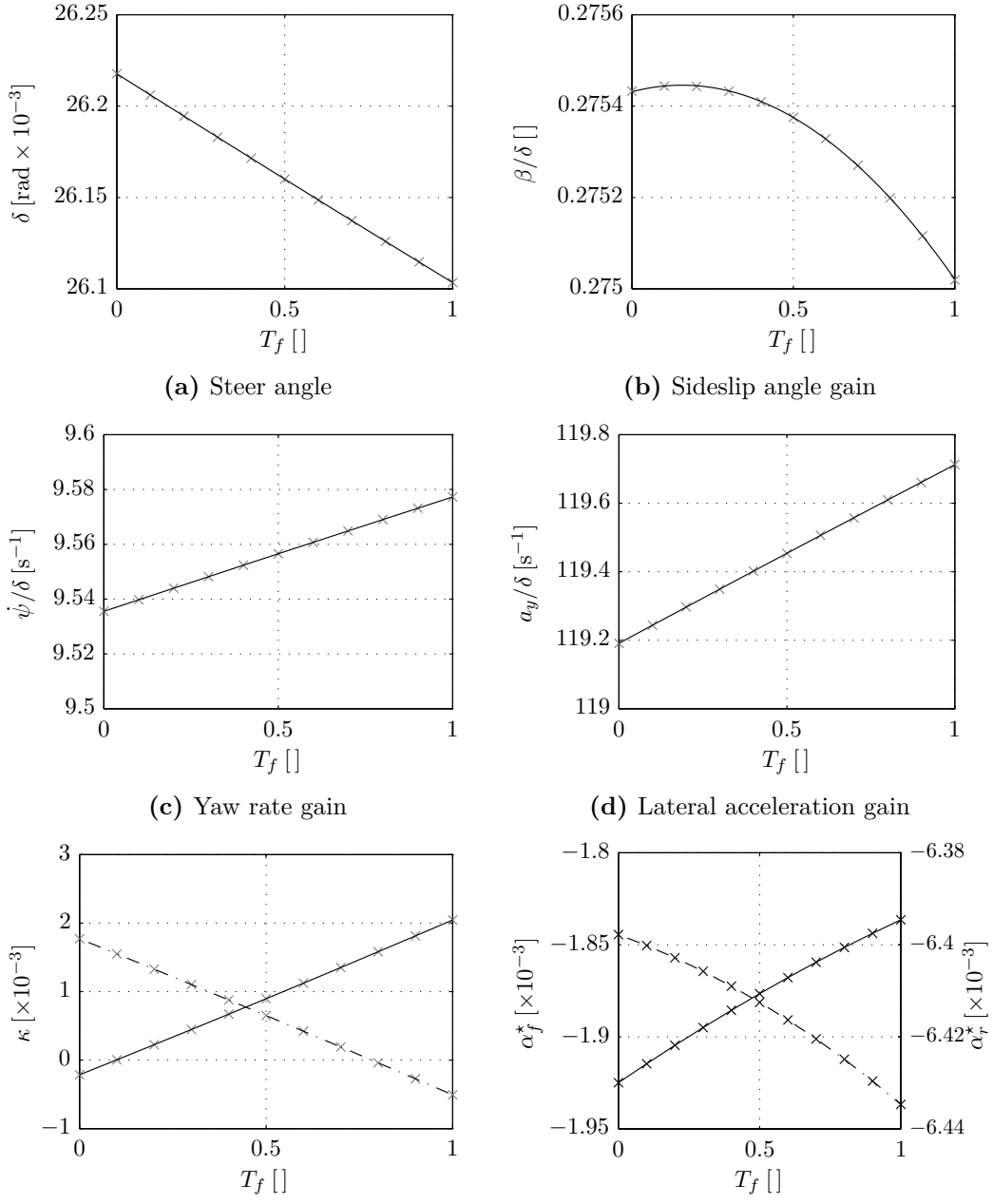

(a) Steer angle **(b)** Sideslip angle gain

(c) Yaw rate gain **(d)** Lateral acceleration gain

(e) Longitudinal slip **(f)** Lateral slip

Figure 5.11: Motorcycle handling diagrams with torque vectoring ($R = 50\,\mathrm{m}$, $v = 12.5\,\mathrm{m\,s^{-1}}$). Figures 5.11e and 5.11f: —— Front wheel; – · – · Rear wheel.

and lateral acceleration gain, shown in Figures 5.11c and 5.11d, increase as the front wheel receives more power. The motorcycle handling characteristic is becoming less understeer, but changes by only a small amount.

Figure 5.11e shows a large variation in longitudinal slip speed as power is transferred, with each of the wheels having a slight negative result when no power is applied there.

The lateral slip ratios of the front and rear wheels are shown in Figure 5.11f. The lateral slip at the rear is approximately 3.4 times that at the front. Putting 100 % of the drive torque to the front wheels increases the lateral slip of the front wheel by around 5 %, and reduces the lateral slip at the rear by around 0.7 % over the standard RWD motorcycle. This could be indicative of the way tyres for motorcycles are currently designed with the front wheels being unsuitable for driving applications.

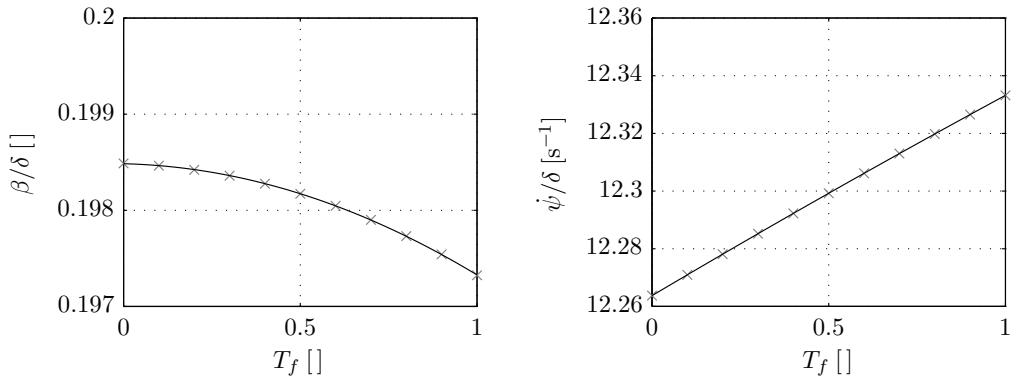

(a) Sideslip angle gain

(b) Yaw rate gain

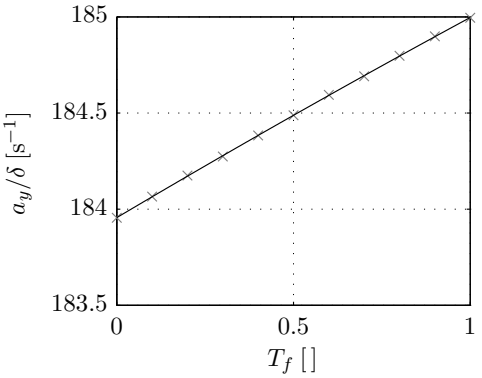

(c) Lateral acceleration gain

Figure 5.12: Motorcycle handling with torque vectoring ($R = 100\,\mathrm{m}$, $v = 15\,\mathrm{m\,s^{-1}}$).

Figure 5.12 shows results for a 100 m radius circle at $15\,\mathrm{m\,s^{-1}}$, which shows qualitatively similar results.

Motorcycle Handling Summary

This section presented a four-degree-of-freedom motorcycle model and used it to obtain steady-state handling results. With the model, it was shown that, in a steady state, steer torque is proportional to steer angle, camber angle, yaw rate and sideslip angle.

Using the fact that steer torque and steer angle are proportional in steady-state, equations were derived for the steady-state handling characteristics of a motorcycle with linear tyres. The equations were used for an investigation into how the weight distribution and tyre properties effects the handling characteristics of the motorcycle.

Finally, the multibody model was used to investigate the effect of torque distribution on handling. In the situations studied herein, the effect on handling is small. Further improvements may be seen as the motorcycle approaches its limits of adhesion by travelling either at faster speeds, or on a lower-friction or loose surface.

5.2 Transient Handling

As well as influencing the steady-state handling characteristics, torque vectoring has the potential to alter the transient characteristics, including the turn-in response, which will be analysed in this section. Mavros [38] attempted to extend the use of the words understeer and oversteer—which are defined only in steady-state situations—to transient manoeuvres by comparing the response of various vehicles to that of a standard case: a similar approach will be used here.

5.2.1 Automobiles

Introduction

What happens immediately after a steer input is applied to the vehicle is another important handling characteristic. Following the application of a steer angle, there are two interconnected characteristics that need to be considered: the stability of the vehicles, and their responsiveness.

Stability After a steer angle input, the transient yaw rate response can approach the steady-state yaw rate expected for the given steer angle and become stable, or it might diverge and become unstable, depending on the handling characteristics. It can be shown mathematically from the *bicycle model* that the transient response of all vehicles is well damped at low speeds, and the yaw rate approaches the steady-state yaw rate without oscillation [2, 75]. Indeed, for a NS vehicle, this is true at all speeds. For an US vehicle at high speeds, the transient yaw rate will oscillate with damping around the steady-state value, whereas the yaw rate of an OS vehicle at

high speeds will diverge from the value and vehicle spins. The speeds above which these responses are apparent are known as the *characteristic speed* and the *critical speed*, respectively.

The natural frequency and damping ratio of the response can be calculated from the linear model, given vehicle and tyre parameters, from Equations (5.1) and (5.2). The roots of the characteristic equation, which vary with speed for a given vehicle, determine the stability of the response: for further detail see [2, 38].

Clearly, oscillations and divergences of the yaw rate response are generally unwanted, especially in road vehicles.

Responsiveness The responsiveness is another important handling parameter and is a measure of how quickly the yaw rate increases after a steer input. The rate of increase influences how a vehicle feels to drive: too slow a response would make a vehicle feel *sluggish*, while to fast a response would feel *twitchy*.

Increases in responsiveness will often lead to a reduction in stability; thus, designing the vehicle to have acceptable responsiveness and stability is a challenge for a dynamicist. Since torque vectoring offers the ability to continuously adjust the drive torques, it offers the potential to improve both responsiveness and stability at the same time.

In this section, the multibody vehicle model will be used to investigate the transient response of vehicles. Firstly, the response of vehicles with various weight distributions will be analysed, then the effect of varying the torque distribution will be investigated.

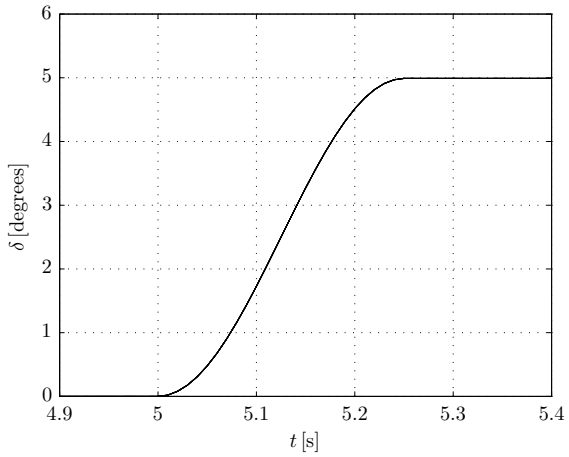

Figure 5.13: Turn-in response simulation steer angle input, created using half a sine wave. A steer angle of 5° is applied over 0.25 s.

In each case, a steer angle input is specified as shown in Figure 5.13, which gives the vehicle model 5 s for any initial transient behaviours to die away, then increases

the steer angle rapidly, but smoothly, to 5°. Half a sine wave is used to define the curve prevents issues with infinities in the model that would occur with step inputs.

Weight Distribution Effects

Firstly, the effect of weight distribution will be analysed to provide a basis for comparison of the influence of torque distribution. As defined in Table 5.1, *Vehicles A, B* and *C* were controlled to a speed of $10\,\mathrm{m\,s^{-1}}$, while their steer angles were increased from 0 to 5° as shown in Figure 5.13. The automobile parameters are defined in Appendix C.1.

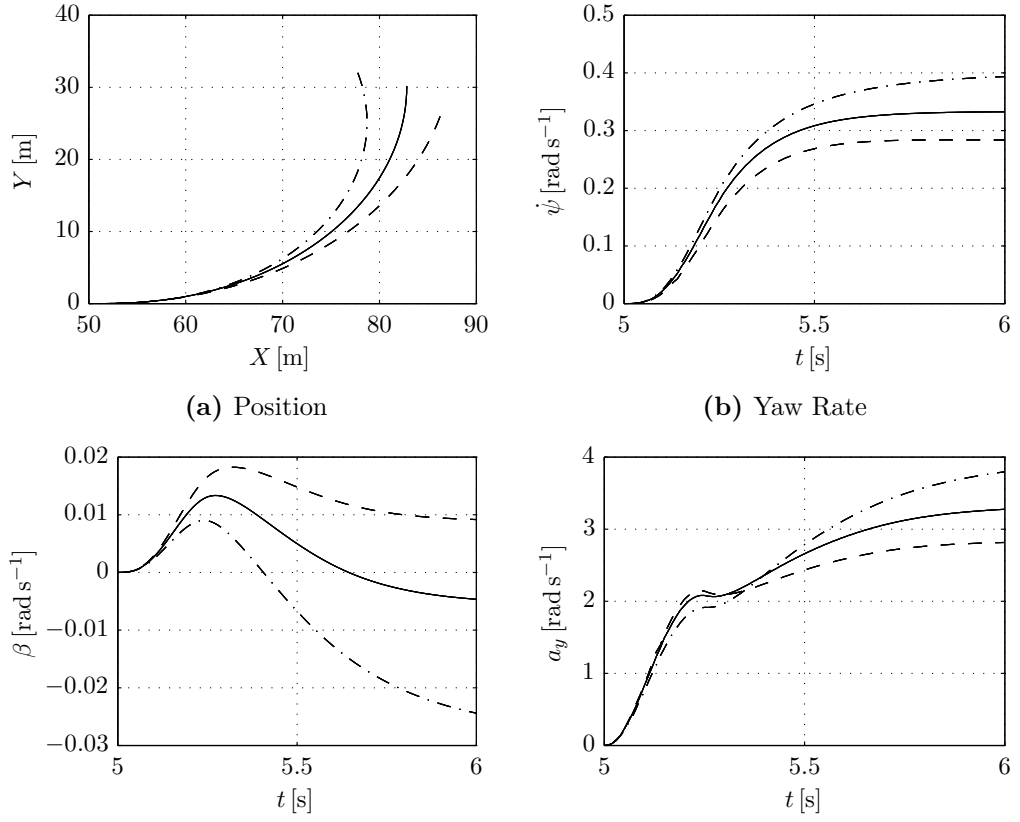

(a) Position **(b)** Yaw Rate

(c) Sideslip angle **(d)** Lateral acceleration

Figure 5.14: Turn-in response at $10\,\mathrm{m\,s^{-1}}$. – – – *Vehicle A*; —— *Vehicle B*; – · – · *Vehicle C*.

Figure 5.14 shows the effect of weight distribution on the handling response of the vehicle. At these speeds, all vehicles exhibit a stable response: the yaw rate rises to the steady-state value without oscillation. As discussed in Section 5.1.1, for a given steer input, the steady-state yaw rate of the OS *Vehicle C* will be greater than the NS *Vehicle B*, while the US *Vehicle A* will have a lower steady-state yaw rate.

The lateral acceleration of *Vehicle A* rises quickest initially, but *Vehicle C* ultimately has the higher lateral acceleration, as expected from the steady-state analysis.

The linear derivation with a step input predicts that the US vehicle would have a higher responsiveness, and a OS vehicle, a lower one; however, the three vehicles show similar initial rates of change of yaw rate and lateral acceleration. This is because the input is smoothly increased, and because of lag in the tyres and dynamic weight transfer effects.

Front–Rear Torque Distribution

The ideal front–rear torque vectoring driveline can distribute up to 100 % of the torque to the front or rear wheels; thus, looking at the range of results between these extremes will give the range achievable through torque vectoring.

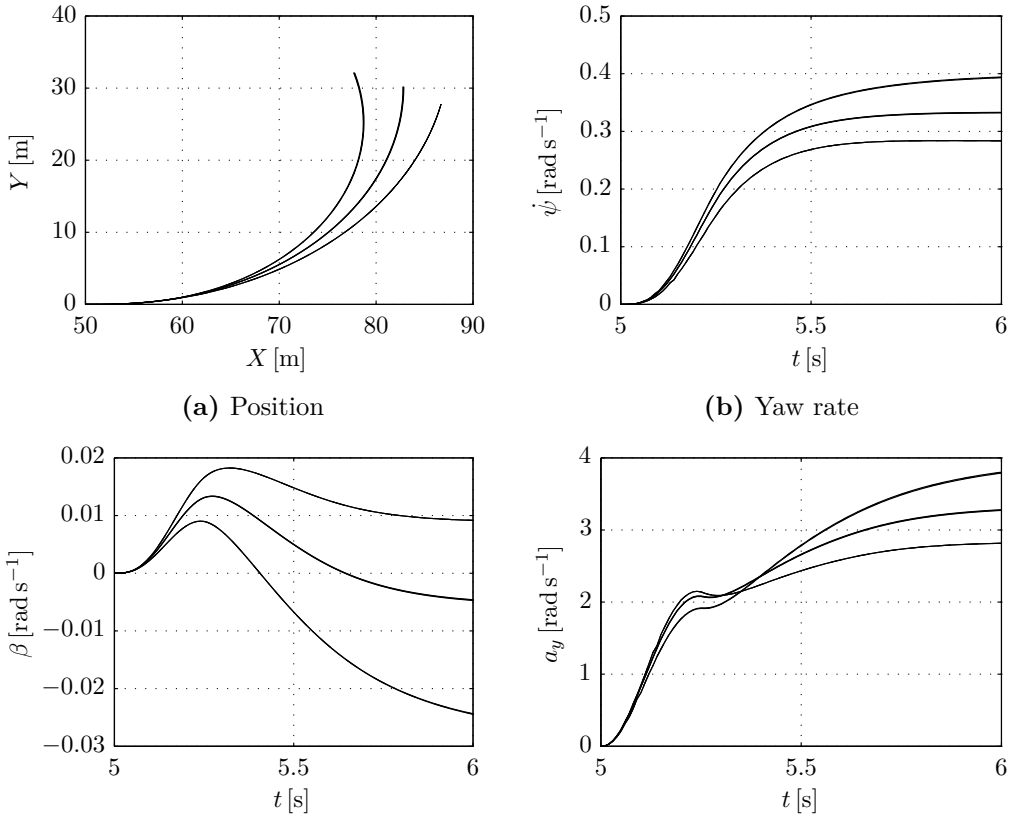

(a) Position **(b)** Yaw rate

(c) sideslip angle **(d)** Lateral acceleration

Figure 5.15: Turn-in response of vehicles with varying front–rear torque distribution at 10 m s^{-1}. – – – *Vehicle A*; ——— *Vehicle B*; – · – · *Vehicle C*; ------ 100 % front wheel torque bias in each case.

Figure 5.15 shows the transient response for vehicles with FWD, 4WD, and RWD drivelines. The ranges provided by front–rear torque vectoring appear as lines in the

above plots because they responses are almost indistinguishable from those of the standard vehicles.

By comparison with Figure 5.14, it is clear that front–rear torque distribution has little effect on the transient response of the vehicles, at this speed. This is because the tyre forces are not approaching their maximum values in either of the principle directions, thus, shifting the drive torque to the front or rear has little effect on the lateral slip force generation capacity.

Left–Right Torque Distribution

Left–right torque vectoring provides more potential to influence the transient handling characteristics, since a yaw moment can be generated through the drive torque difference. This section will analyse the effect of left–right torque distribution at a moderate and high speed. In each case, the total amount of drive torque required to maintain a constant speed is distributed according to the left–right torque distribution ratio, T_l. To obtain the maximum range, this is set to 0 and 100 %. The equal distribution case is also plotted for comparison. The vehicles are assumed to have a 4WD driveline with equal front–rear torque distribution. Similar results are obtain for vehicles with FWD and RWD drivelines, and are omitted.

Moderate Speed *Vehicles A, B* and *C* were controlled to $10\,\mathrm{m\,s^{-1}}$, and their steer angles increased from 0 to 5° over 0.25 s, as shown in Figure 5.13. Results, shown in Figure 5.16, now show a significant change in the vehicle path, caused by the difference in torque between the left and right wheels. For *Vehicles A, B* and *C* there are increases in responsiveness and steady-state yaw angle caused by increasing the drive torque apportioned to the outside wheels. Small increases are also seen in the lateral acceleration.

Despite the application of torque to only the inside or outside wheels, all vehicles remain stable, approaching their steady-state values without oscillation.

High Speed *Vehicles A, B* and *C* were controlled to $20\,\mathrm{m\,s^{-1}}$, with the same steer input as for the moderate speed case. Figure 5.17 shows that, at this speed, there are significant differences in the response of the vehicle to a steer input. Considering the response of the equal torque distribution, represented as dashed, solid and dash-dot lines, oscillations are seen in the vehicle output; however, all vehicles still converge on steady state values. Oscillations are most significant in *Vehicle C* and least significant in *Vehicle A*.

The response of *Vehicle C* is most significantly affected by the distribution of drive torque. As this vehicle is oversteer, its natural yaw rate response will diverge at high speed. The response predicted by the multibody model with equal torque

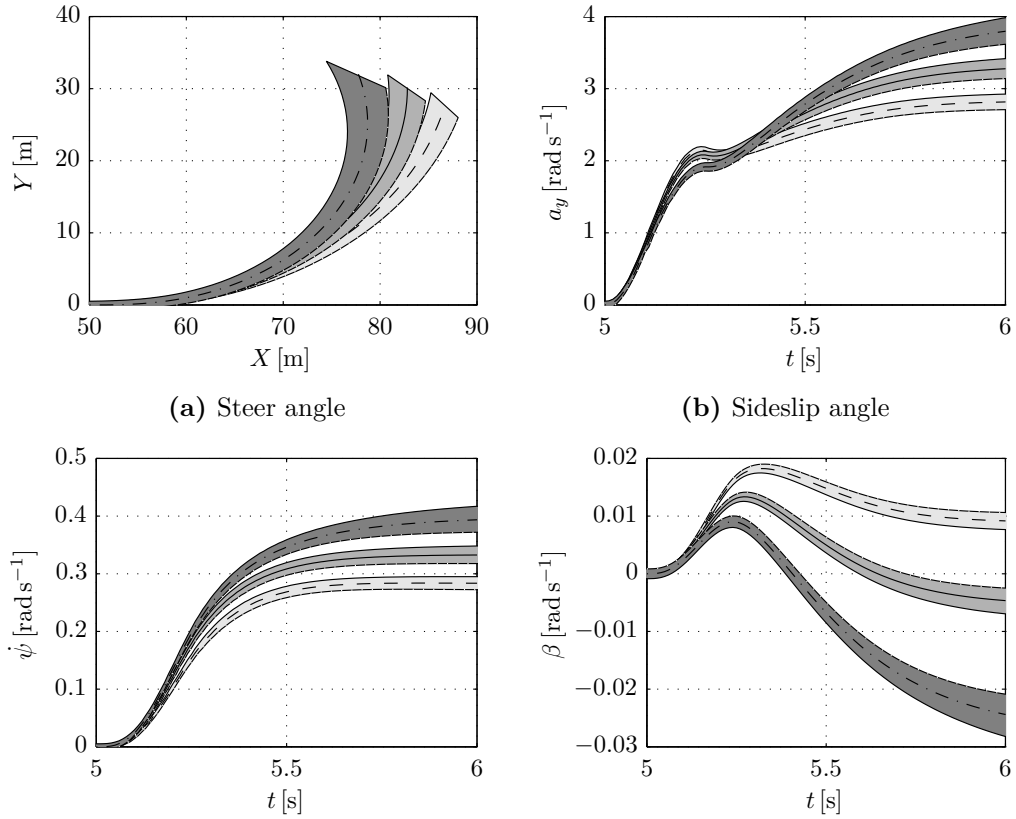

(a) Steer angle

(b) Sideslip angle

(c) Lateral acceleration gain

(d) Yaw velocity gain

Figure 5.16: Turn-in response of vehicles with varying left–right torque distribution at $10\,\mathrm{m\,s^{-1}}$. – – – *Vehicle A*; —— *Vehicle B*; – · – · *Vehicle C*; ------ 100 % inside wheel torque bias in each case.

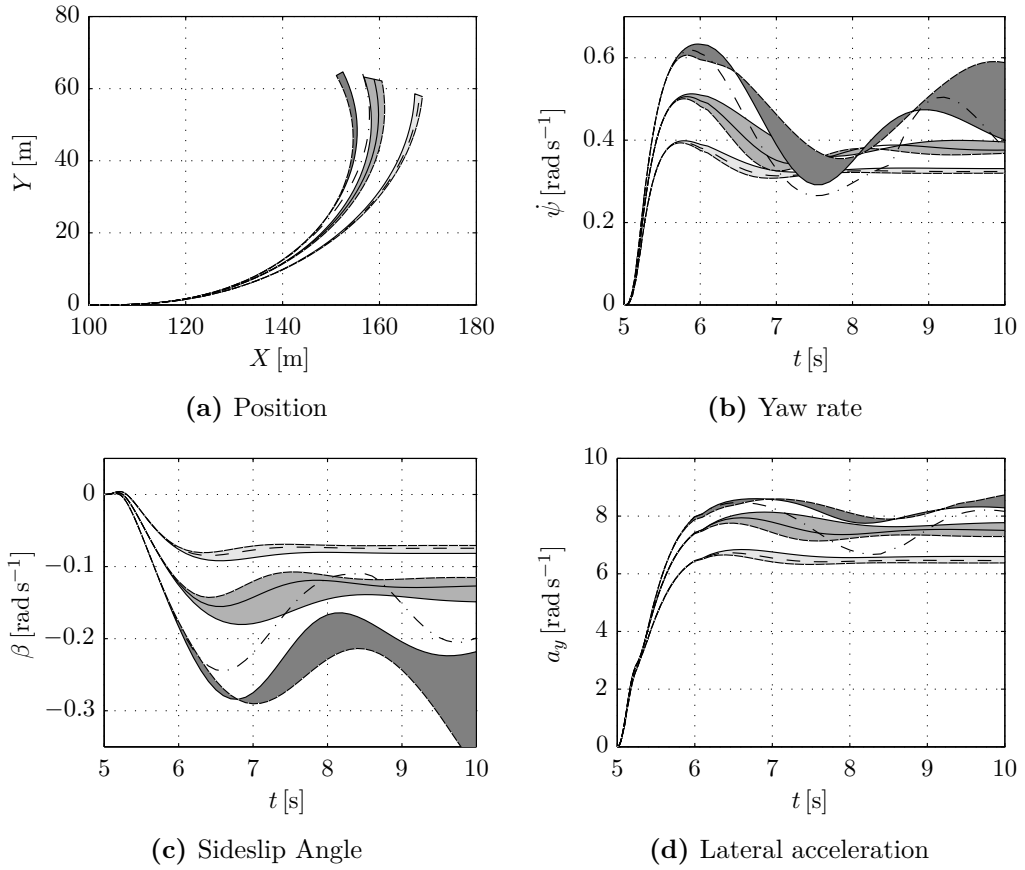

(a) Position **(b)** Yaw rate

(c) Sideslip Angle **(d)** Lateral acceleration

Figure 5.17: Turn-in response of vehicles with varying left–right torque distribution at $20\,\mathrm{m\,s^{-1}}$. – – – *Vehicle A*; ——— *Vehicle B*; –·–·– *Vehicle C*; ------ 100 % front wheel torque bias in each case.

distribution stabilizes and approaches the steady-state value; however, altering the distribution of torque pushes it closer to its limit. Figure 5.17a shows that the turning radii predicted for both the 0 and 100 % cases are smaller than that of the standard vehicle.

The introduction of a torque difference between the wheels the vehicle does not significantly alter the responsiveness of the vehicles in this case: there is little change in the initial rate of increase yaw rate and lateral acceleration of the vehicles. At these high speeds, the tyres are already approaching their limit of adhesion in the lateral direction; therefore, apportioning extra drive torque there has little effect due to the reduced capacity to generate longitudinal force.

Transient Handling Summary

The study of the effect of torque distribution on transient handling characteristics of the automobile has shown that at moderate speeds, the responsiveness of the vehicle can be changed, without significantly reducing stability through the use of left–right torque vectoring. Front–rear torque vectoring has little effect on the transient response in this case. Croft-White and Harrison [12] also report improvements in handling following left–right torque vectoring, after using a mathematical model to analyse a double lane change manoeuvre.

At high speeds, when the tyres are already approaching the limits of adhesion, torque distribution has little effect on the responsiveness, and can further destabilize the vehicle, if it exhibits oversteer tendencies. Therefore, at high speeds, brake-based stability control should still be used (see Section 2.2.1).

5.3 Chapter Summary

Using the linear *bicycle model* of a four-wheeled vehicle, quantities were derived to represent the handling performance of automobile, including the well-known *understeer gradient* [18]. These were applied to the multibody automobile model and good agreement was seen between the linear and non-linear models, during handling tests at low speed. At high speed, however, differences begin to appear because the tyre forces and moments are non-linear, and inertial, aerodynamic and gyroscopic effects influence the results; thus the necessity of a complex model for limit handling situations it demonstrated.

Ideal torque vectoring drivelines were simulated by specifying left–right and front–rear torque distribution ratios; thus, the total drive torque remains the same. At moderate speeds below $a_y = 0.5\,\mathrm{g}$, in a steady-state turn, front–rear torque distribution has negligible effect, because the only way for the drive torque to influence the yaw moment is to create a reduction in lateral tyre force through the

effect of combined lateral and longitudinal slip. At low and moderate speeds, the slip ratios in both principle directions are small; therefore, an increase in longitudinal slip does not have an associated reduction in lateral force. At higher speeds, there is a small effect on handling, where, for example, a vehicle that is US, according to its weight-distribution, could be made less so by a shift of the drive force from the front to the rear. This could be contradictory to literature presented by Osborn and Shim [45], who found that during an acceleration manoeuvre, "Control of front–rear torque distribution alone delivers almost the same performance enhancement as fully independent control." Results will differ because of the effect of acceleration on the vehicles, and because of the tyre models used: [45] used a simple model presented by Dugoff *et al.* [14].

Left–right torque vectoring offers more opportunity to influence the steady-state handling of automobiles. Throughout the whole speed range, a yaw moment can be generated through variation of the torque distribution ratio, but the effect is greatest at high speed when the total drive torque is higher and the magnitude of the difference greater. OS and US automobiles can be made to approach the handling characteristics of a NS vehicle by distributing the drive torque to the inside and outside wheels, respectively. A NS vehicle can have its handling characteristic altered to demonstrate US or OS characteristics, meaning the driver could choose how the vehicle handles for a given situation. Distributing the torque solely to the inside of outside wheels does mean that the vehicles become uncontrollable at a lower speed than its equally-distributed counterpart, because the tyre forces saturate when drive torque is concentrated at one wheel. Similar ranges in handling characteristics are seen in vehicles with FWD, 4WD and RWD drivelines. At high speed, the variation in handling characteristic with left–right torque distribution is greatest with FWD for an US vehicle, and with RWD for an OS vehicle.

The transient response of an automobile to a steer input was also considered, with focus on two aspects: the responsiveness and the stability. It was shown that the responsiveness is not significantly affected by the torque distribution ratio. At moderate speeds, a small increase in the yaw acceleration can be achieved through left–right torque distribution variation, but the effect all but disappears at high speeds when tyres are nearer the limit of adhesion. The front–rear torque distribution ratio has negligible affect on the transient response at moderate speeds. The stability of the vehicles is maintained at moderate speeds, with all vehicles approaching their steady-state values without oscillation or divergence. At high speed, however, the torque distribution significantly affects the stability of the vehicles, increasing the size of oscillations before the vehicle converges on its steady-state response, and can exacerbate the diverging response of an oversteer vehicle.

A mathematical four-DoF model presented by Seffen *et al.* [59] after Sharp and

Limebeer [66], was used to simulate the response of a motorcycle to various steer torque inputs. The steady-state values of steer angle, camber angle and yaw rate were shown to be proportional to the steer torque. Using this fact, a two-DoF eight-parameter steady-state model was derived that is similar to the *bicycle model* for automobiles. The model was used to investigate changes in the handling response caused by variation in weight distribution, and tyre lateral and camber stiffnesses.

Finally, the effect of torque distribution on the steady-state handling of a motorcycle was demonstrated. Steady-state handling characteristics are not well-defined for the motorcycle [34]; for this comparative analysis, a method similar that of the four-wheeled vehicle was used. The motorcycle, which was *understeer* according to the linear handling analysis, was made less understeer through a shift of the drive torque from the rear wheel to the front, as shown by a reduction in the required steer angle. There are corresponding increases in yaw rate and lateral acceleration gains, although the changes were small. A similar effect was seen at higher speeds. Overall, torque vectoring in motorcycles realises only small changes in the handling characteristics, in these steady-state situations. While this may be disappointing from the point of view of improving handling dynamics, it does mean that torque can be applied at the front wheel, for purposes such as increasing traction on low-friction ground, without adversely affecting the handling characteristics.

Chapter 6

Energy Efficiency

There are various ways to alter the distribution of torque between the wheels of a vehicle; for example, through the use brakes or clutches in the differential(s) of automobiles [24, 29, 56], or by using electric or hydraulic motors to power the front wheel of a motorcycle [10, 28]. The aim of this has, thus far, generally been to improve handling, stability and safety, but torque vectoring also has the potential to reduce power consumption. Ongoing research by Abe and Kano [1] has shown limited reduction in tyre dissipation energy in an experimental Active Torque Distribution (ATD) automobile. To study the effect in two- and four-wheel vehicles is the aim of this investigation.

Using models developed in the previous chapters, this chapter will present the results of an investigation into how torque distribution affects the energy consumption of automobiles and motorcycles. Simulated vehicles with various torque distributions will be controlled to undertake straight-line and cornering manoeuvres, so that power consumption can be analysed. The amount of power consumed as slip at the tyres will also be investigated. Conclusions are drawn about the best way to distribute drive torque between the wheels of the vehicles for maximum energy efficiency.

6.1 Introduction

Changing the distribution of torque between the wheels of a vehicle has the potential to alter the power required to perform a manoeuvre in various ways. Since tyres are generally stiffer in the longitudinal direction than in the lateral direction, generating a yaw moment using a variation in drive torque, rather than a steer-induced lateral force, could potentially present a power saving. Also, horizontal forces generated by the individual tyres increase with vertical load for the same amount of tyre slip and thus, for a given force, the power consumed at that wheel is reduced.

However, the tyre forces and moments depend on many factors including the vertical load, slip speed, camber angle and combined slip situation; hence, complex models of the vehicles are required. An overview of the models is given in the section; for more details regarding the modelling and simulation of the vehicles, please refer to Chapter 3.

6.1.1 Vehicle Models

Models of an automobile and a motorcycle were created in SimMechanics [69], where equations of motion are generated automatically based on the joints and constraints between bodies of specified mass and inertia. Forces and torques can be applied to the system, and the resulting kinematics and reaction forces can be monitored and recorded using Simulink.

Automobile model

In the automobile model, the main vehicle body has four wheel bodies attached to it with the relative positions of the wheel centres-of-mass specified. The longitudinal axis of the wheel Coordinate System (CS) can be rotated about the vehicle's z-axis to steer the wheels; the angles are specified before simulation, or, if a driver model is required for path following, by a controller within the system. The wheel bodies are allowed to rotate about the local y-axes, and translate about the local z-axis giving rolling and suspension motions. The connected bodies are allowed to move with the three linear, and three rotational, degrees of freedom. A simple diagram showing the five bodies and the degrees of freedom of the vehicle model is given in Figure 6.1. For more details regarding the multibody model of the four-wheeled vehicle, please refer to Section 3.3.4.

Motorcycle model

The motorcycle model is similar to the vehicle but, as the relative motions of the rider and other assemblies are important, the connections between the bodies are more complex. Bodies representing the handlebars and upper forks are connected to the rear frame with a joint that allows steer and twist rotations. The lower forks are connected to, but allowed a linear degree-of-freedom from, the handlebars, to model telescopic suspension, and the front wheel is attached with a rolling degree-of-freedom about its y-axis. At the rear, a swingarm is connected about a pivot point and suspension forces are calculated between specified points on the swingarm and frame. The rear wheel is attached, also with a rolling degree of freedom. The rider's upper body is allowed to rotate about the motorcycle frame's longitudinal axis and apply lean and steer torques to the frame and handlebars respectively. A simple diagram

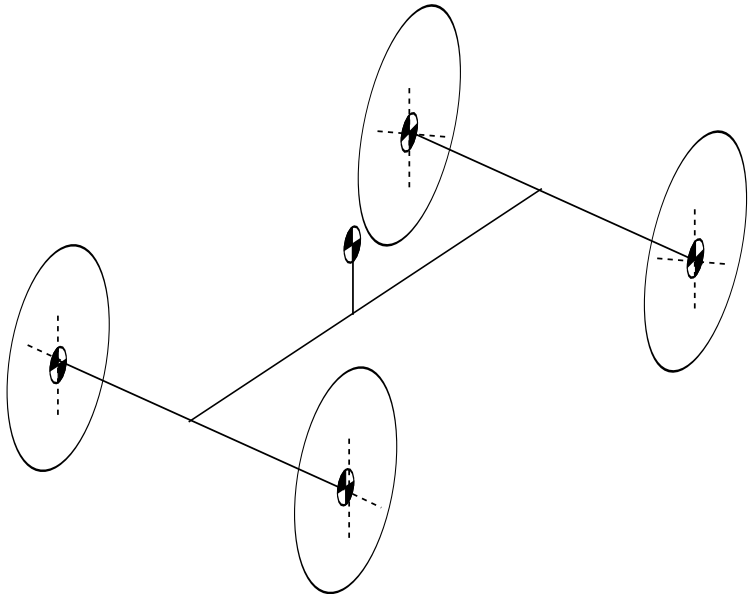

Figure 6.1: Automobile model bodies and degrees of freedom

showing the seven bodies and the degrees of freedom of the motorcycle model is given in Figure 6.2. For further information about the motorcycle model see Section 3.4.4.

Drive Torques

In the cases of both the motorcycle and the automobile, torque is applied individually about the local y-axes of the wheels, simulating an ideal torque vectoring driveline. The amount of torque applied to each wheel is determined through Proportional–Integral (PI) control of the total amount required to achieve a specified vehicle speed, and by the front and outside torque ratios, T_f and T_o, as specified before simulation. These are multipliers specified for each wheel that determines the proportion of torque it should receive, as defined in Equations (3.65) to (3.68).

Tyre Forces and Moments

Normal, longitudinal and lateral tyre forces, and associated moments, are calculated for each wheel using tyre models, coded in Simulink, that use the positions and velocities of the wheels relative to the road surface. The tyre forces for the automobile are calculated using the *Magic Formula* in [46], and for the motorcycle with the tyre model in [40]. Forces and moments are transformed into the global CS, and are applied to the wheel *bodies* using *actuators*, as described in Sections 3.5.5 and 3.5.6.

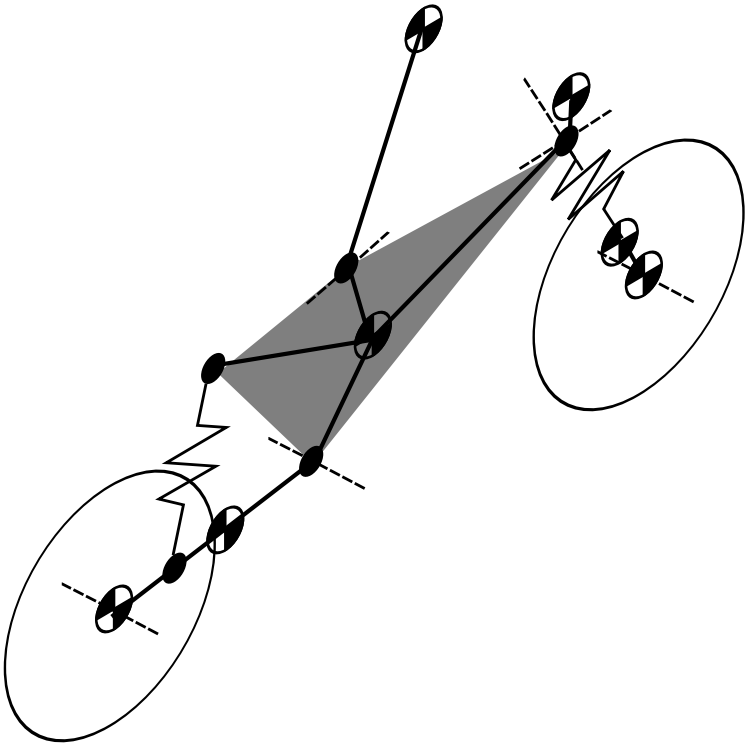

Figure 6.2: Motorcycle model bodies and degrees of freedom

6.1.2 Power Consumption

For both the two- and four-wheeled vehicles, the total power applied is calculated from the sum of each of the SimMechanics *actuators* that apply drive torque to the wheels of the vehicle,

$$P_{\text{total}} = \sum_{i=1}^{n_d} (\tau_i \omega_i) \,, \tag{6.1}$$

for $i = 1, \ldots, n_d$ drive actuators, where τ is the torque applied at the shaft and ω is the rotational velocity. An ideal power source is assumed at each wheel, with sufficient torque capability to cope with the request from the controller.

The power consumed by slip is calculated using

$$\boldsymbol{P}_{\text{slip}} = \sum_{i=1}^{n_w} \left(\boldsymbol{F}_i \boldsymbol{v}_{i\,\text{slip}} \right) , \tag{6.2}$$

for $i = 1, \ldots, n_w$ wheels, where $\boldsymbol{P}_{\text{slip}}$ is a vector of the power consumed in the principle directions of the tyre, $\boldsymbol{F}$ is the tyre force vector and $\boldsymbol{v}_{\text{slip}}$ is the slip velocity vector [1, 35]. The slip velocity is the relative speed of the tyre at the centre of the contact

path, relative to the road surface; thus, the equations are

$$v_{sx} = -\kappa v_x \tag{6.3}$$

$$v_{sy} = \alpha^\star v_x, \tag{6.4}$$

where κ and $\alpha^\star$ are the longitudinal and lateral slip ratios, respectively, and v is the speed of the wheel centre. Other main dissipaters in the model include the aerodynamic drag force, and the rolling resistances of the tyres.

In this chapter, the power consumption of the simulated motorcycle and automobile will be investigated as they perform a range of manoeuvres. In each situation, the various vehicles are controlled to travel at a specified yaw rate, in the same conditions, at the same speed. This is similar to the test method specified in [26].

Firstly, straight-line driving will be considered for the automobile and the motorcycle, as torque distribution between the wheels is altered. Then, the vehicles will be analysed as the undertake steady-state cornering manoeuvres. For the automobile, the influence of front–rear and left–right torque distribution will be shown in each case. The motorcycle is clearly restricted to front–rear torque distribution variation.

6.2 Straight Line Efficiency

6.2.1 Automobile Efficiency

For the investigation into how the torque distribution of automobiles affects the straight line efficiency, three vehicles, with weight distributions specified in Table 6.1, are used with the multibody model specified in Section 3.3.4. The total drive torque and steer angle of the vehicles are controlled to achieve straight driving at $25\,\mathrm{m\,s^{-1}}$. The front–rear torque distribution ratios, T_f, specified for each of the vehicles, range from 0 (Rear Wheel Drive (RWD)) to 1 (Front Wheel Drive (FWD)). Results are also plotted for a Four Wheel Drive (4WD) vehicle with varying left–right torque distribution. In each case, simulations were run for 30 s to achieve the desired speed and path, and for any transient behaviour to die away.

Front–Rear Torque Vectoring

Figure 6.3a shows that the total amount of power consumed by the vehicles is similar in each case, varying by not more than 1.5 %. This is because the main dissipater of energy is the aerodynamic force, which is similar for all the vehicles.

However, trends are clear for the different vehicles: front-heavy *Vehicle A* has the lowest power consumption when torque is biased to the front, while rear heavy *Vehicle C* has the lowest consumption when torque is biased to the rear. *Vehicle B*,

Table 6.1: Vehicle parameter values for the efficiency simulations

Parameter	Symbol	Value		
		Vehicle A	*Vehicle B*	*Vehicle C*
Front axle to CoG	l_f	1.0 m	1.25 m	1.5 m
Back axle to CoG	l_b	1.5 m	1.25 m	1.0 m

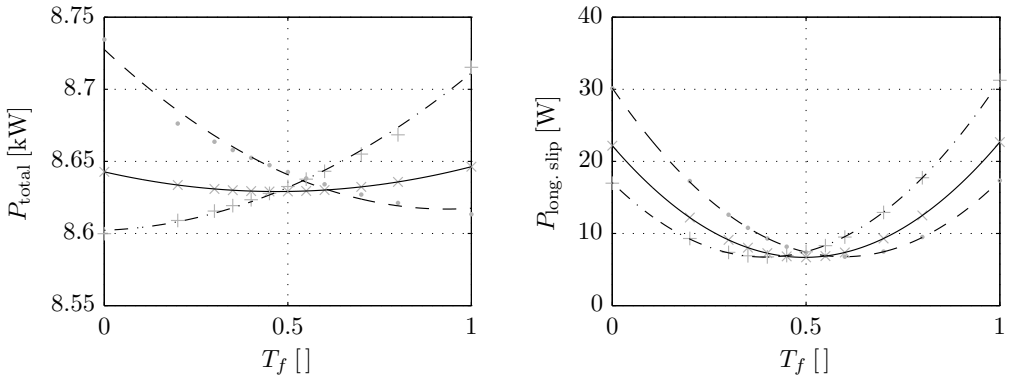

(a) Total **(b)** Longitudinal slip

Figure 6.3: Power consumption of vehicles with varying front–rear torque distribution during straight driving at $25\,\mathrm{m\,s^{-1}}$. – – – *Vehicle A*; —— *Vehicle B*; – · – · *Vehicle C*.

which has an equal weight distribution, has the minimum distribution when it also has equal torque distribution, though the variation is smaller in this case.

Figure 6.3b shows the power consumed by longitudinal slip at the tyre–road contact, as calculated using Equation (6.2). The longitudinal slip power consumption of the three vehicles have minima at torque distribution ratios equal to that of their weight distribution ratios; for example, *Vehicle A* has a weight distribution of 60 % over the front wheels, and a minimum power consumption when 60 % of the torque is delivered there. The variation in longitudinal slip power consumption is large in comparison to the total power consumption: the maximum consumption can be more than four times the minimum. The results suggest that in a straight line, for minimum longitudinal slip power consumption and, therefore, maximum tyre longevity, torque should be distributed according to the weight distribution.

The reason for the discrepancy in the minimum power points of Figures 6.3a and 6.3b is because of the tyre rolling resistances, which vary with vertical load and longitudinal slip situation.

These results indicate that for maximum efficiency in a straight line, the drive torques should be distributed according to the vertical load situation; however, since the potential gains are small, for mechanical drivelines, reduced efficiency of the driveline necessary for torque vectoring may negate any reduction in energy consumption.

Left–Right Torque Vectoring

For completeness, Figure 6.4 shows results for the same $25\,\mathrm{m\,s^{-1}}$ straight-line scenario, this time with the left–right torque distribution ratio, T_o, varying from 0 (left wheel only) to 1 (right wheel only). The vehicles are controlled to drive in a straight line by setting the steering controllers target yaw rate to zero. *Vehicle B* is shown with a 4WD driveline, as the results are representative of other configurations. As would be expected, results are symmetric about the point of equal torque distribution, at which point lateral slip power consumption (Figure 6.4c) drops to zero. Even when power is delivered only to the left or right wheels, the lateral slip consumption is less than that of the longitudinal slip shown in Figure 6.4b.

Figure 6.4a shows that the effect of left–right torque distribution on overall power consumption is minimal; however, using this fact to design a cheaper driveline where only one wheel is driven, would not be sensible because of the effect on handling, as shown in Section 5.1.1. The driver would have to continually correct the steering to account for the amount of power being delivered to the wheels and any yaw moment that is generated.

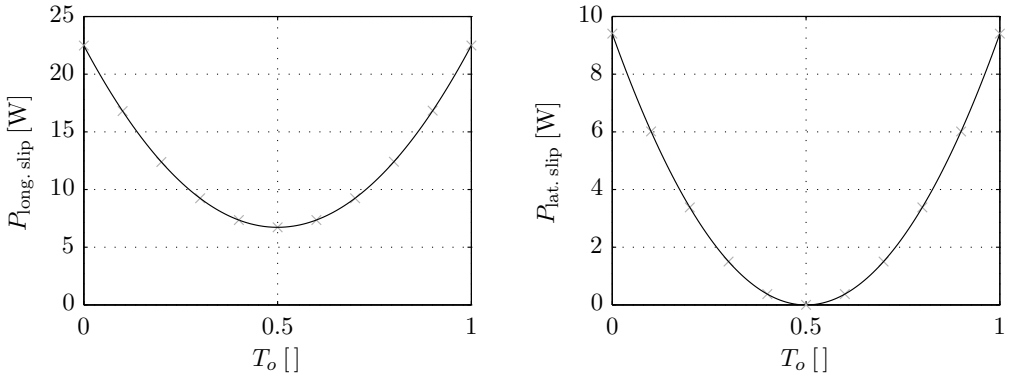

(a) Longitudinal slip **(b)** Lateral slip

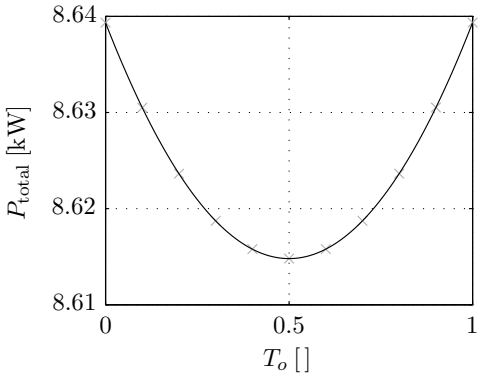

(c) Total

Figure 6.4: Power consumption of *Vehicle B* with varying left–right torque distribution during straight driving at $25\,\mathrm{m\,s^{-1}}$.

6.2.2 Motorcycle Efficiency

The multibody motorcycle model described in Section 3.4 is used to investigate the effect on efficiency of torque distribution in the straight driving of two-wheeled vehicles. The proportion of torque delivered to the front wheel, T_f, is varied from 0 % to 100 %, with corresponding rear wheel torque varying from 100 % to 0 %; thus, a conventional motorcycle with rear wheel drive is represented on the left-hand side of the plots. As the values given here are for steady-state situations, the motorcycle was allowed 60 s to achieve the desired path and for any transient responses to die away.

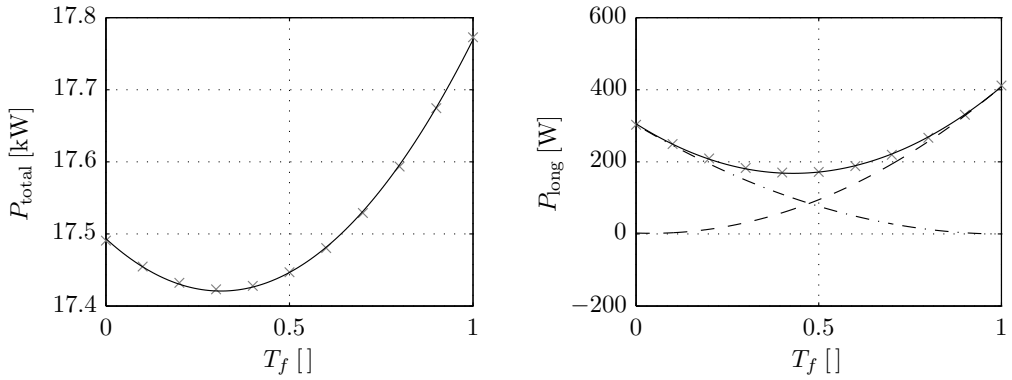

(a) Total **(b)** Longitudinal slip

Figure 6.5: Motorcycle power consumption during straight driving at $45\,\mathrm{m\,s^{-1}}$. —— Total; – – – Front Wheel; – · – · Rear Wheel.

Figure 6.5a shows the total amount of power needed to maintain a speed of $45\,\mathrm{m\,s^{-1}}$ on a straight and level road with the varying torque distributions, as calculated with Equation (6.1). The total power consumed varies with the amount of power apportioned to the front wheel, with the maximum consumption occurring with purely front wheel drive and the minimum occurring with 70 % of the torque applied at the rear wheel ($T_f = 0.3$). The minimum occurs with more torque towards the rear because of the vertical loading situation and dissimilar tyre characteristics.

However, the magnitude of the change in power consumption is small: even at this high speed, the potential improvement over conventional rear wheel drive is only around 0.5 %, which is likely to be insignificant in the real world.

Figure 6.5b shows how much power each wheel dissipates through slip for the various torque distributions. The total longitudinal slip power dissipated by the tyres is at a minimum when around 60 % of the torque is delivered to the rear wheel ($T_f = 0.4$). This suggests that motorcycle tyre longevity could be improved by better distributing the torque, meaning that the rear tyre might not have to be replaced as often. This would be especially useful in motorcycles that do a lot of motorway miles

when a flat band is often worn on the rear wheel, which has an associated impact on handling.

6.3 Steady-State Cornering Efficiency

Actively distributing the torque between the wheels as a vehicle corners presents a greater opportunity to reduce energy consumption than straight driving, because torque vectoring can be used to influence the handling and therefore influence the slip speeds at the wheels. This section investigates the power-reduction potential of torque vectoring for automobiles and motorcycles as they corner in a steady state.

6.3.1 Automobile Efficiency

Firstly, automobiles are considered. The three vehicles, with the weight distributions specified previously in Table 6.1, have their drive torques and steer angles controlled to maintain a constant 50 m radius turn at $17\,\mathrm{m\,s^{-1}}$. This situation might be experienced on the road when negotiating a motorway roundabout at around $61\,\mathrm{km\,h^{-1}}$ (38 mph). The power consumptions, with a range of torque distributions, are compared for various drivelines.

Front–Rear Torque Vectoring

The effect of front–rear torque distribution for *Vehicles A, B* and *C* is shown in Figure 6.6. The longitudinal slip power consumption in Figure 6.6a shows similar results to the straight driving case: the minimum power consumption corresponds roughly to the weight distribution, although in this case, the minimum power point is slightly forward of the centre of mass.

However, the longitudinal slip power consumption is small in comparison with the lateral slip power consumption shown in Figure 6.6b. Lateral slip power consumption does not vary significantly with torque distribution, but does vary between the three vehicles: *Vehicle B*, with its equal weight distribution consumes least energy as lateral slip, while *Vehicles A* and *C* use more. This is because *Vehicles A* and *C* require additional power to counteract their natural tendencies to understeer and oversteer, respectively. *Vehicle A* uses more than *Vehicle C* because at this speed, the magnitude of its understeer gradient is greater; that is, *Vehicle A* is more understeer than *Vehicle C* is oversteer. This means its sideslip angle is greater and therefore lateral velocity is higher; lateral force is similar for all vehicles.

Considering Figure 6.6c, the total power consumed is, on average, around 5 % lower for *Vehicle B* than the other vehicles because of reduced lateral slip power consumption. Minimum power consumption during cornering, for a vehicle with

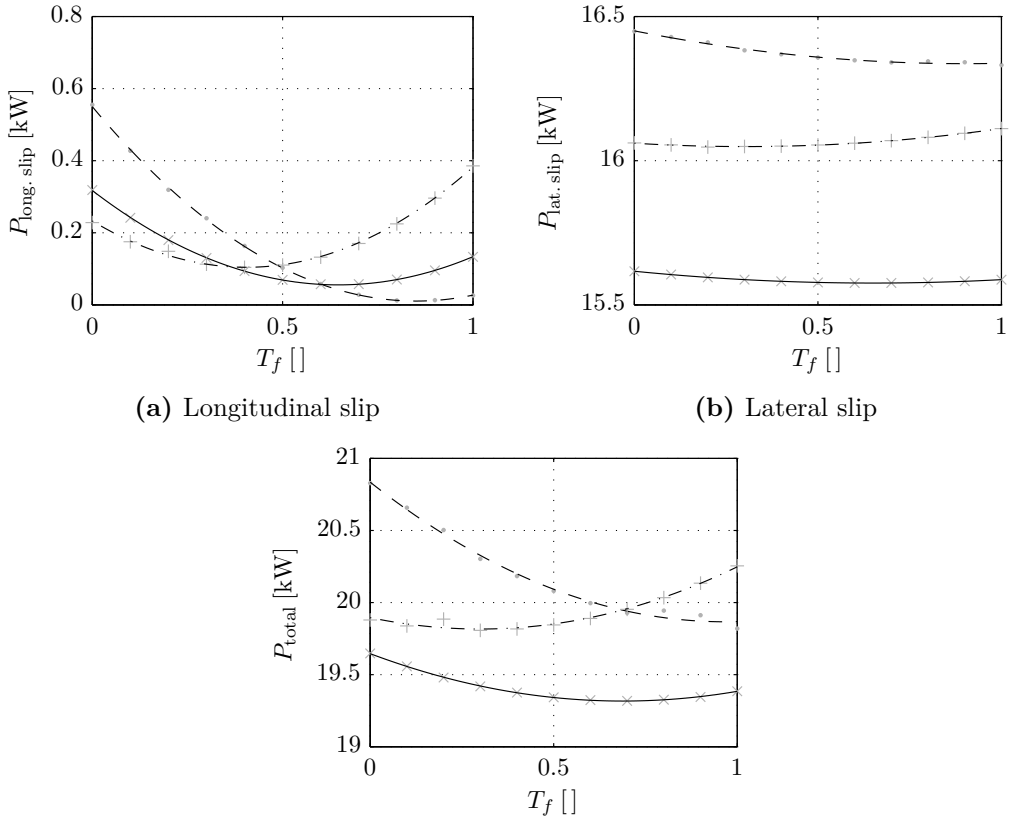

(a) Longitudinal slip

(b) Lateral slip

(c) Total

Figure 6.6: Power consumption during cornering at $17\,\mathrm{m\,s^{-1}}$ with varying front–rear torque distribution. – – – *Vehicle A*; —— *Vehicle B*; – · – · *Vehicle C*.

front–rear torque distribution, seems to occur when the torque distribution is slightly forward of the centre of mass.

Left–Right Torque Vectoring

To investigate the effect on efficiency of left–right torque vectoring during cornering, the three vehicles were again controlled to negotiate a 50 m radius corner at $17\,\mathrm{m\,s^{-1}}$. Each vehicle was simulated with FWD, 4WD and RWD drivelines that are capable of left–right torque vectoring. Figure 6.7 shows longitudinal and lateral slip power consumptions for various drivelines, with *Vehicles A, B* and *C* shown on separate axes. The total power consumptions are shown in Figure 6.8. The results are plotted against the proportion of torque delivered to the outside wheels, T_o, which varies between 0 and 1.

Considering the longitudinal slip power consumption of all vehicles and all drivelines in Figures 6.7a, 6.7c and 6.7e, the minima are all located when $0.6 < T_o < 0.75$; i.e., when slightly more power is going to the outside wheels than the inside. Distributing all of the power to the outside wheels results in a slight increase in longitudinal slip power consumption, while transferring all the power to the inside wheels gives even worse performance. For front-heavy *Vehicle A*, RWD is the worst performing driveline for all left–right distribution ratios, as is FWD for rear-heavy *Vehicle C*.

Figures 6.7b, 6.7d and 6.7f show the lateral slip power consumption: results are generally similar for all drivelines in each vehicle case. *Vehicle A* has minima for all drivelines when 100 % of the torque is apportioned to the outside wheels, where the tyre force acts to induce a yaw moment that helps to counteract the vehicles natural understeer tendency. Lateral slip power consumption could be reduced by around 3 % compared to a vehicle with equal left–right torque distribution.

Vehicles B and *C* have minima in the lateral direction at lower distribution ratios. *Vehicle C* with a RWD driveline, which is naturally the most oversteer of all the vehicles, has a minimum power point with slightly more power to the inside wheel ($T_o = 0.4$).

A significant proportion of the total power consumption of the vehicle is used as lateral slip in this situation. The total power consumption for each of the vehicles and drivelines is shown in Figure 6.8. For the front-heavy *Vehicle A*, all drivelines are more efficient when 100 % of the torque is sent to the outside wheels; the most efficient driveline is FWD. *Vehicle B* is most efficient when torque is biased around 80 % towards the outside wheels, and with a 4WD driveline, though the minimum for FWD is similar. For *Vehicle C*, the minimum consumptions are around 70 %, and 4WD and RWD drivelines give similarly good results.

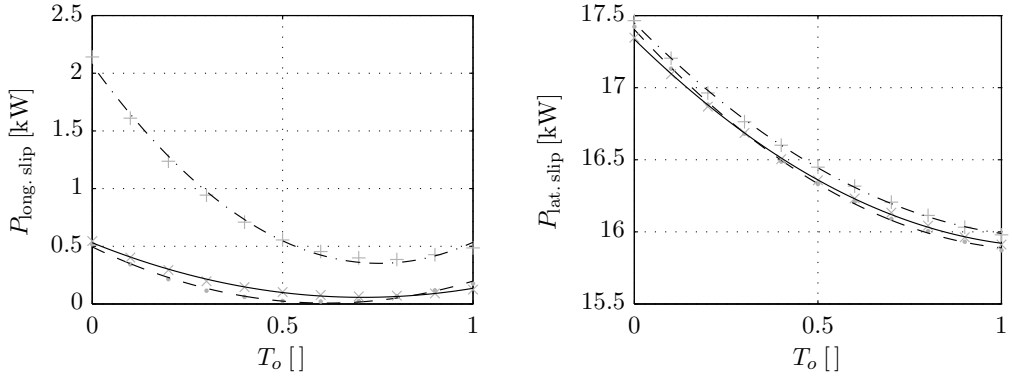

(a) *Vehicle A*, Longitudinal slip

(b) *Vehicle A*, Lateral slip

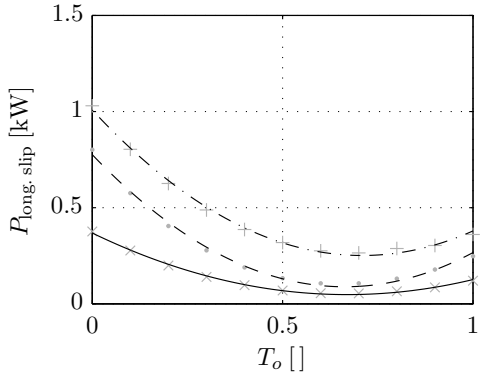

(c) *Vehicle B*, Longitudinal slip

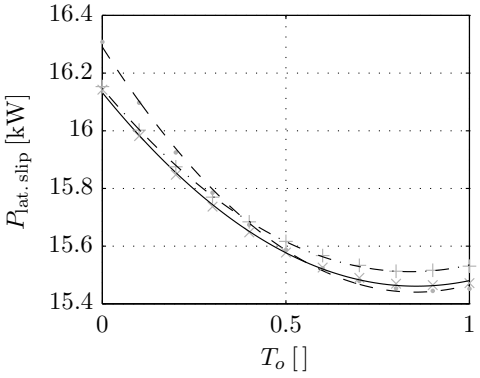

(d) *Vehicle B*, Lateral slip

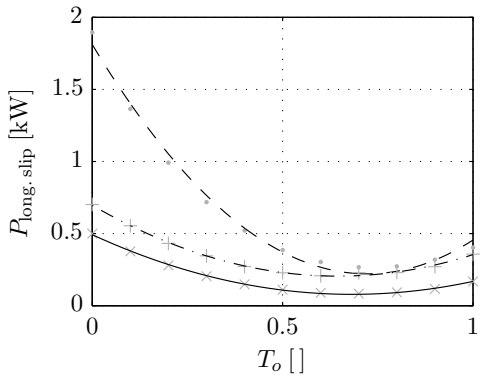

(e) *Vehicle C*, Longitudinal slip

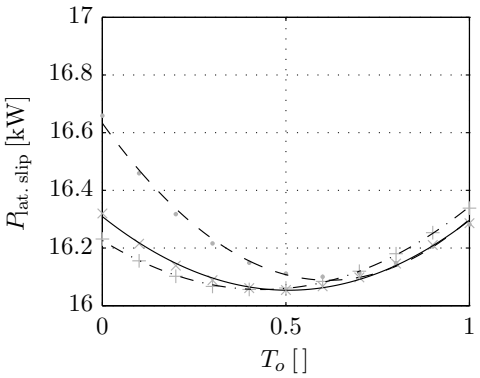

(f) *Vehicle C*, Lateral slip

Figure 6.7: Slip power consumption during cornering at $17\,\mathrm{m\,s^{-1}}$ with varying left–right torque distribution. – – –FWD; ——4WD; – · –RWD.

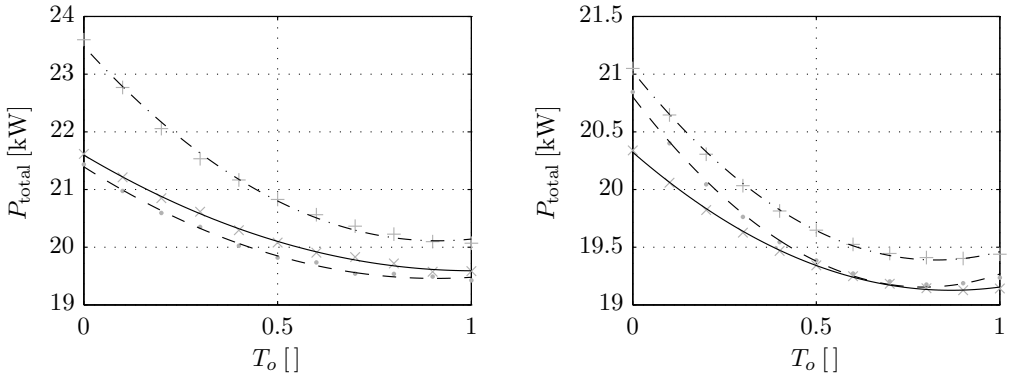

(a) *Vehicle A*, Total

(b) *Vehicle B*, Total

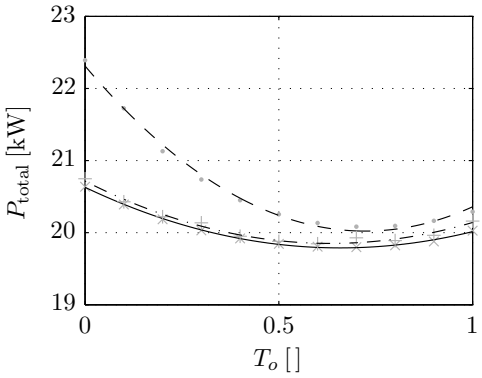

(c) *Vehicle C*, Total

Figure 6.8: Total power consumption during cornering at $17\,\mathrm{m\,s^{-1}}$ with varying left–right torque distribution. – – – FWD; —— 4WD; – · – · RWD.

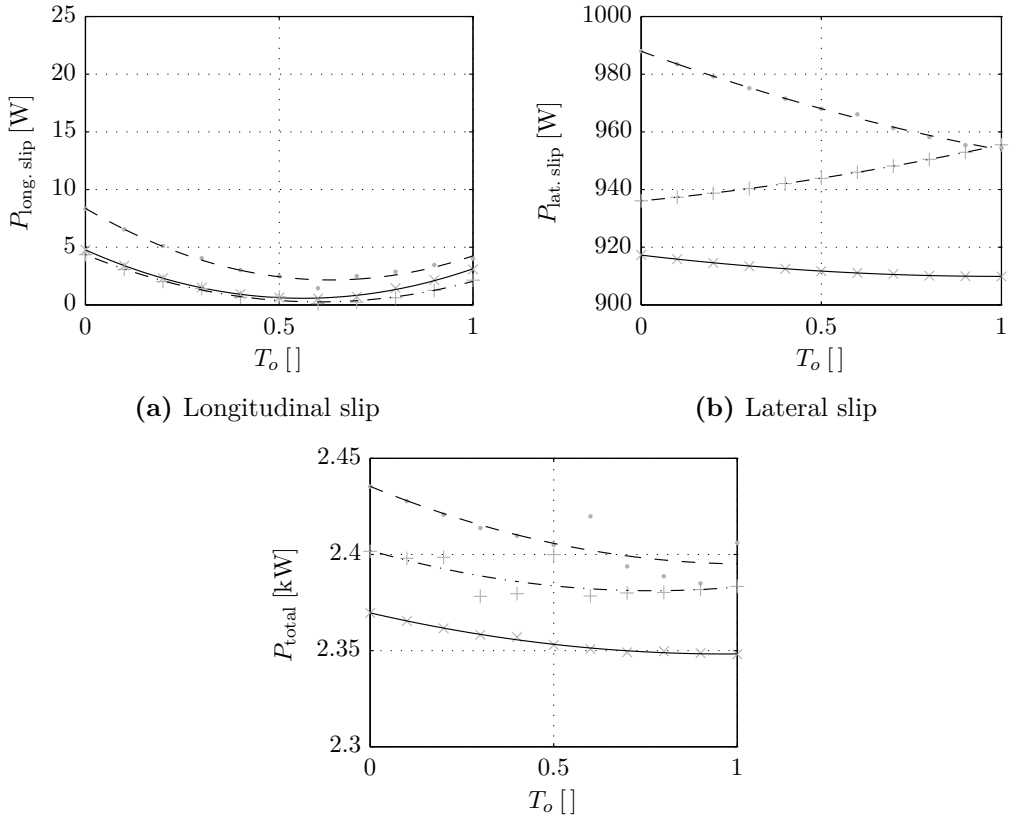

(a) Longitudinal slip

(b) Lateral slip

(c) Total

Figure 6.9: Power consumption during cornering at $10\,\mathrm{m\,s^{-1}}$ with varying left–right torque distribution (4WD). – – – *Vehicle A*; —— *Vehicle B*; – · – · *Vehicle C*.

Figure 6.9 shows results for a similar situation at a lower speed: a 50 m radius corner at $10\,\mathrm{m\,s^{-1}}$. The results are plotted only for the 4WD driveline, with the different vehicle weight distributions on the same axes. Longitudinal slip power consumption, shown in Figure 6.9a, has a minimum with around 60 % torque to the outside for all vehicle weight distributions, while the trend for lateral slip is different for the three individual vehicles. The lateral slip consumption of *Vehicle A* falls as power is biased toward the outside, while for *Vehicle C* it rises. This corresponds to the counteracting of the natural handling characteristics of the vehicles.

The total power consumptions of the vehicles are shown in Figure 6.9c, where the general trend is for power to reduce as torque is biased to the outside wheels, though changes above $T_o = 0.7$ are minimal.

6.3.2 Motorcycle Efficiency

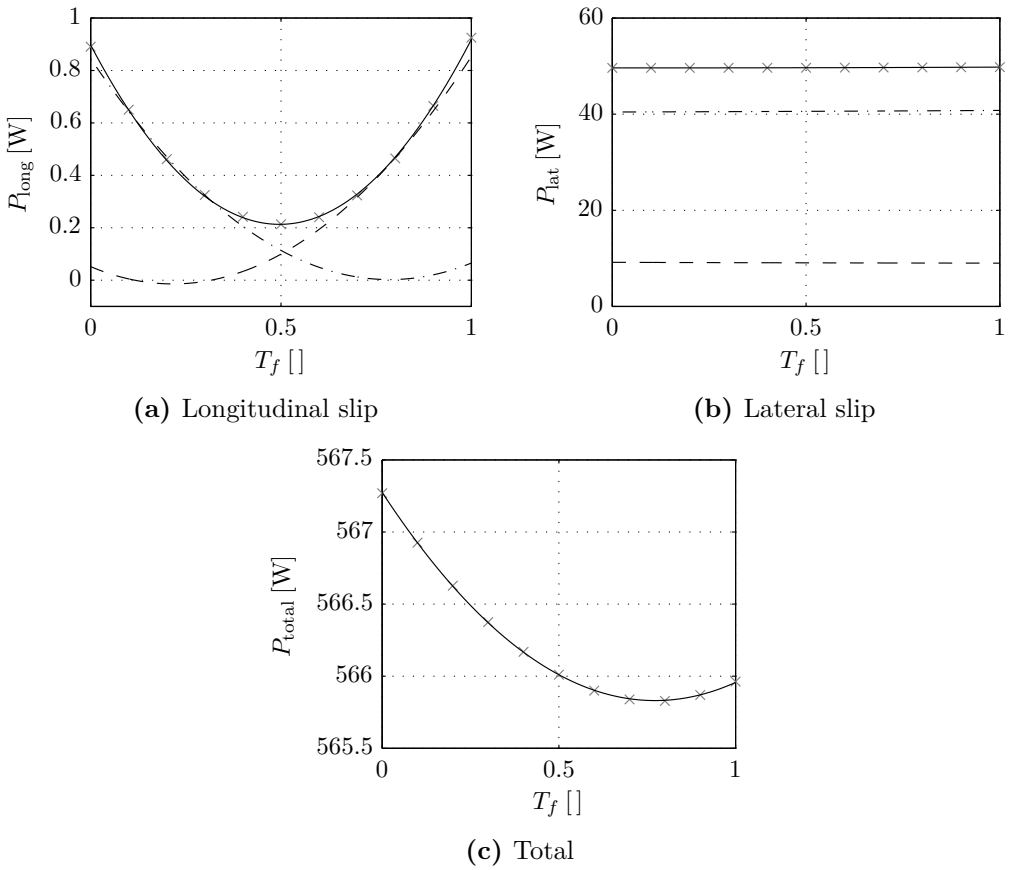

(a) Longitudinal slip

(b) Lateral slip

(c) Total

Figure 6.10: Motorcycle power consumption during cornering at $12.5\,\mathrm{m\,s^{-1}}$. ——Total; – – –Front Wheel; –·–·Rear Wheel.

Finally, the case of a motorcycle negotiating a constant radius corner is investigated to find the effect of torque vectoring on efficiency. The speed, in each case,

is controlled to $12.5\,\mathrm{m\,s^{-1}}$ and the turn radius to 50 m. Figure 6.10a shows that longitudinal slip power consumption is significantly affected by the torque distribution ratio, though magnitudes at this speed are small, at less than 1 W. Lateral slip power consumption, on the other hand, is hardly affected by torque distribution ratio, as shown in Figure 6.10b. Lateral slip power consumption is significantly higher at the rear wheel, for all ratios. Figure 6.10c shows that in this situation, the most efficient way to distribute the torque is with only 30 % going to the rear wheel ($T_f = 0.7$); the least efficient distribution is with the conventional method of supplying all the torque to the rear wheel. Again, however, the magnitude of the potential improvement is small at around 0.7 %.

6.4 Chapter Summary

The results in this chapter have shown that the maximum energy efficiencies of the automobiles occur when the front–rear torque distribution ratio is the same as, or slightly greater than, the weight distribution ratio; for example, if a vehicle has 60 % of its weight over the front wheels, it should have 60 %, or slightly more, of the drive torque at the front wheels for maximum efficiency. It appears that the torque distribution bias should be more towards the front during cornering. The results concerning the most efficient way to distribute power in a motorcycle are similar to that of the automobile.

In the automobile, the most efficient left–right torque distribution ratio depends on the handling characteristic of the vehicle without torque vectoring, though in general, a bias of drive torque towards the outside wheel(s) increases efficiency. A torque distribution ratio that helps to counteract the effect of the handling characteristic reduces the power consumption; for example, a vehicle that is significantly understeer would benefit most, in terms of efficiency, from having drive torque biased towards the outside wheels. Similarly, the power consumption of a vehicle that is significantly oversteer can be reduced by vectoring torque to the inside wheels.

The impact that torque vectoring has on efficiency is speed dependent: at very low speeds, the impact is negligible; at moderate speeds, putting slightly more power to the outside wheels reduces the energy consumption. At high speeds, the most efficient way to distribute power is to use it to counteract any understeer or oversteer tendency.

During straight running, the motorcycle is at its most energy efficient when drive torque is distributed according to the vertical load seen at the tyres. During cornering, the torque to the front wheel should be increased slightly from the straight-running ideal.

Happily, it seems that torque vectoring systems can achieve both an improvement in vehicle handling and a reduction in energy efficiency at the same time. This is a feat not achieved by other driveline augmentations, such as traditional limited slip differentials or brake-based stability control systems, both of which reduce vehicle energy efficiency.

However, improvements in energy efficiency over the standard vehicles are small, in the demonstrated steady-state situations. Recent research by Abe and Kano [1] also showed small reductions, and, in some cases, increases in the power consumed by an ATD automobile undertaking a lane-change manoeuvre. The power savings offered by torque vectoring may be negated by the added mass and losses associated with the drivelines used to achieve it. There may well be more improvement possible during acceleration or for hill-climbing manoeuvres, especially on soft ground. Indeed, Senatore and Sandu [60] found that on a loose surface, it was possible to improve efficiency with more torque towards the rear wheels; however, in off-road vehicles, the *multi-pass* effect of the axles will affect the results.

Chapter 7

Conclusions and Future Work

The research presented herein was initiated after developments were made in automobile and motorcycle technology that allow more control of the amount of drive torque that each wheel receives [10, 28, 54, 57]. History has shown that improvements in traction, handling and stability of automobiles can be made through better control over the individual wheel torques, [3, 71], where control was traditionally achieved through a reduction in the overall drive torque, or application of a brake at one, or more, of the wheels. Electronically controlled systems include the Traction Control System (TCS) and the Electronic Stability Program (ESP) developed by Bosch. Improvements in one performance aspect of a vehicle often come at the expense of worse performance in another; for example, when stability in a corner is improved through a the application of a brake, the vehicle speed might suffer.

Most current electronic chassis enhancements are active only when the system detects that the vehicle is in danger of becoming unstable, at which point it will interfere with the driver's request of the vehicle. The issues with this method of working are two-fold: the system is not active most of the time, leading to expensive components being idle, and when they are active, they might interfere with the driver's intentions. A benefit of a system that aims to influence vehicle performance through active distribution of the drive torque is that they can be permanently active, and thus utilised by a driver in away that is not imposing. Additionally, they can be used in parallel with existing stability enhancements when a dangerous situation is detected. Many researchers have considered the potential for torque vectoring systems to improve the handling of automobiles [1, 48], but there exists the potential for efficiency gains to be realised through better distribution of the drive torque and associated reduction in wheel slip power losses.

In the case of motorcycles, there is a very limited number of production motorcycles that can apply drive torque to the front wheel, and research is needed in this area to investigate the effect on handling and efficiency, and to determine whether it

is beneficial.

This thesis provides details of investigations that have been made in the areas of Active Torque Distribution (ATD) in two- and four-wheeled vehicles. In this chapter, conclusions drawn from those investigations are summarised. Their presentation here is intended to supplement the conclusions in the previous chapter summaries. Work that represents original contributions will also be highlighted. Finally, recommendations for further work will be made.

7.1 Conclusions

Conclusions will be sectioned according to corresponding chapters in the thesis, and supplement the more detailed summaries at the end of each chapter. Chapters 1 and 2 presented an introduction to the topic and a review of the literature and current technology. Aims and objectives of the research were set accordingly.

7.1.1 Vehicle Modelling

Chapter 3 presented the modelling of both the automobile and the motorcycle. A wheel model that is suitable for use in both models was also developed. Various tyre models for the automobile and motorcycle were coded for use with the vehicle models. Simple driver models, capable of controlling the yaw rate and longitudinal speed of the vehicles were created.

Mathematical automobile models were created first, using the well-known *bicycle model*, and then a seven-Degree-of-Freedom (DoF) model similar to one presented by Osborn and Shim [45], but with a more realistic and versatile tyre model. These were used to provide the basis for a multibody model that was ultimately used for the torque vectoring investigations. The multibody automobile model has 14 degrees of freedom, including simple suspension models and the individual rotations of the wheel masses, and accounts for dynamic weight transfer, inertial and gyroscopic effects, and aerodynamic lift and drag. The model, created in SimMechanics [69], is specified using a block diagram approach that is intuitive to use. The model provides a sufficiently detailed representation of the vehicle for handling and efficiency studies, in an environment that is well-documented and user-modifiable; it therefore avoids proprietary issues with commercially available vehicle dynamics software.

Modelling of the motorcycle followed a similar approach: firstly, mathematical models were created, upon which the multibody modelling was based. A steady-state two-DoF model was derived, based on the *bicycle model* for automobiles, but which accounts for the camber of the cornering motorcycle. This model is not widely used in motorcycle dynamics, and presents a method of analysing the handling characteristics

with only eight parameters. A four-DoF model presented by Seffen *et al.* [59] was also coded for initial handling investigations.

The multibody motorcycle model, again created in SimMechanics, is based on literature [40, 66], and accounts for steer and twist of the steering system, front and rear suspensions, rider lean, toroidal tyres and aerodynamic forces. Gyroscopic and inertial effects are also included. The model is sufficiently accurate for handling and efficiency investigations without being computationally expensive.

A generic wheel model was developed in SimMechanics, for use with both the automobile and the motorcycle models. It accounts for the change in radius as the wheel cambers. For motorcycle tyres, the migration of the contact patch due to the toroidal radius is also accounted for. Care was also taken to calculate the various radii generated in dynamic situations, such as the effective, deformed, and rolling radii. A peculiarity of SimMechanics is that forces have to be applied to a Coordinate System (CS) attached to, and moving with, a body; thus, tyre forces and moments must be applied at the wheel centre. The model accounts for this shift in forces from the contact patch on the road and applies the additional moment. These characteristics are believed to be important for accurate simulation results.

The tyre models presented include linear models, various *Magic Formula* models [46] for both automobiles and motorcycles, and a motorcycle tyre model presented by Meijaard and Popov [40]. The most complex of the tyre models calculate all six principle forces and moments, and includes the effects of the vertical load and combined slip situations. They are implemented in SimMechanics in a format designed to be reusable. Simple Proportional–Integral (PI) controllers control speed and steer inputs, if required, to allow simulated vehicles to undertake similar manoeuvres, and, thus, the different vehicles can be directly compared.

Together, these components form advanced models of an automobile and a motorcycle that are suitable for detailed investigations into the effects of torque distribution.

7.1.2 Model Verification

Chapter 4 verified the models of Chapter 3, firstly, with each other, and also through checks on instantaneous radius of curvature and conservation of energy.

The automobile multibody matched both the *bicycle model* and the 7-DoF model at low speeds, giving confidence in its results. At higher speeds, and when the complex tyre is used, differences begin to appear due to the varying influence of vertical load on horizontal force generation, tyre aligning moments and gyroscopic effects. This highlights the fact that the simple *bicycle model* and the 7-DoF model are not suitable for torque vectoring investigations at high speeds and lateral accelerations.

All of these effects influence the handling of real vehicles, and thus it is important to account for them in the simulation model, if accurate results are to be obtained.

The motorcycle model was verified by checking with the expected camber angle of a cornering motorcycle, with good accuracy. The small discrepancies are though to be caused by gyroscopic and aerodynamic effects and sideslip at the wheels. Again, including these effects are key to obtaining accurate simulation results.

Finally, following Evangelou [16], the forces and moments were balanced against the resulting motions, and the power applied to the driving wheels was balanced against the amount dissipated through aerodynamics and slip.

This thorough verification of the models gives good confidence that they are suitable for their intended purpose: to analyse the effects of torque distribution on handling and efficiency in motorcycles and automobiles.

7.1.3 Vehicle Handling

The handling characteristics of the automobile and the motorcycle were studied in Chapter 5, and the conclusion will be presented separately.

Automobile Handling

For automobiles, the chapter was introduced with a summary of steady-state handling characteristics, including yaw rate and sideslip angle gains and the *understeer gradient* [18]. Equations for a quantitative analysis were derived from the linear *bicycle model* and the effect of weight distribution on the characteristics was shown using the multibody model with testing methods conforming to [26]. This analysis formed the basis of the torque distribution investigation.

Considering front–rear torque vectoring, at lateral accelerations of up to around $0.5\,g$, there is very little influence on handling properties. This is because the lateral force generation capacity of the tyres is unaffected by the longitudinal demand at these low speeds, therefore, no effect is seen on the handling characteristics. Above this value, small alterations in the handling characteristics could be made; for example, transferring power to the rear wheels could reduce understeer tendency at high speeds. However, a significant increase in the maximum speed achievable over the equally-distributed vehicle in a given constant-radius manoeuvre was not seen.

On the other hand, left–right torque vectoring has much more effect on the vehicle handling, and the effects are similar for left–right torque vectoring in vehicles with Front Wheel Drive (FWD), Four Wheel Drive (4WD) and Rear Wheel Drive (RWD) drivelines. At low speeds, the torque distribution was shown to affect the steer angle required to achieve a specified cornering radius, and as speeds increase, the influence on lateral acceleration and yaw rate gains becomes more significant. Oversteer (OS)

and Understeer (US) vehicles can be made less so, by transferring drive torque to the inside and outside wheels, respectively; however, at high speeds, this can cause the vehicles to become unstable earlier than their equally-distributed counterpart. The actual range of adjustment to handling that left–right torque vectoring system provides is small in comparison with the effect of weight distribution.

The responsiveness and the stability of an automobile was also considered, following the application of a steer angle input. At moderate speeds, left–right torque vectoring had a small effect on the responsiveness; for example, the yaw acceleration was higher when torque was distributed at the outside wheels. However, the effect was small and disappeared as the tyres forces became saturated at higher longitudinal speed. The stability of the vehicles was also reduced at high speeds, where any oscillations seen in the response were exacerbated, and the OS vehicle would spin if drive torque were distributed solely to the outside wheels. Front–rear torque vectoring had negligible effect on the transient response.

In conclusion, left–right torque vectoring can significantly affect the steady-state handling characteristics of the automobile at moderate and high speeds; where as front–rear torque vectoring has a lesser effect and only at high speeds. In these situations, it appears that left–right torque vectoring is almost as effective in vehicles with FWD or RWD as those with 4WD.

Motorcycle Handling

Firstly, the steady-state response of a motorcycle with range of steer inputs and speeds was calculated using a four-DoF mathematical model presented by Seffen *et al.* [59]. This was used to demonstrate that steer angle, camber angle, yaw rate and lateral acceleration, are proportional to the steer torque input, and thus, the model can be simplified. A two-DoF eight-parameter model was derived to calculate the steady-state response, which was used for initial investigations into how weight distribution and tyre properties affect handling.

The impact on handling of varying the drive torque distribution between the front and rear wheels was then considered. It appears that in motorcycles the effect is small, although the motorcycle, which was naturally oversteer according to the multibody model handling analysis, could be made slightly less so, by application of the drive torque to the front wheel. The fact that torque vectoring does not significantly alter the handling dynamics means that torque can be applied to the front wheel to increase traction, for example, without adversely affecting the handling properties. In conditions of low-friction, or on loose surfaces, the influence on handling may be more significant.

7.1.4 Energy Efficiency

Changing the distribution of power between the wheels of a vehicle could alter the efficiency in a number of ways. The forces generated by the tyres are dependent on the vertical load and the lateral and longitudinal slip situation, amongst other things; thus altering the distribution of torque to take advantage of the situation could present energy savings. In automobiles, where tyres are generally stiffer longitudinally than laterally, generating a yaw moment through a difference in longitudinal force could reduce the slip magnitude required, and therefore, reduce power consumption.

Chapter 6 considered the impact on automobile and motorcycle efficiency. In straight line situations, for maximum efficiency, it appears that torque should be distributed according the the vertical loading situation; for example, a vehicle with 60 % of the weight over the front wheels, should also have 60 % of the torque at the front wheels. In a cornering situation, the minimum power point appear to be with slightly more of the torque to the front wheels than the straight line case. This is true of both motorcycles and automobiles.

Concerning left–right torque distribution in automobiles, during cornering at moderate speeds, energy-efficiency can be increased by applying slightly more power to the outside wheels than the inside. At high speed, efficiency can be improved by distributing the torque according to the handling characteristic: a vehicle that is OS can be made more efficient by biasing the torque to the inside wheels to counteract the effect of its OS tendency, and vice versa for the US vehicle.

However, the impact of torque vectoring on the overall power consumption of the vehicles is only a few percent. This is because the majority of dissipation is due to aerodynamic forces, and, during a corner, the lateral tyre forces.

7.1.5 Overall Conclusions

Mechanical methods of torque vectoring are complex, and will add weight and cost to a vehicle; thus, for most situations, it is difficult to justify the addedexpense. However, with electric motors becoming cheaper and more common in vehicles, it is foreseeable that vehicles with drive sources at each wheel will become available. In this situation, it would be sensible to take advantages of the gains that ATD can provide in both handling and efficiency. It is interesting that almost the same effect on handling can be achieved through left–right torque vectoring with two-wheel drive, as with four-wheel drive.

Currently, powering the front wheel of a motorcycle mechanically is difficult and expensive: such motorcycles are sold at a premium for speciality purposes. Because ATD in motorcycles has the potential to save only a small amount of energy in the steady-state cases presented here, associated losses in the necessary drive

system may well negate the reduction completely. As for automobiles, if the trend is towards electric propulsion, and powering the front wheel becomes easier, this research has shown the on-road handling characteristics will not be adversely affected, and improvements in low-friction traction could be realised.

The models presented in this thesis will be of use to vehicle designers, when deciding what type of driveline to use in vehicles of the future. When rough vehicle parameters are known, they models can easily be modified to represent different vehicles. One benefit of the SimMechanics block-diagram-based approach is that the vehicle models can be modified without an in-depth knowledge of the equations that they represent. For example, it would be relatively simple to add an extra rear wheel at each side, to simulate the handling and efficiency of light trucks.

Similarly, the models can be used by future researchers who wish to develop, for example, torque vectoring control strategies, or for further parameters studies in different situations or conditions.

7.2 Original Contributions to Knowledge

This section outlines the elements of work contained in this thesis that, in the author's opinion, represent original contributions to knowledge.

- A multibody automobile model has been created that is useful for investigating the effects of torque vectoring. It has 14-DoFs, including pitch and roll motions with a simple suspension model. A complex tyre model is used that includes the effects of vertical load, combined slip, and camber angle on tyre forces and moments. Previous vehicle models for torque vectoring investigation have made assumptions that mean they may be unsuitable for use in limit-handling situations. The automobile model was thoroughly verified using mathematical models, and with various other numerical checks. The importance of including complex tyre models and dynamic weight distribution was shown.

- The possible range of impact that torque vectoring could have on automobile handling at a range of speeds has been shown for vehicles with three different weight distributions. Ideal FWD, 4WD and RWD drivelines that can variably distribute torque between the left and right wheels were used. In the 4WD case, front–rear torque distributions were also investigated.

- The impact of torque distribution on the energy efficiency of automobile has been investigated by monitoring the amount of power consumed as slip at the wheels and the overall power consumption of the vehicles as the undertake various manoeuvres. A range of automobile weight distributions were simulated

with ideal torque vectoring drivelines in straight line and steady-state cornering situations.

- Steady-state handling characteristics are commonly used in the study of automobiles; however, they are seldom used in the study of motorcycle dynamics. Linearised equations of motion have been derived for a steady-state cornering situation and equations for the calculation of the handling characteristics were presented. Their application to real two-wheeled vehicles was considered using the multibody model.

- A multibody model of a motorcycle has been created, with a moderately complex tyre model implemented in it, that is suitable for the simulation of a motorcycle with ideal power sources at both the front and rear wheels. The results of an investigation into how torque vectoring in motorcycles affects their handling were presented.

- The motorcycle was analysed in straight line and steady-state cornering situations in order to find the effect of torque vectoring on efficiency. Real all-wheel-drive motorcycles are rare; this investigation considers one of the advantages they might offer.

7.3 Future Work

This work provides a foundation for many further interesting research topics. This section aims to provide recommendations for areas of future work that would build on the current understanding of ATD and its influences.

- With an electric motor at each wheel, it is feasible that energy could be recovered from one wheel and applied to another; thus, a torque imbalance could be generated regardless of the torque request from the driver. This is generally not the case with mechanical devices that distribute engine torque, although exceptions do exist [56]. It would be interesting to see the effect of this additional torque difference in automobiles and motorcycles, especially at low speeds, when distributing the torque according to a ratio has less effect.

- Further parameter studies should be undertaken, to investigate the performance of vehicles in other situations or conditions. The performance on loose or low-friction ground may have more potential for improvement than the situations examined in this thesis.

- A more advanced controller should be developed, capable of calculating the torque that would, for example, minimise slip power, or understeer, or maximise

tractive effort. The effect on the minimum lap time of an ATD-equipped race car would be particularly interesting. The controller could interface with the presented vehicle models to determine its efficacy.

- The way in which torque vectoring coexists with other stability and safety systems should be investigated. Integrated chassis control has the potential to integrate existing brake-based stability control with torque vectoring and other possible future trends, such as active steering and active suspension [51].
- Test vehicles with ATD drivelines should be built, to validate results and provide human feedback on the quality of such a vehicle, which is hard, if not impossible, to calculate.

Bibliography

[1] M. Abe and Y. Kano. A study on active vehicle chassis control reducing dissipation energy by tire slip for full drive-by-wire electric vehcile. In *The 23rd international symposium on dynamics of vehicles on road and tracks*. Qingdao, China, 2013.

[2] M. Abe. *Vehicle handling dynaimcs: theory and application*. Elsvier, Oxford, UK, 2009.

[3] A. F. Andreev, V. I. Kababau and V. V. Vantsevich. *Driveline systems of ground vehicles - theory and design*. CRC Press, Boca Raton, Florida, USA, 2010.

[4] Bosch. Bosch safety technology for motorcyclists. 2014. URL: http://www.bosch-presse.de/presseforum/details.htm?txtID=6819&tk_id=108&locale=en.

[5] M. Burgess. Torque vectoring. Lotus Engineering. 2009. URL: http://www.vehicledynamicsinternational.com/downloads/VDI_Lotus_Vector.pdf.

[6] R. Capitani, G. Masi, A. Meneghin and D. Rosti. Handling analysis of a two-wheeled vehicle using msc. adams/motorcycle. *Vehicle system dynamics*, 44(sup1):698–707, 2006.

[7] C. C. Chan. The state of the art of electric, hybrid, and fuel cell vehicles. In *Proceedings of the IEEE*. Volume 95. (4), April 2007, pages 704–718.

[8] C. C. Chan, A. Bouscayrol and K. Y. Chen. Electric, hybrid, and fuel-cell vehicles: architectures and modeling. *IEEE transactions on vehicular technology*, 59(2):589–598, February 2010. ISSN: 0018-9545.

[9] K. T. Chau and Y. S. Wong. Overview of power management in hybrid electric vehicles. *Energy conversion and management*, 43(15):1953–1968, 2002. ISSN: 0196-8904.

[10] Christini Technologies Inc. The Basics of AWD. 2013. URL: http://www.christini.com/awd-technology/about-the-technology.

[11] V. Cossalter. *Motorcycle dynamics*. Lulu.com, 2006.

[12] M. Croft-White and M. Harrison. Study of torque vectoring for all-wheel-drive vehicles. *Vehicle system dynamics*, 44(sup1):313–320, 2006.

[13] L. De Novellis, A. Sorniotti and P. Gruber. Design and comparison of the handling performance of different electric vehicle layouts. *Proceedings of the institution of mechanical engineers, part d: journal of automobile engineering*, 228(2):218–232, 2014.

[14] H. Dugoff, P. S. Fancher and L. Segel. An analysis of tire traction properties and their influence on vehicle dynamic performance. *SAE technical papers*, 1970.

[15] European Commission. Vehicle safety systems - transport. 2014. URL: http://ec.europa.eu/transport/themes/its/road/application_areas/vehicle_safety_systems_en.htm.

[16] S. Evangelou. Control and stability analysis of two-wheeled road vehicles. PhD thesis. University of London, 2004.

[17] E-VECTOORC. Electric-vehicle control of individual wheel torque for on- and off-road conditions. 2014. URL: www.e-vectoorc.eu/.

[18] T. Gillespie. *Fundamentals of vehicle dynamics*. Society of Automotive Engineers, 1992. ISBN: 9781560911999.

[19] L. Guzzella and A. Sciarretta. *Vehicle propulsion systems: introduction to modeling and optimization*. L. Guzzella and A. Sciarretta, editors. Springer, Berlin, Germany, 2005.

[20] M. Hancock. Vehicle handling control using active differentials. 2006.

[21] M. Hancock, R. Williams, E. Fina and M. Best. Yaw motion control via active differentials. *Transactions of the institute of measurement and control*, 29(2):137–157, 2007. ISSN: 0142-3312.

[22] J. Happian-Smith. *An introduction to modern vehicle design*. Butterworth-Heinemann, 2001.

[23] J. He, D. A. Crolla, M. C. Levesley and W. J. Manning. Coordination of active steering, driveline, and braking for integrated vehicle dynamics control. *Proceedings of the institution of mechanical engineers, part d: journal of automobile engineering*, 220(10):1401–1420, 2006.

[24] Honda. Honda's innovative SH-AWD technology add a whole new dimension of handling power. URL: http://world.honda.com/automobile-technology/SH-AWD/.

[25] I. Hussain. *Electric and hybrid vehicles design fundamentals*. CRC Press, Boca Raton, USA, 2nd edition, 2011.

[26] International Organization for Standardization, 2004. ISO4138:2004 Passenger Cars – Steady-state circular driving behaviour – Open-loop test methods, Geneva, 2004.

[27] International Organization for Standardization, 2011. ISO8855:2011 Road vehicles – Vehicle dynamics and road-holding ability – Vocabulary, Geneva, 2011.

[28] L. Jansson. 2WD - The Complete Story. 2013. URL: http://www.ohlins.com/Checkpoint-Ohlins/2WD---The-Complete-Story/.

[29] JTEKT Torsen North America Inc. Torsen Traction Home Page. 2011. URL: http://www.torsen.com/.

[30] I. Kageyama and Y. Kuriyagawa. Study on influence of rider's lean angle on two-wheeled vehicle behavior. In *10th international symposium on advanced vehicle control*. Loughborough, 2010, pages 355–360.

[31] G. Kaiser, F. Holzmann, B. Chretien, M. Korte and H. Werner. Torque vectoring with a feedback and feed forward controller - applied to a through the road hybrid electric vehicle. In *Intelligent vehicles symposium (iv), 2011 IEEE*, June 2011, pages 448–453.

[32] C. Koenen. The dynamic behaviour of a motorcycle when running straight ahead and when cornering. PhD thesis. 1983.

[33] J. Kooijman and A. Schwab. A review on bicycle and motorcycle rider control with a perspective on handling qualities. *Vehicle system dynamics*, 51(11):1722–1764, 2013.

[34] J. Kooijman and A. Schwab. A review on handling aspects in bicycle and motorcycle control. In *ASME 2011 international design engineering technical conferences and computers and information in engineering conference*. American Society of Mechanical Engineers, 2011, pages 597–607.

[35] D. J. Limebeer, R. Sharp and S. Evangelou. The stability of motorcycles under acceleration and braking. *Proceedings of the institution of mechanical engineers, part c: journal of mechanical engineering science*, 215(9):1095–1109, 2001.

[36] M. Lin. Driver and vehicle modelling as development tools in vehicle handling design. PhD thesis. University of Nottingham, April 2004.

[37] W. J. Manning and D. A. Crolla. A review of yaw rate and sideslip controllers for passenger vehicles. *Transactions of the institute of measurement and control*, 29(2):117–135, 2007. ISSN: 0142-3312.

[38] G. Mavros. On the objective assessment and quantification of the transient-handling response of a vehicle. *Vehicle system dynamics*, 45(2):93–112, 2007.

[39] Mechanical Simulation Corporation. Mechanical simulation: home page. 2011. URL: `http://www.carsim.com/`.

[40] J. Meijaard and A. Popov. Multi-body modelling and analysis into the non-linear behaviour of modern motorcycles. *Proceedings of the institution of mechanical engineers, part K: journal of multi-body dynamics*, 221(1):63–76, 2007.

[41] J. Meriam and L. G. Kraige. *Engineering mechanics: dynamics*. John Wiley & Sons, 7th edition, 2012.

[42] M. Milehins, C. Cheng, T.-W. Chu and R. P. Jones. Handling behaviour of a TTR hybrid electric vehicle with independent rear wheel torque control. In *10th international symposium on advanced vehicle control*. Loughbrough, UK, August 2010, pages 556–561.

[43] F. C. Moon. *Applied dynamics: with applications to multibody and mechatronic systems*. John Wiley & Sons, 2008.

[44] MSC Software. Adams the multibody dynamics simulation solution. 2014. URL: `http://www.mscsoftware.com/product/adams`.

[45] R. P. Osborn and T. Shim. Independent control of all-wheel-drive torque distribution. *Vehicle system dynamics*, 44(7):529–546, July 2006.

[46] H. B. Pacejka. *Tyre and vehicle dynamics*. Butterworth-Heinemann, Oxford, UK, 3rd edition, 2012.

[47] L. Pinto, S. Aldworth, M. Watkinson, P. Jeary and M. Franco-Jorge. Advanced yaw motion control of a hybrid vehicle using twin rear electric motors. In *10th international symposium on advanced vehicle control*. Loughborough, UK, August 2010, pages 640–645.

[48] D. Piyabongkarn, J. Lew, R. Rajamani and J. Grogg. Active driveline torque-management systems. *IEEE control systems magazine*, 30(4):86–102, August 2010. ISSN: 1066-033X.

[49] D. Piyabongkarn, J. Y. Lew, R. Rajamani, J. A. Grogg and Q. H. Yuan. On the use of torque-biasing systems for electronic stability control: limitations and possibilities. *IEEE transactions on control systems technology*, 15(3):581–589, May 2007. ISSN: 1063-6536.

[50] R. Rajamani. *Vehicle dynamics and control*. Springer, New York, 2006.

[51] C. Rengaraj and D. Crolla. Integrated chassis control to improve vehicle handling dynamics performance. Technical report. SAE Technical Paper, 2011.

[52] R. J. Rieveley. The effect of direct yaw moment on human controlled vehicle systems. PhD thesis. Canada: University of Windsor, 2010.

[53] R. J. Rieveley and B. P. Minaker. Variable torque distribution yaw moment control for hybrid powertrains. *Avanced hybrid vehicle powertrains, SAE 2007-01-0278*, 2007.

[54] K. Rikiya, I. Akihiro, A. Yoshihiro and M. Atsushi. Development of sh-awd (super handling-all wheel drive) system. *Honda R&D technical review*, 16(2):9–16, 2004.

[55] Robert Bosch GmbH. *Automotive handbook*, 9th edition, 2014.

[56] K. Sawase and Y. Ushiroda. Improvement of vehicle dynamics by right-and-left torque vectoring system in various drivetrains. Technical report (20). Mitsubishi Motors Technical Review, 2008.

[57] K. Sawase, Y. Ushiroda and T. Miura. Left-right torque vectoring technology as the core of super all wheel control (S-AWC). Technical report. Mitsubishi Motors Technical Review, 2006.

[58] A. Schwab and J. Meijaard. How to draw Euler angles and utilize Euler parameters. In *ASME 2006 international design engineering technical conferences and computers and information in engineering conference*. American Society of Mechanical Engineers, 2006, pages 259–265.

[59] K. Seffen, G. Parks and P. Clarkson. Observations on the controllability of motion of two-wheelers. *Proceedings of the institution of mechanical engineers, part I: journal of systems and control engineering*, 215(2):143–156, 2001.

[60] C. Senatore and C. Sandu. Torque distribution influence on tractive efficiency and mobility of off-road wheeled vehicles. *Journal of terramechanics*, 48(5):372–383, 2011. ISSN: 0022-4898.

[61] A.-H. M. Sharaf. Investigation of all-wheel-drive off-road vehicle dynaimcs augmented by visco-lock devices. PhD thesis. Loughborough University, September 2007.

[62] R. S. Sharp. Stability, control and steering responses of motorcycles. *Vehicle system dynamics*, 35(4-5):291–318, 2001.

[63] R. S. Sharp. The stability and control of motorcycles. *Journal of mechanical engineering science*, 13(5):316–329, 1971.

[64] R. Sharp, S. Evangelou and D. Limebeer. Advances in the modelling of motorcycle dynamics. *Multibody system dynamics*, 12:251–283, 3, 2004. ISSN: 1384-5640.

[65] R. Sharp, S. Evangelou and D. Limebeer. Improved modelling of motorcycle dynamics. In *Eccomas thematic conference on advances in computational multibody dynamics*. Lisbon, 2003.

[66] R. Sharp and D. Limebeer. A motorcycle model for stability and control analysis. *Multibody system dynamics*, 6:123–142, 2, 2001. ISSN: 1384-5640.

[67] M. Shino and M. Nagai. Independent wheel torque control of small-scale electric vehicle for handling and stability improvement. *JSAE review*, 24(4):449–456, 2003. ISSN: 0389-4304.

[68] Tesla Motors, Inc. Tesla motors | premium electric vehicles. 2010. URL: http://www.teslamotors.com/.

[69] The Mathworks. Mathworks United Kingdom - products and services. 2012. URL: http://www.mathworks.co.uk/products/.

[70] Toyota GB Plc. The new toyota prius - the original hybrid car by toyota. 2011. URL: http://www.toyota.co.uk/cgi-bin/toyota/bv/frame_start.jsp?id=MSR_PRIUS.

[71] A. G. Ulsoy, H. Peng and M. Çakmakci. *Automotive control systems*. Cambridge University Press, 2012.

[72] Unknown. Mitsubishi motors develops S-AWC vehicle dynaimcs control system & twin clutch sst automated manual transmission. Technical report. Mitsubishi Motors Corporation, October 2007.

[73] Y. Ushiroda, K. Sawase, N. Takahashi, K. Suzuki and K. Manabe. Development of super AYC. *Mitsubishi motors tech rev*, 15:73–76, 2003.

[74] F. J. W. Whipple. The stability of the motion of a bicycle. *The quarterly journal of pure and applied mathematics*, 30:312–348, 1899.

[75] J. Y. Wong. *Theory of ground vehicles*. John Wiley & Sons, 2001.

[76] G. Wood. Motorcycle: full nonlinear motion. 2013. URL: www.mathworks.co.uk%20/help/physmod/sm/examples_v1/motorcycle-full-nonlinear-motion.html.

[77] A. T. van Zanten. Evolution of electronic control systems for improving the vehicle dynamic behavior. In *6th international symposium on advanced vehicle control*. Hiroshima, Japan, September 2002.

Appendix A

The Rotation Matrix

The orientation of a body relative to a fixed Coordinate System (CS) can be given by a rotation matrix. The rotation matrix, $\mathbf{R}$, is a matrix that transforms a vector from the body-fixed CS to the global, or space-fixed, CS, as in,

$$\boldsymbol{r} = \mathbf{R}\boldsymbol{r}', \tag{A.1}$$

with space-fixed coordinates $\boldsymbol{r}$ and body-fixed coordinates $\boldsymbol{r}'$ [43, 58]. Its inverse, inv($\mathbf{R}$), can be used to transform space-fixed coordinates into body-fixed coordinates. In three-dimensional space, it is a 3×3 matrix,

$$\mathbf{R} = \begin{bmatrix} R_{11} & R_{12} & R_{13} \\ R_{21} & R_{22} & R_{23} \\ R_{31} & R_{32} & R_{33} \end{bmatrix}, \tag{A.2}$$

which, if known, can be solved to find three parameters that characterise the rotation.

A.1 Calculation of the Rotation Matrix

Using aeroplane terminology of yaw, roll and pitch, and notation from tyre studies, rotation matrices representing the three individual rotations are given below.

Yaw is an anti-clockwise rotation of ψ about the *global* Z-axis, with a rotation matrix

$$\mathbf{R}_{\psi} = \begin{bmatrix} \cos\psi & -\sin\psi & 0 \\ \sin\psi & \cos\psi & 0 \\ 0 & 0 & 1 \end{bmatrix}. \tag{A.3}$$

Roll, or camber when referring to tyres, is an anti-clockwise rotation of γ about the body's x-axis, with a rotation matrix

$$\mathbf{R}_\gamma = \begin{bmatrix} 1 & 0 & 0 \\ 0 & \cos\gamma & -\sin\gamma \\ 0 & \sin\gamma & \cos\gamma \end{bmatrix}. \tag{A.4}$$

Pitch is an anti-clockwise rotation of Ω about the body's y-axis, with a rotation matrix

$$\mathbf{R}_\Omega = \begin{bmatrix} \cos\Omega & 0 & \sin\Omega \\ 0 & 1 & 0 \\ -\sin\Omega & 0 & \cos\Omega \end{bmatrix}. \tag{A.5}$$

The above rotation matrices can be used to apply the individual transformations sequentially, or the rotation matrix representing the complete transformation can be used, which is found by multiplying the matrices together:

$$\mathbf{R} = \mathbf{R}_\psi \mathbf{R}_\gamma \mathbf{R}_\Omega = \begin{bmatrix} \cos\Omega\cos\psi - \sin\Omega\sin\gamma\sin\psi & -\cos\gamma\sin\psi & \sin\Omega\cos\psi + \cos\Omega\sin\gamma\sin\psi \\ \cos\Omega\sin\psi + \sin\Omega\cos\psi\sin\gamma & \cos\gamma\cos\psi & \sin\Omega\sin\psi - \cos\Omega\cos\psi\sin\gamma \\ -\sin\Omega\cos\gamma & \sin\gamma & \cos\Omega\cos\gamma \end{bmatrix}. \tag{A.6}$$

A.2 Calculation of Yaw and Camber Angles From the Rotation Matrix

In the SimMechanics model, the rotation matrix is known, and the individual rotations are required. By simplifying the rotation matrix calculated in Equation (A.6), the following equations are obtained for the yaw, roll and pitch angles, respectively:

$$\psi = -\arctan\left(\frac{R_{12}}{R_{22}}\right), \tag{A.7}$$

$$\gamma = \arctan\left(\frac{R_{32}}{\sqrt{R_{31}^2 + R_{33}^2}}\right), \tag{A.8}$$

$$\Omega = -\arctan\left(\frac{R_{31}}{R_{33}}\right). \tag{A.9}$$

Appendix B

MATLAB scripts

B.1 The *Bicycle Model*

Listing B.1: Bicycle Model Function

```
function ydot = planar_model(t,y,vehicle,F_zf,F_zr,v_x,delta)
%planar vehicle model
%y=[lat vel; yaw rate]

%side slip angles [rad]
alpha_f = ((y(1)+(vehicle.l_f*y(2)))/v_x)-delta; %front
alpha_b = ((y(1)-(vehicle.l_b*y(2)))/v_x);  %rear

%lat tyre force [N]
gamma=0; %camber=0
F_yf = tyreforceLIN(F_zf,alpha_f,gamma); %front
F_yb = tyreforceLIN(F_zr,alpha_b,gamma); %rear

%equations of motion
v_ydot=((2*F_yf + 2*F_yb - (v_x*vehicle.m*y(2)))/vehicle.m); %lateral ...
    vel change [m/s^2]
psi_ddot= (((vehicle.l_f*2*F_yf)-(vehicle.l_b*2*F_yb))/vehicle.I); % ...
    yaw acc [rad/s^2]

ydot = [v_ydot; psi_ddot];
end
```

B.2 Seven-Degrees-of-Freedom Model

Listing B.2: Seven-Degrees-of-Freedom Model Function

```
function y_dot = planar_7dof (t, y, vehicle, driver_inputs)
%planar vehicle model function J Griffin 2014-01-21
%y=[v_x v_y psi_dot omega_FL omega_FR omega_RL omega_RR]
%driver_inputs=[delta; tau_FL; tau_FR; tau_RL; tau_RR];

persistent a_x a_y
```

```
if isempty(a_x) % initialise a_x and a_y
    a_x=0; a_y=0;
end

delta=driver_inputs(1);

%calculate wheel velocities (in tyre coordinate system)
%longitudinal
v_xFL=(y(1) - y(3)*vehicle.track_f/2)*cos(delta) ...
    + (y(2)+y(3)*vehicle.l_f)*sin(delta);
v_xFR=(y(1) + y(3)*vehicle.track_f/2)*cos(delta) ...
    + (y(2)+y(3)*vehicle.l_f)*sin(delta);
v_xRL= y(1) - y(3)*vehicle.track_r/2;
v_xRR= y(1) + y(3)*vehicle.track_r/2;

%lateral
v_yFL=(y(2) + y(3)*vehicle.l_f) *cos(delta) ...
    - (y(1) - y(3)*vehicle.track_f/2) *sin(delta);
v_yFR=(y(2) + y(3)*vehicle.l_f) *cos(delta) ...
    - (y(1) + y(3)*vehicle.track_f/2) *sin(delta);
v_yRL= y(2) - y(3)*vehicle.l_r;
v_yRR= y(2) - y(3)*vehicle.l_r;

%rotational
omRe_FL=y(4).*vehicle.R_f;
omRe_FR=y(5).*vehicle.R_f;
omRe_RL=y(6).*vehicle.R_r;
omRe_RR=y(7).*vehicle.R_r;

%calculate vertical loads
F_zFL=vehicle.m*vehicle.g*vehicle.l_r/(2*vehicle.l) ... %stationary
    - vehicle.h_CoG*vehicle.m*a_x/(2*vehicle.l) ... %longitudinal
    - vehicle.l_r*vehicle.m*a_y/(2*vehicle.track_f); %lateral

F_zFR=vehicle.m*vehicle.g*vehicle.l_r/(2*vehicle.l) ...
    - vehicle.h_CoG*vehicle.m*a_x/(2*vehicle.l) ...
    + vehicle.l_r*vehicle.m*a_y/(2*vehicle.track_f);

F_zRL=vehicle.m*vehicle.g*vehicle.l_f/(2*vehicle.l) ...
    + vehicle.h_CoG*vehicle.m*a_x/(2*vehicle.l) ...
    - vehicle.l_f*vehicle.m*a_y./(2*vehicle.track_r) ;

F_zRR=vehicle.m*vehicle.g*vehicle.l_f/(2*vehicle.l) ...
    + vehicle.h_CoG*vehicle.m*a_x/(2*vehicle.l) ...
    + vehicle.l_f*vehicle.m*a_y./(2*vehicle.track_r);

%calculate tyre forces
[F_xFL, F_yFL]=tyre_forces_MF_combined(F_zFL, v_xFL, v_yFL, omRe_FL);
[F_xFR, F_yFR]=tyre_forces_MF_combined(F_zFR, v_xFR, v_yFR, omRe_FR);
[F_xRL, F_yRL]=tyre_forces_MF_combined(F_zRL, v_xRL, v_yRL, omRe_RL);
[F_xRR, F_yRR]=tyre_forces_MF_combined(F_zRR, v_xRR, v_yRR, omRe_RR);

%calculate drag
F_drag=-0.5*1.23*2*0.3*y(1)^2; % 0.5*rho*A*C_d*v^2

%calculate change in velocities
v_x_dot = ( cos(delta)*(F_xFL+F_xFR) - sin(delta)*(F_yFL+F_yFR) ...
    + F_xRL + F_xRR + F_drag + y(2)*y(3)*vehicle.m ) / vehicle.m;
```

```
v_y_dot = ( sin(delta)*(F_xFL+F_xFR) + cos(delta)*(F_yFL+F_yFR) ...
    + F_yRL + F_yRR - y(1)*y(3)*vehicle.m ) / vehicle.m;

psi_ddot=((cos(delta)*(-F_xFL+F_xFR) ...
    + sin(delta)*(-F_yFL+F_yFR))*vehicle.track_f/2 ...
    + (-F_xRL+F_xRR)*vehicle.track_r/2 ...
    + (cos(delta)*(F_yFL + F_yFR)...
    + sin(delta)*(F_xFL+F_xFR) )*vehicle.l_f ...
    - (F_yRL+F_yRR)*vehicle.l_r ) /vehicle.I;

%calculate wheel accns
omega_dotFL= (driver_inputs(2)-(F_xFL.*vehicle.R_f))./vehicle.I_fw;
omega_dotFR= (driver_inputs(3)-(F_xFR.*vehicle.R_f))./vehicle.I_fw;
omega_dotRL= (driver_inputs(4)-(F_xRL.*vehicle.R_r))./vehicle.I_rw;
omega_dotRR= (driver_inputs(5)-(F_xRR.*vehicle.R_r))./vehicle.I_rw;

y_dot=[v_x_dot; v_y_dot; psi_ddot; ...
    omega_dotFL; omega_dotFR; omega_dotRL; omega_dotRR];

a_x=v_x_dot-(y(3)*y(2));
a_y=v_y_dot+(y(3)*y(1));
end
```

B.3 The Simple *Magic Formula* Tyre Model

Listing B.3: Simple Magic Formula Function

```
function [F_x, F_y] = tyreforceMFcombined(F_z, v_x, v_y, v_r)
%function to calculate tyre force based on simple Magic Formula and the
%friction cricle. J Griffin. 2014-01-21

if F_z≤0 %tyre off the ground
F_x=0;
F_y=0;
else
%account for zero longitudinal speed
if abs(v_x)<0.1
v_x=0.1;
end

%longitudinal
v_sx=v_x-v_r; % [m/s] longitudinal slip speed (-ve in acceleration)
kappa=-v_sx./abs(v_x); %[] longitudinal slip (+ve in acceleration)
B=5; C=2.55; D=1; E=0.99; % Magic Formula coefficients
F_x= F_z.*(D*sin(C*atan(B*kappa - E*(B*kappa - atan(B*kappa)))));

%lateral
alpha=atan(v_y./abs(v_x)); %[] lateral slip (-ve in a left-hand turn)
By=4.5; Cy=2.2; Dy=1; Ey=1.04; % Magic Formula coefficients
F_y= -F_z.*(Dy*sin(Cy*atan(By*alpha - Ey*(By*alpha - atan(By*alpha)))));

% scale to magnitude of the friction circle
resultant = hypot(F_x, F_y);
if resultant > F_z
```

```
F_x=F_x.*F_z/resultant;
F_y=F_y.*F_z/resultant;
end
end
end
```

B.4 Steady-State Linear Motorcycle Handling Calculation

Listing B.4: Motorcycle Handling Function

```
function [beta, psidot]=MC_SS_handling(delta,v,params)
%function to calculate steady-state handling response of a motorcycle
%J Griffin, 2014

%parameters read from structure "params"
g=params.g; m=params.m; lf=params.lf; lr=params.lr;
Kyf=params.Kyf; Kyr=params.Kyr;
Kcf=params.Kcf; Kcr=params.Kcr;

A= [ (Kyf + Kyr) , (lf*Kyf - lr*Kyr)/v + (Kcf+Kcr)*v/g + m*v;
    (lf*Kyf - lr*Kyr), (lf*lf*Kyf + lr*lr*Kyr)/v + (lf*Kcf-lr*Kcr)*v/g];
B=[Kyf*delta; Kyf*lf*delta];
X=A\B; % inv(A)*B
beta=X(1); %sideslip angle [rad]
psidot=X(2); %yaw rate [rad/s]
end
```

B.5 Mathematical Motorcycle Model

The four MATLAB files in this section form the model presented by Seffen *et al.* [59].

B.5.1 Script

Listing B.5: Motorcycle Model Script

```
% script to calculate motorcycle response to a steer torque input
% from "Observations on the controllability of motion of two-wheelers"
% Seffen, Parks, Clarkson. IMechE 2001.
% J Griffin, 2014-10-28

clear all; close all; clc

%% calculate coefficients
v=15;
tau_s=-1;
MC_params %run parameter script
MC_calcs %calculate matrices
clearvars -except MM N PP G tau_s v

%% initialise
y_0=0;
```

```
yaw0=0;
delta_0=deg2rad(0);
camber_0=deg2rad(0);
v_y0=0;
yaw_rate0=0;
delta_rate0=0;
camber_rate0=0;
X_init = ...
    [y_0;yaw0;delta_0;camber_0;v_y0;yaw_rate0;delta_rate0;camber_rate0];

%% solve ODE
tspan = [0 60];
options=[];%odeset('RelTol',1e-3,'InitialStep',1e-5);
f=@(t,X) MC_ode(t,X,MM,N,PP,G,tau_s); %anonymous function
[t,X]=ode45(f,tspan,X_init,options);
clearvars -except t X tau_s v

y=X(:,1);
yaw=X(:,2);
delta=X(:,3);
camber=X(:,4);
v_y=X(:,5);
yaw_rate=X(:,6);
delta_rate=X(:,7);
camber_rate=X(:,8);
```

B.5.2 Motorcycle ODE function

Listing B.6: MC_ODE.m

```
function Xdot=MC_ode(t,X,MM,N,PP,G,tau_s)
X1=X(1:4);
X2=X(5:8);
Xdot1=X2;
Xdot2=-MM\(N*X2 + PP*X1 + G*tau_s);
Xdot=[Xdot1;Xdot2];
end
```

B.5.3 Motorcycle Parameters

Listing B.7: MC_params.m

```
%% from Table 1
M_r     =217.45;    M_f     =30.65;     I_rxx   =31.184;
I_fxx   =1.234;     I_rzz   =21.070;    I_fzz   =0.442;
I_rxz   =1.735;     i_fwy   =0.719;     lamdai_rwy =1.051;
h_r     =0.615;     h_f     =0.467;     p_f     =0.854;
b       =0.480;     L       =0.935;     e       =0.0244;
c       =0.0226;    Eps     =0.4712;    t_r     =0.1158;
R_r     =0.3048;    R_f     =0.3048;    gamma_s =6.780;
C_fs    =11173.9;   C_fc    =0938.6;    C_rs    =15831.2;
C_rc    =1325.6;
```

```
%% Also required
M_u     =0;          h_u     =0;          p_u     =0; %upper torso
I_uxx   =0;          I_uzz   =0;          I_uxz   =0;
M_l     =0;          h_l     =0;          p_l     =0; %lower torso
I_lxx   =0;          I_lzz   =0;          I_lxz   =0;
I_fxz=0; %not specified for MC
g=-9.81; %gravity (Simulation works if this is -ve, contradicts Fig 1bii)
```

B.5.4 Calculation of Matrices

Listing B.8: `MC_calcs.m`

```
%% Calcs from Appendix
M=M_f+M_r+M_l+M_u; %total mass
p=(M_f*p_f - M_u*p_u - M_l*p_l)/M; %distance to Centre of Mass
h=(M_f*h_f + M_r*h_r + M_l*h_l + M_u*h_u)/M; %height of combined CoM
w=L+b;
M_jge=M_f*g*e + M*t_r*(b+p)*g/w;

I_fss=I_fzz + M_f*e^2;
I_fss__r=i_fwy/R_f + lamdai_rwy/R_r;

I_1=M_f*e*p_f + I_fzz*cos(Eps) + I_fxz*sin(Eps);
I_2=M_f*e*h_f + I_fzz*sin(Eps) - I_fxz*cos(Eps);

I_Ozz=M_f*p_f^2 + M_u*p_u^2 + M_l*p_l^2 + I_rzz + I_fxx*sin(Eps)^2 ...
    +I_fzz*cos(Eps)^2 + I_fxz*sin(2*Eps) + I_uzz - I_lzz;
I_Oxx=M_r*h_r^2 + M_f*h_f^2 + M_u*h_u^2 + M_l*h_l^2 + ...
    I_fzz*sin(Eps)^2 ...
    +I_fxx*cos(Eps)^2 - I_fxz*sin(2*Eps) + I_rxx + I_uxx + I_lxx;
I_Oxz=-M_f*p_f*h_f + M_u*p_u*h_u + M_l*p_l*h_l ...
    +(I_fxx-I_fzz)*sin(Eps)*cos(Eps) + I_fxz*cos(2*Eps)...
    + I_rxz + I_uxz + I_lxz;

C_1=C_fs+C_rs;
C_2=(b*C_rs-L*C_fs)/w;
C_3=C_fs*cos(Eps)+C_fc*sin(Eps);
C_4=C_fc+C_rc;
C_5=(b^2*C_rs + L^2*C_fs)/w^2;
C_6=(L*C_fc - b*C_rc)/w;

%% matrix Calcs
MM=[M, M*p, M_f*e, M*h;
    M*p, I_Ozz, I_1, -I_Oxz;
    M_f*e, I_1, I_fss, I_2;
    M*h, -I_Oxz, I_2, I_Oxx];

N=[C_1/v^2, -w*C_2/v^2+M, -t_r*C_fs/v^2, 0;
    -w*C_2/v^2, ...
        w^2*C_5/v^2+M*p,-t_r*L*C_fs/v^2-i_fwy*sin(Eps)/R_f,-I_fss__r;
    -t_r*C_fs/v^2, -t_r*L*C_fs/v^2+M_f*e+i_fwy*sin(Eps)/R_f, ...
        t_r^2*C_fs/v^2+gamma_s/v, -i_fwy*cos(Eps)/R_f;
    0, M*h+I_fss__r, i_fwy*cos(Eps)/R_f, 0];

P=[-C_3,-C_4;
    -L*C_3, -w*C_6;
```

```
    t_r*C_3-M_jge*sin(Eps), t_r*C_fc-M_jge;
    -M_jge, -M*g*h];
PP=[zeros(4,2), P]; % for ode script (if required)

G=[0;0;-1;0];

%% for state space model (if required)
A=[zeros(2,4) eye(2,2);
    -MM\P -MM\N]; % -inv(MM)*P -inv(MM)*N]; %

B=[zeros(2,1);
    -MM\G]; % -inv(MM)*G]; %

U=tau_s;
```

Appendix C

Multibody Model Parameters

This chapter lists the parameters used for the multibody model simulations of the automobile and motorcycle. Values given here are used unless otherwise stated in the text.

C.1 Automobile Model Parameters

Table C.1: Vehicle parameters

Parameter	Symbol	Value
vehicle mass	m_v	$1560\,\mathrm{kg}$
vehicle inertia	$\mathbf{I}_v$	$\begin{bmatrix} 1500 & 0 & 0 \\ 0 & 1500 & 0 \\ 0 & 0 & 2500 \end{bmatrix}\,\mathrm{kg\,m^2}$
gravitational acceleration	$\boldsymbol{g}$	$\begin{bmatrix} 0 & 0 & -9.81 \end{bmatrix}\,\mathrm{m}$
Centre of Mass (CoM) position	$\boldsymbol{s}_{\mathrm{CoM}}$	$\begin{bmatrix} 0 & 0 & 0.5 \end{bmatrix}\,\mathrm{m}$
Centre of Pressure (CoP) position	$\boldsymbol{s}_{\mathrm{CoP}}$	$\begin{bmatrix} 0 & 0 & 0.5 \end{bmatrix}\,\mathrm{m}$
drag coefficient	C_{drag}	0.3
lift coefficient	C_{lift}	0.1
frontal aera	A	$2\,\mathrm{m^2}$

Table C.2: Wheel parameters

Parameter	Symbol	Value
wheel mass	m_w	10 kg
wheel inertia	$\mathbf{I}_w$	$\begin{bmatrix} 0.9 & 0 & 0 \\ 0 & 0.9 & 0 \\ 0 & 0 & 0.9 \end{bmatrix}$ m
front-left wheel position	$\boldsymbol{s}_{fl}$	$\begin{bmatrix} 1.25 & 0.75 & 0.3 \end{bmatrix}$ m
front-right wheel position	$\boldsymbol{s}_{fr}$	$\begin{bmatrix} 1.25 & -0.75 & 0.3 \end{bmatrix}$ m
rear-left wheel position	$\boldsymbol{s}_{rl}$	$\begin{bmatrix} -1.25 & 0.75 & 0.3 \end{bmatrix}$ m
rear-right wheel position	$\boldsymbol{s}_{rr}$	$\begin{bmatrix} -1.25 & -0.75 & 0.3 \end{bmatrix}$ m
wheel radius	r_w	0.3 m
suspension stiffness	K	30 000 $\mathrm{N\,m^{-1}}$
suspension damping	C	2000 $\mathrm{N\,s\,m^{-1}}$
suspension offset	s_z	-0.13 m

C.2 Motorcycle Model Parameters

Table C.3: Motorcycle Coordinate System (CS) locations

CS	Location	
mainframe CoM	$\begin{bmatrix} 0.680 & 0 & 0.532 \end{bmatrix}$	m
rider CoM	$\begin{bmatrix} 0.600 & 0 & 0.990 \end{bmatrix}$	m
rear wheel CoM	$\begin{bmatrix} 0.000 & 0 & 0.315 \end{bmatrix}$	m
front wheel CoM	$\begin{bmatrix} 1.539 & 0 & 0.318 \end{bmatrix}$	m
forks CoM	$\begin{bmatrix} 1.539 & 0 & 0.318 \end{bmatrix}$	m
handlebars CoM	$\begin{bmatrix} 1.165 & 0 & 0.869 \end{bmatrix}$	m
swingarm CoM	$\begin{bmatrix} 0.100 & 0 & 0.350 \end{bmatrix}$	m
aerodynamic CoP	$\begin{bmatrix} 0.634 & 0 & 0.696 \end{bmatrix}$	m
mainframe–rider joint	$\begin{bmatrix} 0.600 & 0 & 0.800 \end{bmatrix}$	m
mainframe–handlebars joint	$\begin{bmatrix} 1.169 & 0 & 0.834 \end{bmatrix}$	m
handlebars–forks joint	$\begin{bmatrix} 1.125 & 0 & 0.867 \end{bmatrix}$	m
mainframe–swingarm joint	$\begin{bmatrix} 0.400 & 0 & 0.321 \end{bmatrix}$	m
mainframe–rear suspension	$\begin{bmatrix} 0.200 & 0 & 0.700 \end{bmatrix}$	m
swingarm–rear suspension	$\begin{bmatrix} 0.100 & 0 & 0.330 \end{bmatrix}$	m

Table C.4: Motorcycle body masses

Body	Mass
mainframe	192 kg
rider	45 kg
rear wheel	16 kg
front wheel	11.4 kg
handlebars	6.34 kg
forks	7.61 kg
swingarm	7.35 kg

Table C.5: Motorcycle body inertias

Body	Inertia	
mainframe	$\begin{bmatrix} 16.582 & 0 & 0.733 \\ 0 & 34.758 & 0 \\ 0.733 & 0 & 23.632 \end{bmatrix}$	$\mathrm{kg\,m^2}$
rider	$\begin{bmatrix} 1.3 & 0 & 0.3 \\ 0 & 2.1 & 0 \\ 0.3 & 0 & 1.4 \end{bmatrix}$	$\mathrm{kg\,m^2}$
rear wheel	$\begin{bmatrix} 0.1 & 0 & 0 \\ 0 & 0.3895 & 0 \\ 0 & 0 & 0.1 \end{bmatrix}$	$\mathrm{kg\,m^2}$
front wheel	$\begin{bmatrix} 0.1 & 0 & 0 \\ 0 & 0.2624 & 0 \\ 0 & 0 & 0.1 \end{bmatrix}$	$\mathrm{kg\,m^2}$
handlebars	$\begin{bmatrix} 0.1995 & 0 & 0 \\ 0 & 0.1210 & 0 \\ 0 & 0 & 0.0900 \end{bmatrix}$	$\mathrm{kg\,m^2}$
forks	$\begin{bmatrix} 0.2476 & 0 & 0 \\ 0 & 0.1880 & 0 \\ 0 & 0 & 0.0963 \end{bmatrix}$	$\mathrm{kg\,m^2}$
swingarm	$\begin{bmatrix} 0.0563 & 0 & 0 \\ 0 & 0.2501 & 0 \\ 0 & 0 & 0.2659 \end{bmatrix}$	$\mathrm{kg\,m^2}$

Table C.6: Motorcycle suspension characteristics

Parameter	Value
rear suspension stiffness	98000 $\mathrm{N\,m^{-1}}$
rear suspension damping	16000 $\mathrm{N\,s\,m^{-1}}$
rear suspension preload	1800 N
front suspension stiffness	16000 $\mathrm{N\,m^{-1}}$
front suspension damping	1000 $\mathrm{N\,s\,m^{-1}}$
front suspension offset	-0.057 m
steer stiffness	0 $\mathrm{N\,rad^{-1}}$
steer damping	8 $\mathrm{N\,s\,rad^{-1}}$
twist stiffness	34100 $\mathrm{N\,rad^{-1}}$
twist damping	100 $\mathrm{N\,s\,rad^{-1}}$
rider lean stiffness	1000 $\mathrm{N\,rad^{-1}}$
rider lean damping	1000 $\mathrm{N\,s\,rad^{-1}}$

Table C.7: Further motorcycle parameters

Parameter	Symbol	Value
steer tube inclination	ϵ	-0.418 rad
coefficient of drag	C_{drag}	0.312
coefficient of lift	C_{lift}	0.114
front tyre radius	$r_{0\,f}$	0.325 m
front tyre toroid radius	$r_{t\,f}$	0.075 m
rear tyre radius	$r_{0\,b}$	0.332 m
rear tyre toroid radius	$r_{t\,b}$	0.120 m